THE UNIVERSITY OF CALGARY

Effects of Molecular Structure on the Sintering of Ethylene/α-Olefin Copolymers

by

Sergio Alejandro Guillén Castellanos

A THESIS

SUBMITTED TO THE FACULTY OF GRADUATE STUDIES IN PARTIAL FULFILLMENT OF THE REQUIREMENTS FOR THE DEGREE OF

MASTER OF SCIENCE IN CHEMICAL ENGINEERING

Department of Chemical and Petroleum Engineering

Calgary, Alberta

August 2001

ABSTRACT

The objective of this work is to determine the effects of the polymer molecular structure on the sintering process. An experimental study on polymer sintering has been conducted in conjunction with an extensive characterization of the resins used in this work. A combination of rheological, thermal, and spectroscopic techniques was found to be effective in determining the molecular characteristics of the resins.

Sintering experiments were conducted under isothermal and non-isothermal conditions using both powder and cylindrical particles. It was found that the trends observed for the sintering of powder were consistent with the predictions of Newtonian sintering models. Sintering results obtained using cylindrical particles, however, showed significant differences not seen when using powder particles. These were attributed to the differences in the surface area between the two types of particles. It is speculated that the effect of material properties other than viscosity and elasticity are enhanced when cylindrical particles are used. It was shown that an increase in the molecular weight, which translates into higher viscosity values, has a negative impact on polymer sintering. It was also shown that as the comonomer content increases, the sintering rate decreases. The presence of more side branches in the polymer chain causes a reduction in the degree of crystallinity. The resulting amorphous regions represent an obstacle to self-diffusion that negatively impacts the sintering process. On the other hand, an increase in the comonomer content generally results in a decrease in the melting temperature and the heat of fusion, which favors the onset of sintering. For the resins used in this study, it was difficult to evaluate the effect of the molecular weight distribution, comonomer type, and comonomer distribution on the sintering process. Experimental evidence suggested that copolymers with a more homogeneous structure generally sinter faster than their heterogeneous counterparts. Nevertheless, the presence of some heterogeneities in the molecular structure, while maintaining a relatively narrow molecular weight distribution, seemed to favor the sintering process in a few cases, especially with experiments conducted under non-isothermal conditions.

ACKNOWLEDGEMENTS

I want to thank my supervisor, Dr. Céline T. Bellehumeur, for having given me the opportunity to work under her supervision. I very much appreciate her continuous support and guidance. I would like to thank my committee members: Dr. Robert A. Heidemann and Dr. William J. D. Shaw for taking the time to read my thesis and to critique my work. Also, I want to express my gratitude for the many helpful comments provided by Dr. Mark Weber, NOVA Chemicals Corporation. The discussions we have had played a major role in both the content and presentation of my work.

This research would not have been possible without the help of many people. These include: Dr. Anil Mehrotra for letting me use the DSC apparatus; Dr. George Shimizu and Ms. Dorothy Fox in the Chemistry Department for their help with TGA and FTIR experiments. I am indebted to Mr. Jen Shueng Tiang, Mr. Sebastian Kosciolek and Mr. Wen Lin for conducting experiments which were crucial to my discussion. I also thank the research staff of the NOVA Chemicals Technical Centre. In particular, I express my appreciation to Mr. Craig Ellefson and Mr. Cheng Luo for their help and comments about rotomolding and part testing.

I am thankful to NOVA Chemicals Corporation for supplying the resins and for funding part of this project. The financial support from the Department of Chemical and Petroleum Engineering and the Natural Science Engineering and Research Council of Canada was also appreciated.

I would like to thank the faculty, staff and fellow graduate students at the Department of Chemical and Petroleum Engineering for making my studies at the University of Calgary so memorable. In particular, I want to thank Imtiaz, Jen, Wen, Sebastian, Prashanth, Sung, Yus, Hua, Karen, Helen, Mike, Javier and Laura for sharing time and experiences with me and for their friendship.

To my parents

TABLE OF CONTENTS

TABLE OF CONTENTS

LIST OF TABLES

LIST OF FIGURES

Effect of MWD

Effect of comonomer type and content

Effect of rheological properties: low viscosity

Effect of rheological properties: medium viscosity

Effect of rheological properties: high viscosity

ABBREVIATIONS

ABS	Copoly (acrylonitrile-butadiene-stryrene)
DSC	Differential scanning calorimetry
GPC	Gel permeation chromatography
HDPE	High density polyethylene
IR	Infrared
FTIR	Fourier transform infrared
LCB	Long chain branching
LDPE	Low density polyethylene
LLDPE	Linear low density polyethylene
MW	Molecular weight
MWD	Molecular weight distribution
PC	Polycarbonate
PE	Polyethylene
PET	Polyethylene terephthalate
PDI	Polydispersity index
PMMA	Poly (methyl-methacrylate)
PP	Polypropylene
PS	Polystyrene
PVC	Poly vinyl chloride
SCB	Short chain branching
TREF	Temperature rising elution fractionation
UHMWPE	Ultrahigh molecular weight polyethylene

WAXD	Wide angle X-ray diffraction
ZN	Ziegler-Natta

NOMENCLATURE

a	Particle radius, m
$G'(\omega)$	Storage modulus, Pa
$G''(\omega)$	Loss modulus, Pa
M_n	Number average molecular weight
M_w	Weight average molecular weight
T_m	Melting temperature, °C
y	Neck length, m

Greek Letters

δ	Phase angle, radians
η	Viscosity, Pa.s
γ	Surface tension, N/m
ω	Frequency, rad/s
ω_s	Crossover frequency, rad/s

Introduction

Chapter 1

1.1 Polymer Sintering

Sintering can be defined as the formation of a homogeneous body by the merger of small particles usually under the action of heat and pressure. This term, frequently found in the literature related to metal and ceramics processing, is also being used to describe the coalescence of polymeric materials. While for metals and ceramics the sintering temperature usually does not reach the materials' melting temperature, conditions above the melting or glass transition temperature are often used for polymers. As a result, polymer sintering takes place in the molten state. It can be then studied as a flow phenomenon in which intrinsic forces (surface tension) and externally applied forces (pressure) drive the coalescence. Some of the physical processes associated with polymer sintering include deformation and diffusion (Mazur, 1995).

The coalescence phenomenon is more complicated for polymeric liquids than for simple liquids. Polymeric liquids show a very distinctive behavior in terms of flow and interdiffusion mainly due to their macromolecular characteristics. Entanglements, linearity of the chains, order-disorder transitions, relaxation and retardation phenomena are some of the important factors that affect the behavior of these liquids.

The study of the coalescence of polymeric liquids is relevant to industrial applications. In many processes such as rapid prototyping, powder coating and rotational molding, polymer sintering plays an important role. The processing cycle and the properties of the final product are related to sintering. Moreover, the

information gained while studying coalescence can be used in multiple applications involving interfacial flow, polymer diffusion and adhesion. These fundamental aspects associated with sintering are common, to some extent, to multi-layer extrusion, "welding" of polymers and fused deposition modeling.

1.2 Rotational Molding

Rotational molding is a technique used to produce hollow plastic parts. In a very general way, the process can be divided into four major stages. First, a mold is charged with the resin, usually in powder form. It is then heated in an oven and rotated biaxially at the same time. As the mold is heated, the powder particles melt. The molten particles undergo a densification process that is characterized by the neck growth between the particles (sintering), the entrapment of air bubbles within the melt, and finally the dissolution of bubbles. The rotation speed is relatively slow and a proper rotation ratio ensures a uniform melt covering of the mold. The molding cycle and oven temperature are set with the objective of minimizing the size and number of bubbles in the final part but without compromising the material thermal stability. The presence of bubbles and thermal degradation are undesirable because they affect the impact properties and appearance of the molded part. In the last stage, the mold is cooled down and the final part removed.

Sintering and densification can be seen as fundamental phenomena of rotational molding since they strongly impact both heating times and the properties of the final part. Past studies have shown that the powder characteristics (particle size, shape, particle size distribution) and the material properties (viscosity, elasticity, melting range) are important in the bubble formation-dissolution process (Kontopoulou et al., 2000). However, since the densification process depends on many parameters, the relative importance of each one has to be established. Other factors such as the pulverization conditions during grinding, the presence of additives and the materials' molecular structure must be also taken into consideration in the study of sintering and densification.

Currently, polyethylene (PE) is the most widely used resin in the rotational molding industry due to its good flow properties, thermal stability and impact properties. There is a need for new materials, nevertheless. Some applications require certain optical or impact properties that PE cannot attain. The rotomoldability of materials such as polypropylene (PP), polyamides (nylons), polycarbonate (PC), poly (acrylonitrile-butadiene-styrene) (ABS), polyvinylchloride (PVC) has been tested but each material was found to have limitations that in general, included very high values of viscosity (and/or elasticity) and susceptibility to thermal degradation. It is envisioned that a better understanding of polymer sintering with respect to molecular structure could contribute to the design of new materials suitable for rotational molding.

1.3 Objectives and thesis outline

The current study is part of a research program that focuses on the sintering phenomenon in the rotational molding process. Polymer sintering has traditionally been studied in terms of rheological properties (Bellehumeur et al., 1996). Other aspects, however, need further research. The main objective of this work is to investigate the influence of molecular structure on coalescence of polymeric materials. Sintering experiments are conducted on well-characterized resins. The characterization of the resins involves the study of rheological and thermal properties since they are closely related to the chain microstructure. Additional information about chemical composition of the resins is obtained by infrared spectroscopy. The conditions at which sintering experiments are conducted are set in order to obtain information that can be related to the rotational molding process.

Linear low density polyethylene (LLDPE) resins with different molecular weight and type of comonomer are chosen for this study because of several reasons. Polyethylene (PE) in general and LLDPE in particular occupy a very important place in the thermoplastics market nowadays. In rotational molding alone,

they represent almost 90% of the total consumption in North America (Leaversuch, 1989). Moreover, LLDPE resins are being synthesized by new polymerization techniques based on novel catalysts and their resulting properties need to be studied.

This thesis is divided into five chapters including this introduction. A review of previous studies relevant to the present work is presented in the second chapter. Due to the vast amount of research published on polyethylene, that chapter is limited to recent literature that focuses on LLDPE only. Chapter three deals with the characterization of the different resins. The sintering experiments and their discussion are then presented in chapter four. The final chapter contains the conclusions and recommendations for future work.

Literature review

Chapter 2

Past studies on the sintering of polymers will be discussed in this chapter. This review focuses mainly on experimental work performed with discrete particles and semi-crystalline materials. Then, the influence of molecular structure on the properties of LLDPEs will be briefly discussed. Emphasis will be made on copolymers of ethylene with 1-butene, 1-hexene and 1-octene.

2.1 Experimental studies of polymer sintering

Polymer coalescence of discrete particles has been studied less extensively than sintering of metals and ceramics. One of the first experimental studies on polymer sintering dates from 1970. That was the work of Kuczynski and collaborators who tested the sintering behavior of poly(methyl methacrylate) (PMMA). Their experiments consisted of the observation of the coalescence between spherical particles and a flat block of the same material. In 1979, Narkis conducted experiments using particles of PMMA placed as single layers on flat aluminum surfaces. These two studies were considered qualitative in nature since the experimental measurements were not carried out continuously. Rosenzweig and Narkis (1980) improved the experimental technique by using a hot stage coupled to an optical microscope. The sintering evolution of two particles was monitored with respect to time and more reliable experimental results were obtained. In 1981, these researchers studied the behavior of polystyrene (PS) and PMMA. Their experiments showed that Newtonian viscous flow is the dominant mechanism in polymer sintering as opposed to volume and surface diffusion for metals and ceramics (Kuczynski, 1972). Hornsby and Maxwell (1992) studied the sintering behavior of polypropylene (PP) and PMMA. They showed that, in general, the sintering behavior of

polypropylene beads is in good agreement with Frenkel's model (Frenkel, 1945). However, in their analysis they used Trouton's viscosity (three times larger than the shear viscosity). In the studies reviewed so far, information about material properties other than viscosity was not provided, which makes further comparison of these results very difficult.

Siegmann and his group (1986) conducted experiments on semi-crystalline (PE) and amorphous (PS, PMMA) polymers. Polyethylenes with different molecular weights were tested following the procedure of Rosenzweig and Narkis. Interestingly, they found that an ultra high molecular weight polyethylene resin (UHMWPE) sintered faster than the other PE resins. The viscosity and molecular weight of this UHMWPE were much greater than those of a high molecular weight PE but the sintering time was almost four times shorter. They attributed this behavior to its special fibrillar microstructure consisting of highly oriented chains. Different UHMWPE resins were also studied by Barnetson and Hornsby in 1995. They focused their work on the effect of microscopic structure on polymer sintering. The comparison of results was somehow difficult to make because the resins had different molecular weights and particle sizes. Moreover, material properties such as melting temperature and degree of crystallinity were only superficially mentioned. The conclusion of this work supported observations made by Siegmann et al. (1986) in relation to the effect of microstructure on sintering. Finely divided and porous powders, with high surface area, were found to sinter faster than the coarser grades. They attributed this enhanced sintering ability to the fact that the driving force of the process is caused by the work of surface reduction.

In 1996, Bellehumeur et al. conducted sintering experiments using different grades of polyethylene resins in both powder and cylindrical forms. They found that for some resins, the particle size influenced sintering rate more significantly than for others. In particular, resins with higher viscosity seemed to be strongly affected by the particle size. Important variations in the sintering rate were observed when a HDPE resin was tested at different conditions. Low-viscosity LLDPE resins, on the

other hand, showed fewer variations. The negative impact of viscosity on sintering rate was demonstrated. While this study included information about some material properties such as melting temperature and crystallinity, the number of resins tested was limited. Experimental results were compared to analytical models and the dominance of Newtonian viscous flow mechanism in polymer sintering was confirmed. Liu (1996) studied the behavior of low-density polyethylenes. He concluded that besides surface tension, gravity acts as a driving force for the sintering mechanism. Viscosity is the main resistance. He also incorporated talc into some of the resins and conducted sintering experiments. An increase in sintering rate was observed. He explained this phenomenon based on the higher thermal conductivity of talc compared to polyethylene's conductivity. Unfortunately, additional information about the material properties was not provided.

Analytical models and numerical simulations are often encountered in the literature. They are useful in that parametric studies can be made to determine the relative importance of the variables involved in sintering. In 1945, Frenkel derived the first analytical model by considering surface tension as the driving force and viscous flow as the main resistance in the sintering process. This model is only valid for the initial stages of coalescence. In spite of its simplicity, it correlates relatively well with experimental observations.

$$\left(\frac{y}{a}\right)^2 = \left(\frac{3\gamma t}{2\eta a}\right) \qquad (2.1)$$

Equation 2.1 corresponds to Frenkel's model. In this expression the radius of the interface or neck between two spheres (y/a) is proportional to the surface tension (γ) but inversely proportional to viscosity (η) and the radius of the sphere (a). Several corrections and modifications have been proposed to this model mainly in terms of geometrical considerations (Rosenzweig and Narkis, 1983; Hopper, 1984; Pokluda et al., 1997). The model's predictions were qualitatively in agreement with

experimental results supporting the idea of Newtonian flow under the action of surface tension.

2.2 Polyethylene and linear low density polyethylene

Polyethylene is a semicrystalline polymer which can be classified into major categories according to density and structure of the macromolecular chains. High density polyethylene (HDPE) is composed of linear chains. Polymers with lower densities can be obtained by introducing branches and altering the molecular structure. While the density of low density polyethylene (LDPE) is reduced by the number and size of long chain branches, the density in linear low-density polyethylene (LLDPE) is reduced by increasing the number of short chain branches (Goyal, 1995). The desired mechanical and chemical resistance properties vary according to density. LDPE shows low stiffness and high toughness. HDPE (density >940 kg/m^3) shows better chemical resistance but reduced toughness and stress cracking resistance. LLDPE offers the best combination of properties compared to the other PE grades and its consumption is growing continuously.

LLDPE is the product obtained by copolymerization of ethylene and α-olefins. The chain microstructure of this polymer depends on the type and amount of comonomer used, the distribution of the comonomer along the macromolecules and the molecular weight (MW). The type of comonomer determines the length of the side branches and the comonomer content is related to the number of short chain branches (SCB). As a result, the terms "degree of branching" and "comonomer content" are often used interchangeably. Until recently, LLDPE had been produced using Ziegler-Natta (ZN) technology. The development of new "single site" catalysts has revolutionized the polyolefin industry making it possible to synthesize copolymers with narrower molecular weight distribution (MWD) and more uniform composition. This new technology also allows the use of a wider variety of monomers such as higher α-olefins, cyclo-olefins and polar structures (Starck, 1996). Although the chemical composition of single-site LLDPEs is more uniform

than that of ZN copolymers, inter-molecular (Fu et al., 1997) and intra-molecular heterogeneities (Zhang et al., 2000) have been reported. Both the molecular structure and polymer homogeneity are important because they influence the copolymers' viscoelastic, mechanical, optical and thermal properties (Schouterden et al., 1987; Hosoda, 1988; Adisson et al., 1992).

2.3 Rheological properties of ethylene/α-olefin copolymers

Some researchers have studied the influence of the molecular structure on the rheological properties of LLDPE resins synthesized using conventional (Ziegler-Natta) and single site catalysts (Kim et al., 1996; Goyal et al., 1998; Wood-Adams and Dealy, 1999; Kazatchkov et al., 1999; Wood-Adams et al., 2000). It has been found that the rheological behavior of these materials is a strong function of MW, MWD, degree of branching and branching distribution. In general, an increase in MW results in an increase of viscosity and elasticity if other molecular characteristics remain unchanged. Kazatchkov et al. (1999) studied two series of butene copolymers: the first had comparable MW but different MWD while the second series had very similar MWD but different MW values. Using both oscillatory and capillary measurements, they found that zero-shear viscosity and extrudate swell increased as the MW increases and the MWD broadens. As the MWD broadens, however, the shear thinning behavior is enhanced and the elastic properties (measured as the dynamic moduli: G′ and G″) vary with frequency. Whereas at small frequencies the values of G′ and G″ increased with MWD broadness, they tended to decrease at high frequencies. Wood-Adams et al. (2000) observed similar trends.

It has been reported that the presence of long chain branches (LCB) even in small amounts have a drastic effect on the rheological properties (Kim et al., 1996; Vega et al., 1998; Wood-Adams and Dealy, 1999; Wood-Adams et al., 2000). Kim and collaborators (1996) and Bin-Wadud and Baird (1999) mentioned that small amounts of LCB positively affect the material processability. This was verified by

Vega et al. (1998) and Wood-Adams et al. (2000). They observed that even though the zero-shear viscosity increases with LCB content (same molecular weight), the shear-thinning behavior is enhanced and consequently, the resin is easier to process. According to Wood-Adams et al. (2000), some differences in the linear viscoelastic region can be observed as well. Polymers with LCB show a mode of relaxation at low frequencies that is not observed with non-branched polymers. Bimodal polyethylenes, i. e. resins with two major MW, were studied by Muñoz-Escalona and his group in 1999. Interestingly, the rheological behavior of these polymers was found to be comparable to that of polymers with small amounts of LCB. The amount of short chain branches (SCB), on the other hand, has little influence in rheological properties, at least in the linear viscoelastic region (Kim et al., 1996; Wood-Adams and Dealy, 1999; Wood-Adams et al., 2000). The distribution of SCB along the chains, however, was reported to affect the rheological behavior of ethylene/1-hexene copolymers (Shan et al., 2000).

Goyal (1995) and Goyal and co-workers (1998) examined the effects of molecular characteristics of LDPE and LLDPE on the melt strength, a property related to extensional viscosity. The melt strength represents the resistance of a melt to extension and it is desired information in processes such as film blowing and extrusion coating. They found that as the MW increases so does the melt strength. They also observed that for LLDPE the amount of SCB does not have a significant effect on melt strength but the type of comonomer is, on the other hand, important. They explained those results in terms of chain entanglements. Higher alpha olefin SCB may produce a relatively higher degree of entanglement, in particular at lower temperatures. As the level of entanglement increases, the melt strength also increases. For LDPE in which LCB are normally present, Goyal et al. found that the melt strength was affected by the amount of branches and by their distribution along the chains.

2.4 Morphology and thermal behavior of ethylene/α-olefin copolymers

It is well known that for linear polymers the melting temperature (T_m) increases with MW up to a limiting value (Riande et al., 2000). However, for some LLDPE copolymers with approximately constant comonomer content it has been reported that the melting temperature (T_m) can decrease with increasing MW (Alamo and Mandelkern, 1989; Peeters et al., 1997).

Experiments have shown that the melting temperature and the degree of crystallinity of LLDPE resins decrease very rapidly with increasing branching content (Hosoda, 1988; Alamo and Mendelkern, 1989; Bensason et al., 1996; Alizadeh et al., 1999; Vanden Eynde et al. 2000b). As more non-crystallizing units are introduced, the degree of crystallinity decreases continuously. Moreover, the length and the number of sequences that are available to participate in the crystallization process are progressively reduced. This is a natural consequence of the structure of random copolymers (Alamo and Mandelkern, 1989). Crystallites of different sizes and stabilities are formed from ethylene sequences of different length (Vanden Eynde et al. 2000b). A range of melting and crystallization temperatures is therefore observed and reflected in the DSC endotherms (Peeters et al., 1997; Vanden Eynde et al. 2000c).

There is not a general consensus on whether the chemical nature of the SCB affects the T_m and degree of crystallinity. Hosoda (1988) mentioned that the copolymers of 1-butene showed higher melting temperature and crystallinity than the 1-hexene and 1-octene resins. In 2000, Vanden Eynde and coworkers also attributed some variations of thermal properties to the different types of comonomer. Alamo and Mandelkern (1989) and Alizadeh et al. (1999), on the other hand, concluded that apart from methyl or chlorine substituents, the chemical nature of SCB does not influence the thermal behavior of LLDPEs.

Peeters et al. (1997) worked with monodisperse copolymers of ethylene and 1-octene and linear polymers for comparison. They observed that the thermal history influences the subsequent melting behavior. All the samples were crystallized under different conditions (quenching and slow cooling) and the following trends were observed upon melting:

-For linear and poorly branched samples that were cooled from the melt very rapidly (quenched), the melting range was narrower than that obtained after slow cooling. Also, the reduction of crystallinity with SCB was more prominent in this case. The melting temperature was found to increase slightly with decreasing cooling rate for these samples.

-For branched samples, fast cooling had an opposite effect, i. e. the melting range was broad. For these samples, the reduction of crystallinity with SCB seemed to be independent of cooling rate. Decreasing cooling rate resulted in lower melting temperatures.

The variations in melting temperature were attributed to the different crystalline structures that are formed under different conditions. During slow cooling processes the longer sequences crystallize at higher temperatures and the crystals formed under these conditions are more stable and have a high melting point. On the other hand, during quenching, long and short sequences crystallize together and the formed crystals will be rather unstable and imperfect. Upon re-heating, these imperfect crystals melt and the longer undisturbed sequences can recrystallize into more stable crystals. The crystals formed in slow-cooled samples do not need to rearrange in the melt state because stable crystals were already formed. It was also corroborated by Wide Angle X-Ray Diffraction (WAXD) that an increase of SCB resulted in looser folds in the crystalline structure. Accordingly, linear polyethylene had tighter folds and hence the interfacial (amorphous) regions were more ordered.

Peeters and collaborators (2000) studied the combined effect of comonomer content and annealing on the thermal properties of ethylene copolymers. They observed that annealing gradually increased the thermal stability of the original crystals. Also, it was shown that the size and type of crystalline structure is a function of comonomer (or branching) content. They commented that if the degree of branching is high the average thickness of the lamellae decreases and more and more polymer parts are driven out of the crystal. The amount of chain that can leave the crystal is limited and as a result, shorter and shorter lamellae are formed, ultimately resulting in fringed micellar-type crystals. If the comonomer content is low, then the metastable crystals are of lamellar type. These results supported the observations previously made by Defoor (1992), Lambert and Phillips (1994) and Bensason et al. (1996). The presence of crystals with different thermal stabilities was observed as the broadness of the melting range.

Vanden Eynde et al. studied the morphology and thermal behavior of highly branched LLDPEs (2000b, 2000c) by different techniques. It was found that copolymers of ethylene-propylene, ethylene-1-butene and ethylene 1-octene behave similarly. They also observed that the DSC curves became broader and flatter and shifted to lower temperatures as the comonomer content was increased. The chain length magnified this effect. It was shown that, in general, an increase in the degree of branching shifts the crystallization process to regions of lower temperature where chain mobility (and diffusion) is hindered.

A recent study conducted on metallocene LLDPEs by Fu et al. (1997) showed that the thermal behavior of these copolymers is complex. After thermal segregation in the melt and/or during crystallization, the samples became phase separated and re-heating of the samples led to a heterogeneous melt.

2.5 Studies of polyethylene resins using infrared spectroscopy

Past studies of polyethylene resins using infrared (IR) spectroscopy can be grouped into two major categories. The first category comprises the work carried out to determine the chemical structure of the different grades of polyethylene, i. e. the amount and the length of SCB. The second category includes the study of chain conformations and crystalline states. Usually, infrared spectroscopy is used in combination with other analytical techniques in order to complete and validate the information gained using this experimental method. For comparative purposes, however, it has been found to be useful mostly due to its low cost, short testing times and the ease of sample preparation (Koenig, 1999).

2.5.1 Chemical composition

The quantification of methyl groups has served as an indicator of the degree of branching in polyethylene. Absorption at 1378 cm^{-1} (methyl deformation band) has been used since the 1950's in spite of the fact that this band is overlapped by the bands located at 1367 cm^{-1} and 1350 cm^{-1}, which are associated with methylene vibration. The work of Willbourn (1959) gave rise to the technique that evolved into a standard (ASTM D2238). Basically the absorption at 1378 cm^{-1} is resolved by using a polyethylene wedge in the reference beam that compensates for the interference previously mentioned. Other methods of resolution of bands were proposed because the compensation method was found to be very sensitive to experimental conditions (Rueda et al., 1979) and gave erroneous results for low degrees of branching (Baker and Madams, 1976). The bromination of vinyl groups in polyethylene improved the resolution of some peaks, particularly the band located at 935 cm^{-1} due to methyl vibration (McRae and Maddams, 1976). Curve fitting techniques have been also employed. In 1979, Rueda et al. used a curve fitting method to resolve the peaks located between 1320 and 1400 cm^{-1}. Five gaussian bands were fitted following

theoretical assignments and very good results were obtained. They created a calibration curve using the absorption at 1378 cm^{-1} of materials with known amounts of SCB. Recently, the use of Fourier self-deconvolution has been also employed to resolve peaks (Blitz and McFaddin, 1994). This technique must be used with caution since it requires the knowledge of half-widths of the component peaks. In practice, they are not known. Wrong estimations of half-widths can produce bands with lower resolution or even overconvolution which in turn gives a degree of sharpening greater than expected (Koenig, 1999).

Blitz and McFaddin (1994) conducted a thorough and rigorous study for determining the type and degree of branching of LLDPEs using FTIR and NMR. The spectral region between 700 and 900 cm^{-1} provided information about the different branches. They showed a correlation between the band at 770 cm^{-1} and the amount of ethyl branches following the work of Usami and Takayama (1984). The absorption at ~890 cm^{-1} has been attributed to branches longer than ethyl (McRae and Maddams, 1976; Usami and Takayama, 1984). Blitz and McFaddin demonstrated that this band shifted to 893 cm^{-1} in the case of butyl branches and to 888 cm-1 in the case of hexyl branches. The methyl deformation band at ~1378 cm^{-1} also shifted positions according to the length of the branch. For ethyl branches, for instance, the band was located at 1378-79 cm^{-1}. For butyl and hexyl branches the band moved towards 1377 cm^{-1}.

The bands mentioned in the above paragraph have been proven to be useful in the determination of the comonomer present in LLDPE resins or polyethylene blends (Prasand and Mowery, 1997; Gartner and Sierra, 1998; Sierra et al, 2000). IR spectroscopy has some limitations in that the measurements are semi-quantitative. The use of calibration curves is often required. However, the short testing times and the ease of sample preparation make the use of FTIR suitable as a quality assurance tool in the LLDPE industry (Pandey, 1995).

2.5.2 Chain conformation and crystalline states

A number of investigations about the microstructure of polyethylene using infrared spectroscopy have been published in the literature. The doublet 720-730 cm^{-1} has been assigned to degree of crystallinity because it disappears in the molten state (Stein and Sutherland, 1953). However, quantitative determination of crystallinity using these bands is extremely difficult as their high intensities require that very thin films be used. As an alternative, Okada and Mandelkern (1967) studied the crystallinity of different PEs using the band attributed to crystalline regions located at 1894 cm^{-1} and the bands attributed to amorphous regions at 1303, 1352 and 1368 cm^{-1}. Although good correlation between IR and specific volume crystallinities was observed, the authors suggested more research because the nature of the amorphous bands was not well understood. Painter and collaborators (1977a) studied polyethylene single crystals using subtraction FTIR. They analyzed the "amorphous" bands 1303, 1352 and 1368 cm^{-1} before and after thermal treatments. Different assignments were made based on theoretical calculations of *trans-gauche* interactions. A new band in the spectra of single crystals, located at 1346 cm^{-1} and very sensitive to conformation, was reported. The doublet 720-730 cm^{-1} was further examined and a band characteristic of monoclinic arrangement of chains (716 cm^{-1}) was found in the spectra of single crystals (Painter et al., 1977b). It has also been reported that the IR absorption of the bands related to crystalline and amorphous regions varied linearly with degree of crystallinity (Rueda et al., 1978)

Koenig and Witenhafer (1966) studied the chain folding of solution crystallized and bulk crystallized linear polyethylenes. They mention that the absorption of the bands located at ~1350 and 1304 cm^{-1} is partly due to the folds and partly due to the disordered material in the polymer. After an imposed thermal treatment (annealing) they found that the absorbance of these bands decreased but the ratio between them remained the same. They concluded that after annealing the fold content drops while no significant change in the fold structure occurs. Similar results were obtained for both solution and bulk crystallized linear PEs.

Recently, Tashiro and co-workers (1996; 1998) have studied the transitions of polyethylene using time-resolved FTIR. In their studies the orthorhombic-to-hexagonal phase was investigated using the IR bands in the region 1300 to 1370 cm^{-1}, the bands in the region 700 to 730 cm^{-1} and the band located at 1466 cm^{-1} which has been related to the hexagonal phase. All these bands involve different *trans-gauche* configurations that vary with temperature changes.

2.6 Summary

The qualitative agreement between experimental data and the predictions of Newtonian sintering models indicates that the viscous flow mechanism is dominant in polymer sintering. The quantitative discrepancies between the experimental data and the trends predicted by the models, however, also indicate that other forces need to be taken into consideration. It has been shown that viscosity and elasticity play an important role in polymer sintering. Temperature, particle size and the presence of additives (e. g. talc) also affect the sintering rate. On the other hand, the experimental work carried out on UHMWPE suggests that other material properties may contribute to the controlling mechanism of sintering.

The properties of LLDPE are strongly dependent on molecular structure. Viscosity and elasticity of polymer melts are affected by the MW, MWD and the presence of LCB. The amount of SCB, on the other hand, has little influence on those rheological properties in the linear viscoelastic region. However, there is evidence showing that the melt strength is influenced by the type and distribution of the branches.

LLDPE, being a random copolymer, presents inter- and/or intra-molecular heterogeneity. The catalyst used in the polymerization process is the main factor in determining such heterogeneity. The semicrystalline structure of LLDPE varies according to the amount, distribution and length of SCB (comonomer content). As a

result, thermal properties such as melting and crystallization temperatures are also a function of the macromolecular architecture. Moreover, other factors such as the presence of additives or thermal history of the sample modify the thermal behavior of LLDPEs.

Material Characterization

Chapter 3

3.1 Materials

Twenty-six linear low-density polyethylene resins were used in this study. The resins were named in sequential order using the letters "PE" followed by a number and the letters "B", "H" or "O" that denote the type of comonomer and stand for butene, hexene and octene respectively. They were then grouped into three different categories according to weight average molecular weight (M_w) in order to facilitate the presentation of their properties. Material properties such as molar mass and density are presented in Table 3.1.

The resins with M_w ranging from 53,000 to 67,000 g/gmol are included in category A. It can be seen in Table 3.1 that, in general, the resins have narrow molecular weight distributions. However, some differences in density are observed since different types and amounts of comonomers were used during the copolymerization process. The M_w of the LLDPEs included in category B range from 68,000 to 72,200 g/gmol. Apart from PE-18-H, all the resins show very narrow MWD. Resins with a M_w greater than 76,000 g/gmol are included in category C. PE-26-O is a blend of PE-25-O and PE-27-O (50% w/w). All the resins in this category have a very narrow MWD with the exception of PE-21-H.

Table 3.1 Material properties of LLDPE resins

Resin ID	$M_w \times 10^{-3}$	$(M_w/M_n)^a$	Density[a] (g/cm^3)	Source
Category A				
PE-1-O	53.7	2.47	0.9348	NOVA Chemicals
PE-2-O	58.6	2.09	0.9334	NOVA Chemicals
PE-3-O	61.3	2.93	0.9358	NOVA Chemicals
PE-4-H	61.7	2.09	0.9346	Borealis
PE-5-H	62.1	3.91	0.9350	NOVA Chemicals
PE-6-H	62.8	2.12	0.9391	Borealis
PE-7-O	64.9	2.07	0.9344	NOVA Chemicals
PE-8-B	65.5	3.08	0.9350	NOVA Chemicals
PE-9-O	66.1	3.00	0.9190	NOVA Chemicals
PE-10-H	66.9	3.47	0.9350	NOVA Chemicals
Category B				
PE-11-O	68.5	1.97	0.9383	NOVA Chemicals
PE-12-O	68.6	1.97	0.9376	NOVA Chemicals
PE-13-O	68.9	1.92	0.9378	NOVA Chemicals
PE-14-O	68.9	2.05	0.9388	NOVA Chemicals
PE-15-O	68.9	2.07	0.9371	NOVA Chemicals
PE-16-O	69.2	1.96	0.9378	NOVA Chemicals
PE-17-O	71.7	2.05	0.9402	NOVA Chemicals
PE-18-H	72.2	3.03	0.9380	Exxon
Category C				
PE-19-H	76.1	2.00	0.9402	Borealis
PE-20-O	76.6	1.90	0.9446	NOVA Chemicals
PE-21-H	76.8	3.96	0.9380	NOVA Chemicals
PE-22-O	79.5	2.05	0.9445	NOVA Chemicals
PE-23-O	80.3	2.19	0.9450	NOVA Chemicals
PE-24-O	80.4	1.97	0.9461	NOVA Chemicals
PE-25-O	92.2	2.28	0.9203	NOVA Chemicals
*PE-26-O	n.a	n.a	n.a.	n. a.
PE-27-O	100.5	2.00	0.9458	NOVA Chemicals

[a]Provided by supplier

* Blend of PE-25-O and PE-27-O (50% w/w)

3.2 Rheological characterization

Polymers exhibit viscoelastic behavior, i. e. their response to an applied stress or deformation is located between the responses of fully elastic solids and viscous liquids. If the deformation is sufficiently small that the polymeric molecules are disturbed from their equilibrium configuration and entanglements state to a negligible extent then linear viscoelasticity is observed. Linear viscoelastic responses are easier to measure than the non-linear phenomena and are frequently used as an analytical tool because they are molecular-structure dependent.

In the present work, both the zero-shear viscosity and the elasticity of the resins are of interest. These two properties are recognized as controlling factors in the sintering process. Moreover, the rheological analysis is also performed with the aim of gaining information about the molecular structure of the resins. Dynamic mechanical testing is frequently used to measure the viscoelastic behavior of polymeric materials. Small amplitude oscillatory shear, in particular, has been found to be very useful in the study of these materials. Basically, the shear strain is varied sinusoidally. The stress also varies periodically with frequency but lags behind the strain in phase over δ radians. The stress response can be separated into its elastic and viscous contributions. For a perfectly elastic body, the stress response is in phase with the imposed strain (phase angle equal to zero). Conversely, the phase angle approaches $\pi/2$ for purely viscous fluids. The elastic and viscous contributions in oscillatory measurements are usually referred to as the elastic or storage modulus (G') and the loss modulus (G'') respectively and their use is widely accepted.

The resins were subjected to oscillatory tests using a HAAKE RS150 rotational rheometer. A parallel-plate sensor with a plate diameter of 20 mm and a shearing gap of either 1 or 1.5 mm was used. The samples were prepared by hot pressing approximately 5 g of polymer between two teflon® sheets (or aluminum foil) for 2.5 minutes at 204.4 °C (400 °F). The resulting thin sheet was then immediately quenched in iced water. A cylindrical sample was then cut from the sheet using a 20

mm cutter. Because of the nature of oscillatory measurements, a stress sweep was run at different frequencies in order to determine the linear viscoelasticy region. Values of stress were selected from these measurements and frequency sweep experiments were then performed. In this work, the average of two measurements with less than 10% difference is reported.

3.2.1 Category A

The results of oscillatory measurements conducted on the resins in this category are summarized in Table 3.2. The values of zero-shear viscosity reported in this table were obtained by fitting the Cross model to experimental data. In general, an increase in the shear viscosity with the M_w can be observed. The crossover frequency (ω_s) of the resins is also presented in Table 3.2. At this frequency, the values of elastic and loss moduli are equivalent, i. e. G'=G". The inverse of the ω_s can be considered as a characteristic relaxation time of the melt (Muñoz-Escalona et al., 1999). At frequencies $\omega > \omega_s$ the material behaves in an elastic manner and at frequencies $\omega < \omega_s$ the material acts like a viscous liquid. In other words, as ω_s is shifted to lower frequencies or as the characteristic relaxation time increases, the more elastically the material behaves.

Besides the single values of some rheological properties, the graphs of the measurements carried out over a range of frequencies provide useful information about the molecular structure. It has been reported that the amount of comonomer has little influence on the rheological properties (Wood-Adams et al., 2000) but the type of comonomer has been found to affect properties such as the melt strength (Goyal, 1995). Thus, the rheological curves are grouped and presented according to the type of comonomer whenever possible.

The viscosity curves of the hexene LLDPEs in this category are presented in Figure 3.1. Clearly, two different trends can be identified. A well-defined Newtonian plateau can be distinguished for PE-4-H and PE-6-H. This plateau has been related

Table 3.2 Rheological properties of resins in Category A

Resin ID	Zero-Shear Viscosity (Pa s)[b]		Crossover ω (rad/s) at 170°C	Characteristic relaxation time (ms)[c]
	170°C	190°C		
PE-1-O	2074	1465	460	2.17
PE-2-O	2188	1239	448	2.22
PE-3-O	2236	1599	>500	< 2.0
PE-4-H	1803	1287	>500	< 2.0
PE-5-H	2273	1573	460	2.17
PE-6-H	1911	1237	>500	< 2.0
PE-7-O	3000	1401	446	2.23
PE-8-B	2142	1664	>500	< 2.0
PE-9-O	3265	2905	297.1	3.36
PE-10-H	2724	2067	>500	< 2.0

[b]Predicted by the Cross Model (Appendix A)

[c]Calculated as the inverse of crossover frequency

to polymers with narrow MWD and homogeneous composition (Wood-Adams et al., 2000). For PE-5-H and PE-10-H, however, the shear-thinning behavior starts at low frequencies being more pronounced for the latter. This observation is consistent with the fact that these resins have a broader MWD as observed in Table 3.1.

Figure 3.2 shows the viscosity curves for the octene LLDPEs. All the resins show the onset of shear thinning at low frequencies and a Newtonian plateau is not well defined. Nevertheless, two trends are observed. PE-7-O and PE-9-O show higher values of viscosity than the other octene resins, in particular at low shear rates. Maybe this is due to their slightly higher value of M_w. The effect of MWD, on the other hand, is not evident since all the resins exhibit a relatively narrow distribution. The shear thinning behavior may indicate the presence of other types of heterogeneity, which could be related to the distribution of short chain branches (Shan, 2000).

Only one resin is a butene/ethylene copolymer (PE-8-B). Its rheological behavior will therefore be compared to that of octene and hexene copolymers which exhibit characteristic viscosity trends (Figure 3.3). It can be observed that the viscosity of PE-8-B is lower than the viscosity of the other resins over almost the whole frequency range in spite of having comparable values of M_w and MWD. Furthermore, it shows a pronounced shear-thinning behavior maybe resulting from a heterogeneous composition (broad MWD and branching distribution).

The variation of rheological properties with temperature is examined since some sintering experiments are to be conducted under non-isothermal conditions. Oscillatory measurements were carried out at three different temperatures: 150, 170 and 190 °C. The shape of the viscosity curves with respect to frequency did not vary significantly. However, the temperature dependence of zero-shear viscosity varied from one resin to another. It can be seen in Figure 3.4 that PE-4-H and PE-6-H are less sensitive to temperature than the other hexene resins. PE-8-B shows strong

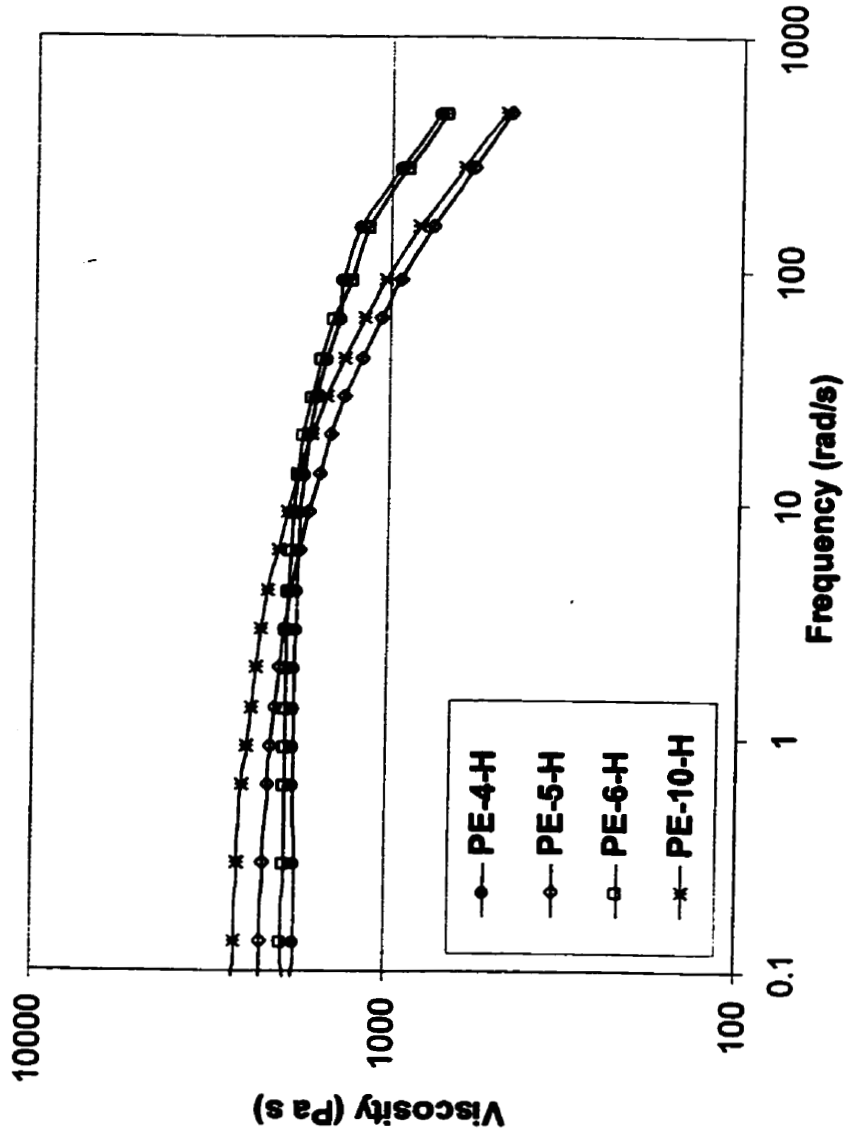

Figure 3.1 Complex viscosity for the hexene resins in Category A (170°C)

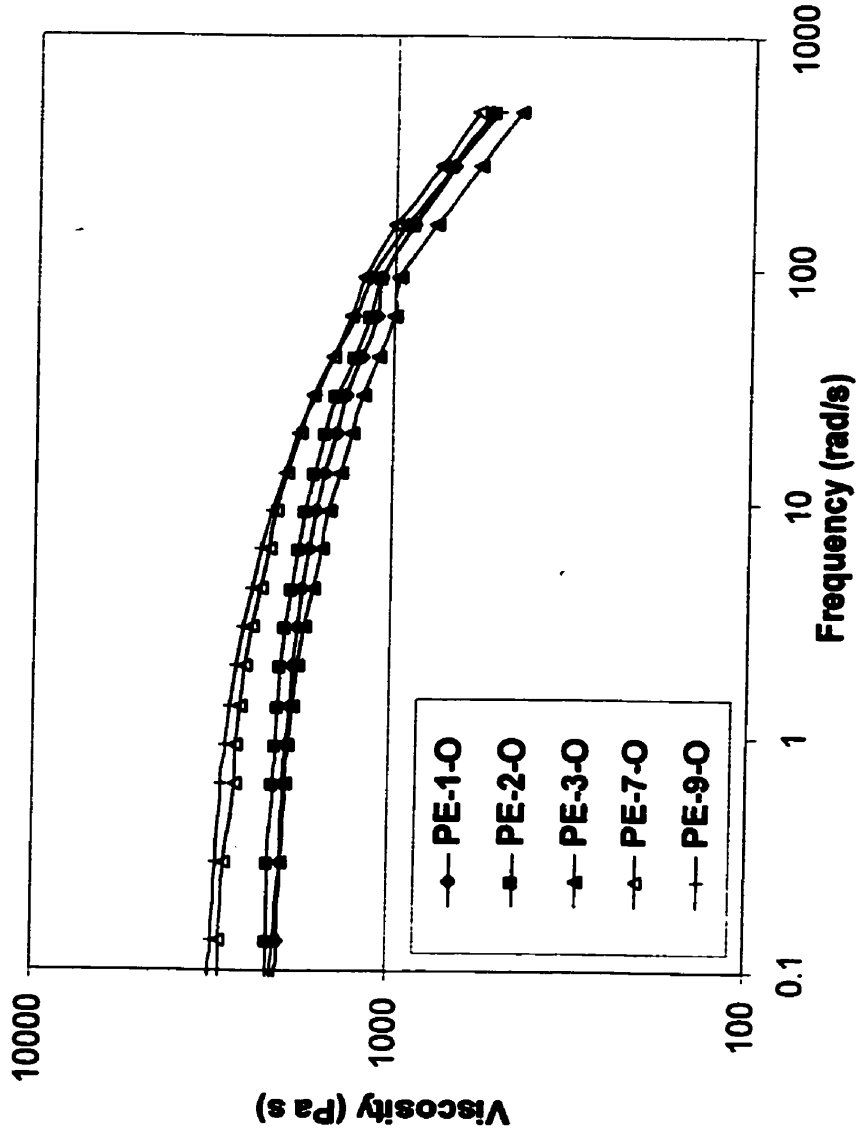

Figure 3.2 Complex viscosity for the octene resins in Category A (170°C)

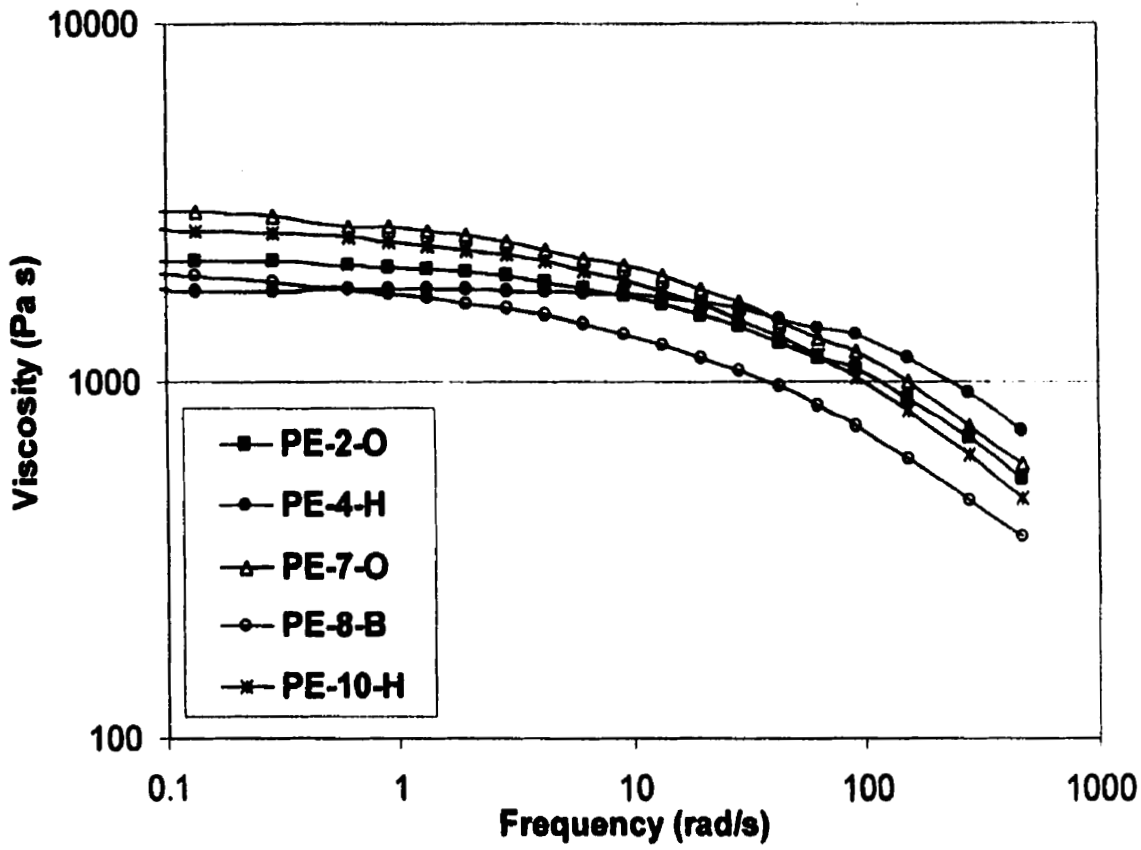

Figure 3.3 Comparison of viscosity curves between resins in Category A (170°C)

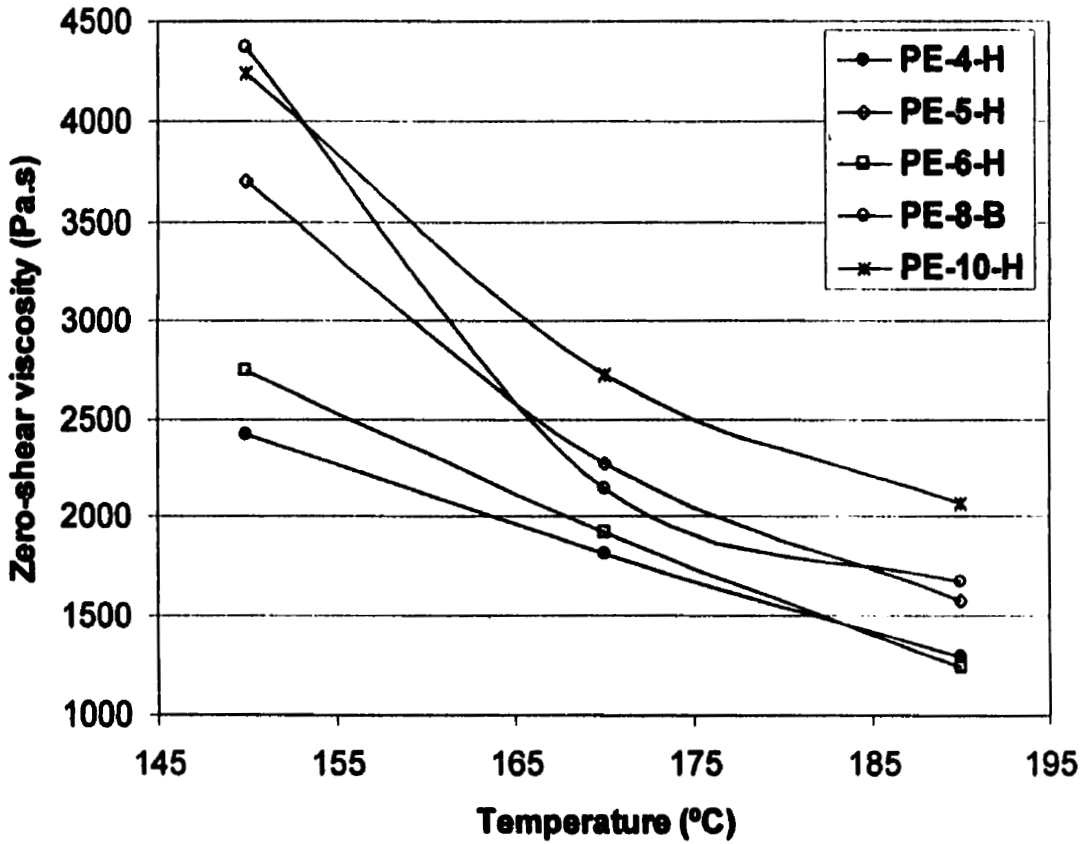

Figure 3.4 Viscosity temperature dependence for hexene and butene resins in Category A

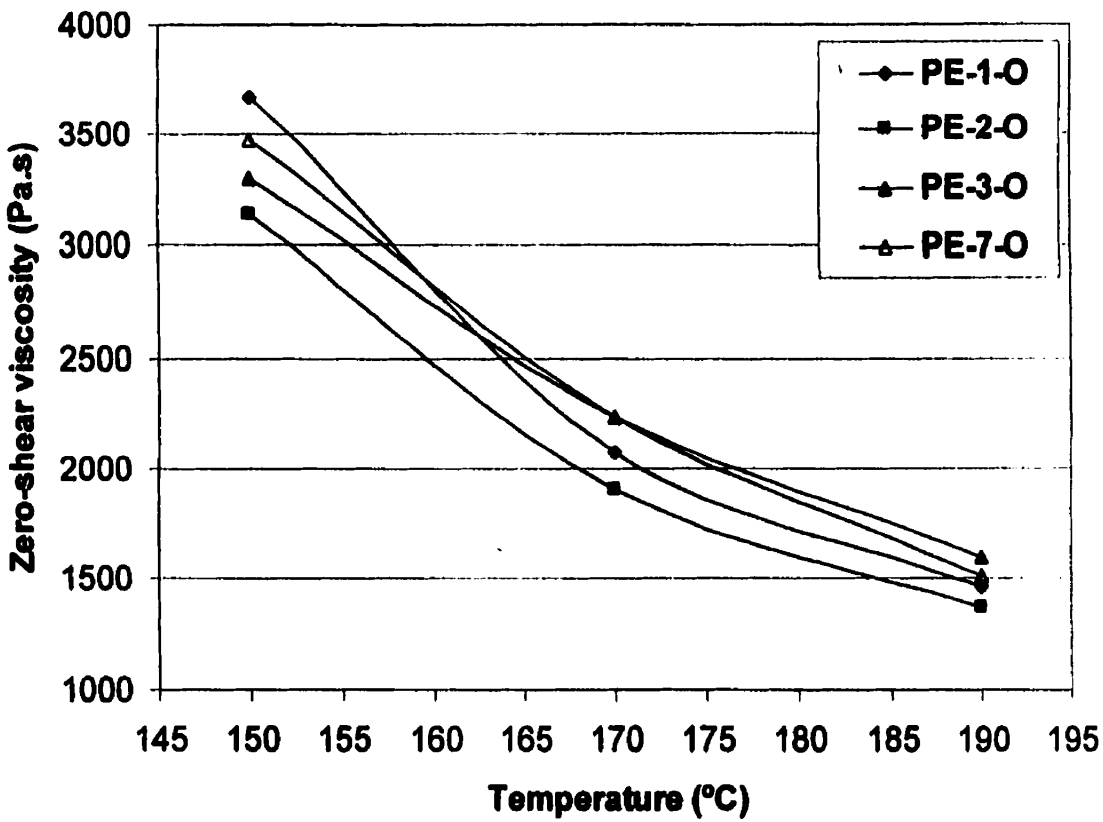

Figure 3.5 Viscosity temperature dependence for octene resins in Category A

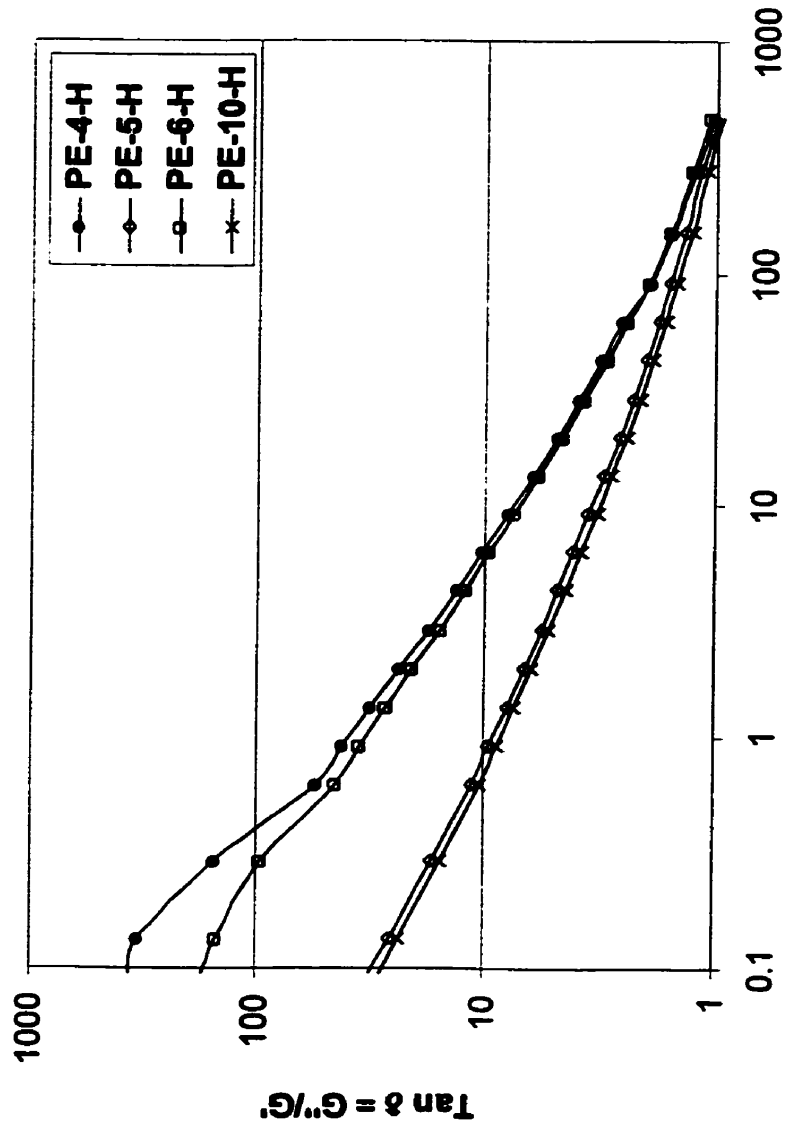

Figure 3.6 Tan δ curves for the hexene resins in Category A (170°C)

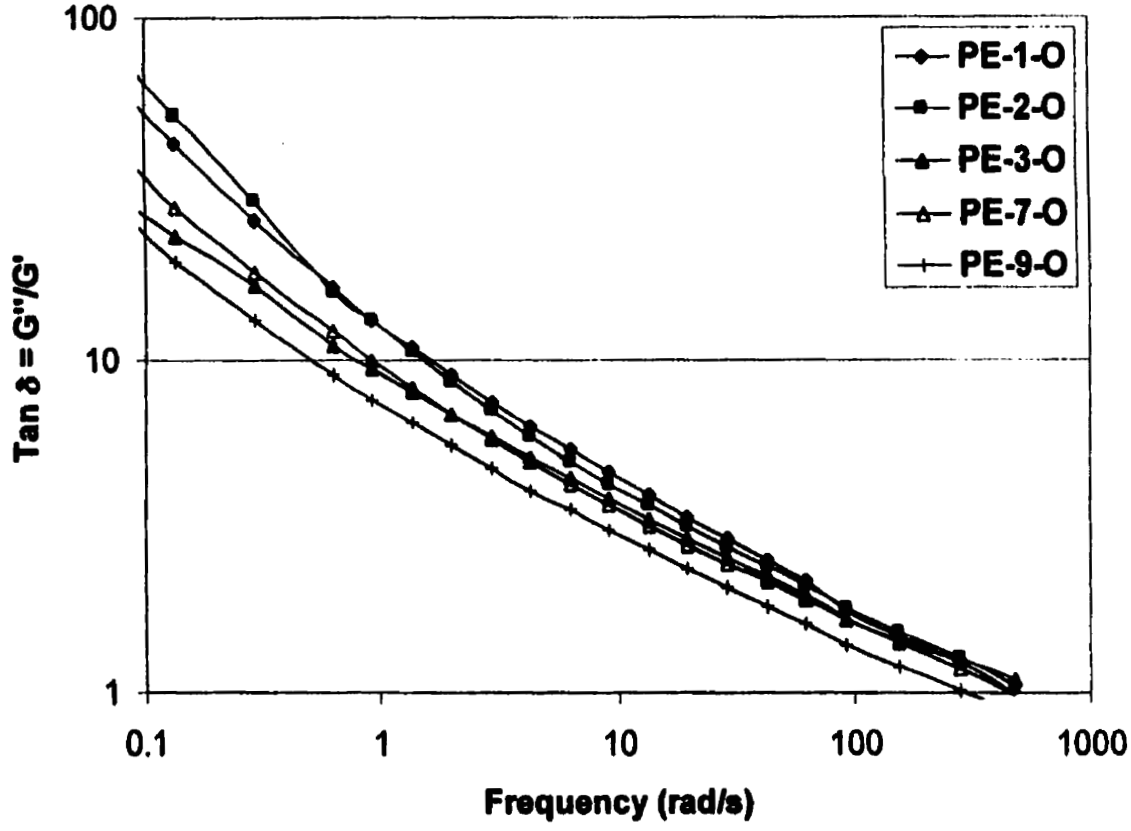

Figure 3.7 Tan δ curves for the octene resins in Category A (170°C)

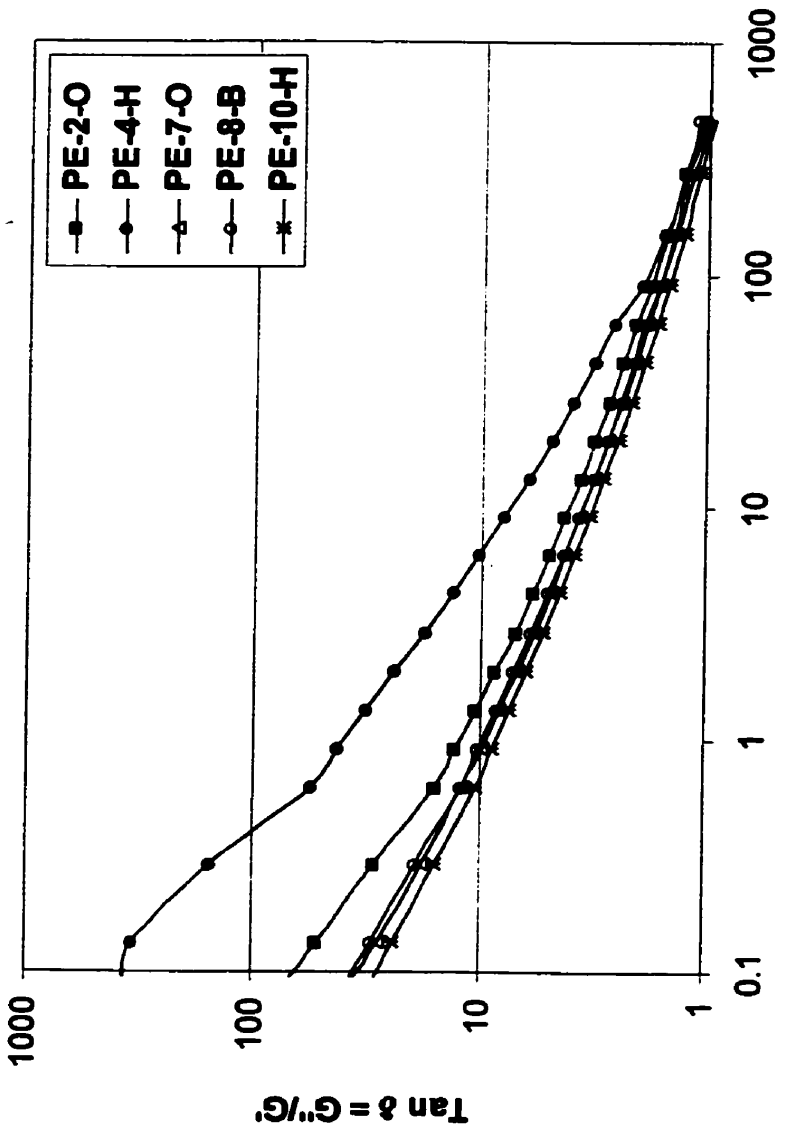

Figure 3.8 Comparison of tan δ curves between resins in Category A (170°C)

temperature sensitivity. The curves in Figure 3.5 indicate that PE-1-O is more sensitive to temperature than the other octene resins.

The values of *tan* δ for the hexene resins are presented in Figure 3.6. High values of *tan* δ indicate that the elastic contribution to the complex modulus is relatively small. It is possible to observe that PE-4-H and PE-6-H are less elastic than PE-5-H and PE-10-H over the range of frequencies tested. These differences can be attributed to the effect of M_w and MWD on elasticity (Kazatchkov et al., 2000; Wood-Adams et al., 2000). Figure 3.7 shows the *tan* δ curves for the octene LLDPEs. It can be seen that the elastic contribution increases with M_w. Accordingly, PE-1-O and PE-2-O are less elastic than the other octene resins. PE-9-O has consistently lower values of *tan* δ indicating a more elastic behavior. A comparison between resins with different comonomer is shown in Figure 3.6. PE-8-B exhibits values of *tan* δ comparable to those of PE-7-O and PE-10-H but lower values than PE-2-O and PE-4-H.

3.2.2 Category B

Results from rheological tests for the resins in category B are presented in Table 3.3. There are only minor variations in the zero-shear viscosity, in agreement with the variation of M_w. Only PE-17-O seems to have a higher value of viscosity. The viscosity and *tan* δ curves are shown in Figures 3.9 and 3.10 respectively. Although the trends are very similar for all the resins, it can be seen that the rheological behaviors of PE-17-O and PE-18-H are slightly different. PE-18-H shows important shear thinning maybe due to the broadness of its MWD. PE-17-O, on the other hand, exhibits higher values of viscosity than the other resins over the range of frequencies tested. It must be pointed out that PE-14-O, PE-16-O and PE-18-H are considered to be more elastic based on their values of crossover frequency and characteristic relaxation times.

Table 3.3 Rheological properties of resins in Category B

Resin ID	Zero-Shear Viscosity (Pa s)[b]		Crossover ω (rad/s) at 170°C	Characteristic relaxation time (ms)[c]
	170°C	190°C		
PE-11-O	3987	2739	380	2.63
PE-12-O	4202	2973	363	2.75
PE-13-O	4176	2924	380	2.63
PE-14-O	3754	2730	275	3.64
PE-15-O	4024	2686	380	2.63
PE-16-O	4725	2531	287	3.48
PE-17-O	5603	3752	400	2.50
PE-18-H	4551	3770	238.7	4.18

[b]Predicted by the Cross Model (Appendix A)

[c]Calculated as the inverse of crossover frequency

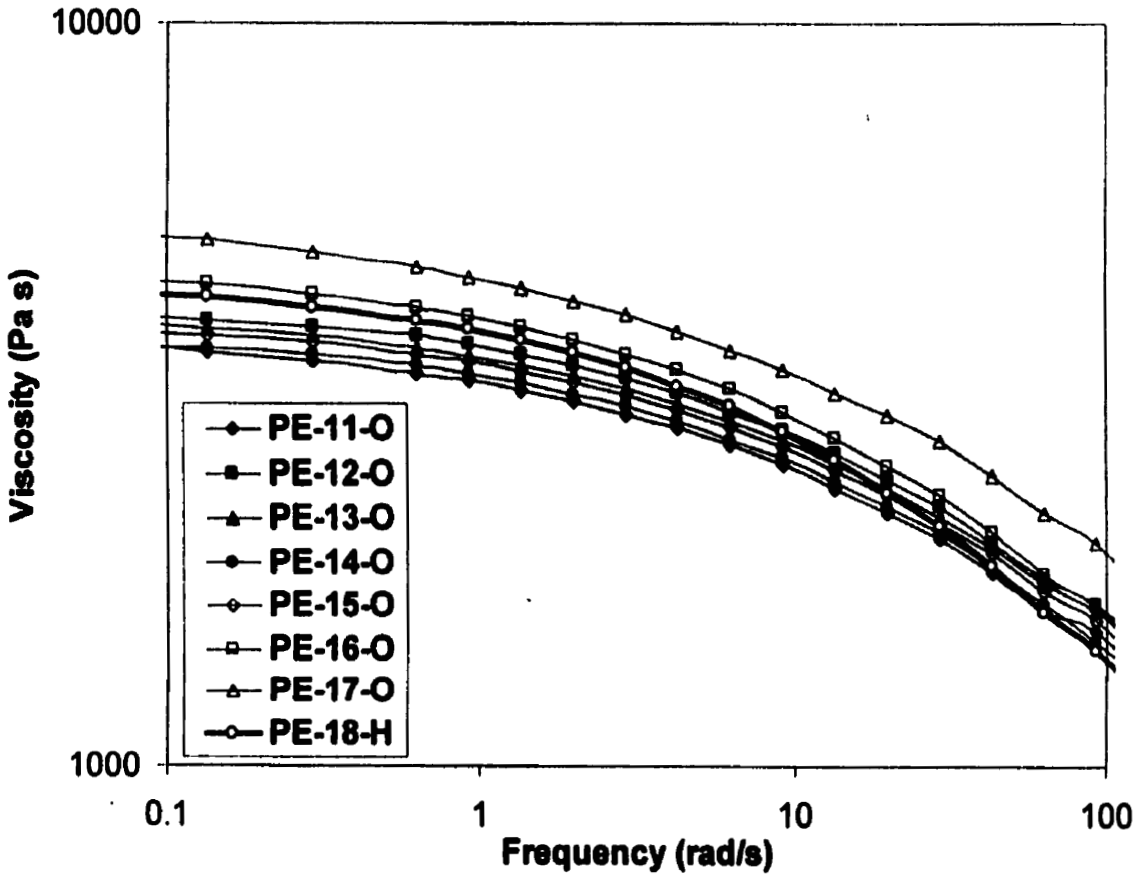

Figure 3.9 Complex viscosity for all the resins in Category B (170°C)

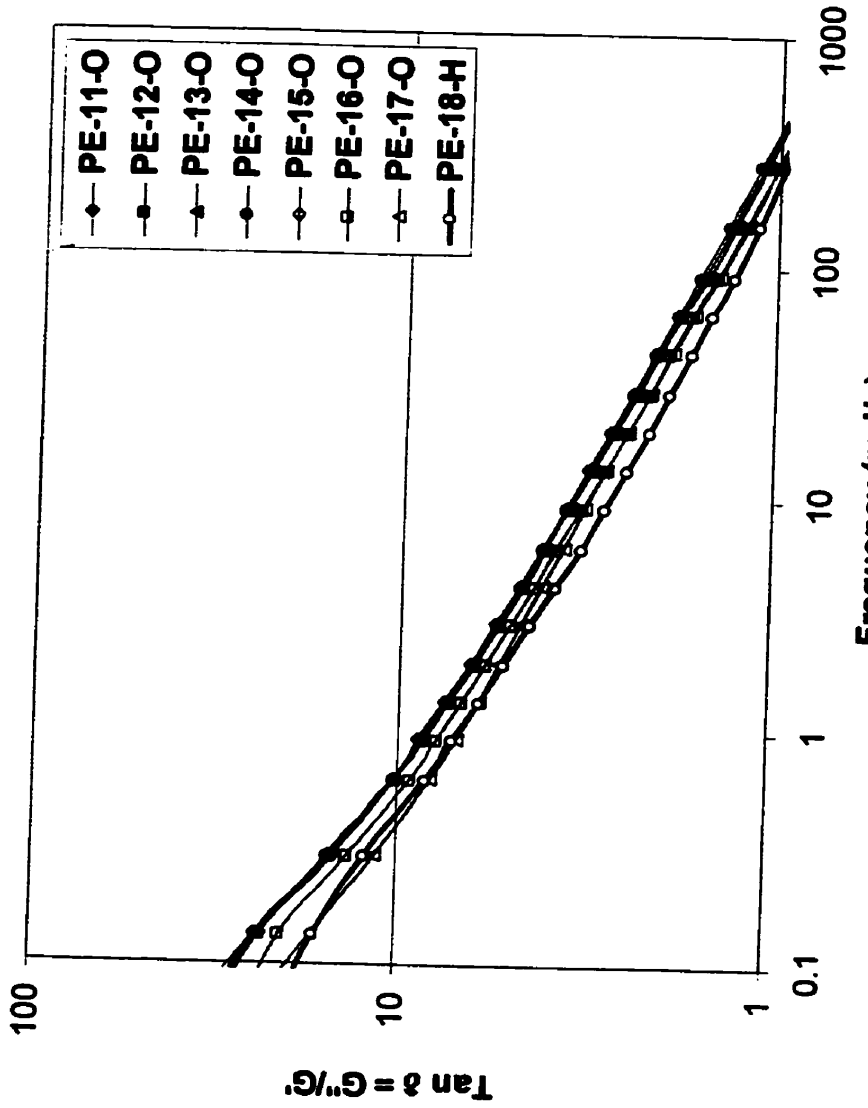

Figure 3.10 Tan δ curves for all the resins in Category B (170°C)

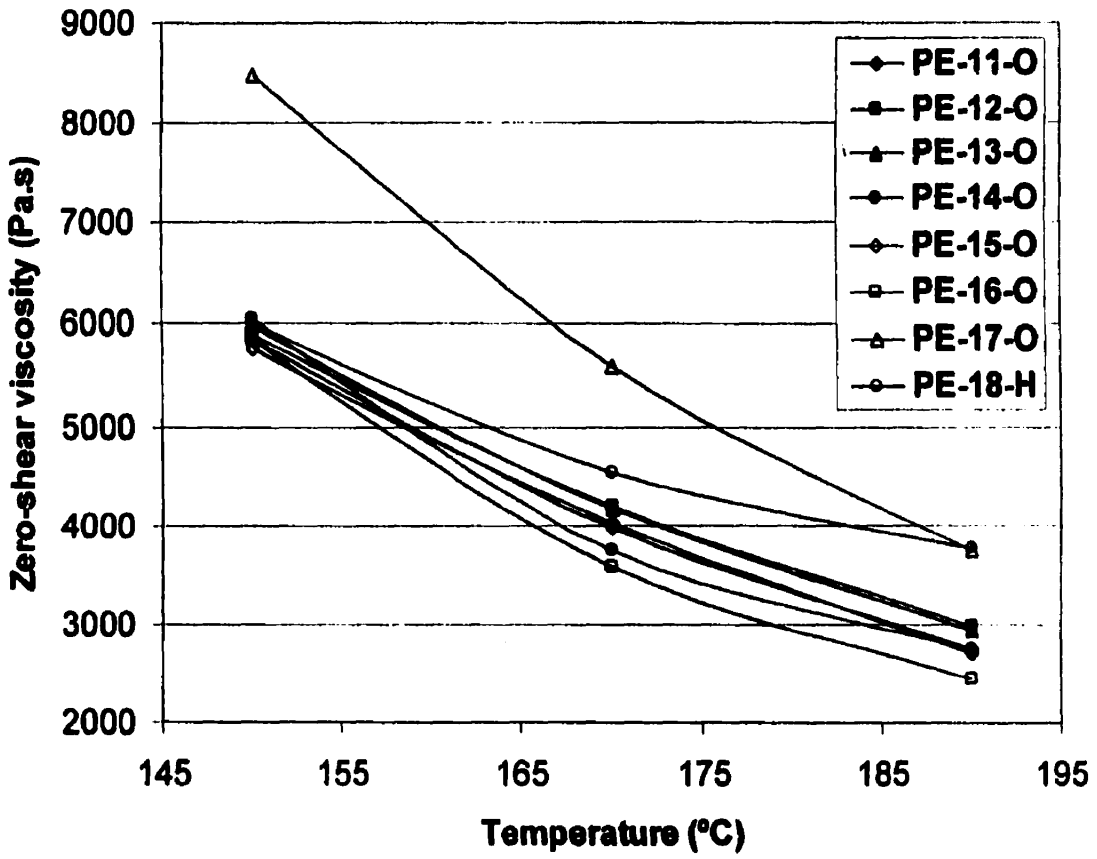

Figure 3.11 Viscosity temperature dependence for all the resins in Category B

Figure 3.11 presents the viscosity-temperature dependence for all the resins in this category. Interesting trends can be observed. At low temperatures, PE-17-O shows an important increase of zero-shear viscosity. PE-18-H is not very sensitive to temperature. Even thought the differences between the other resins are small, some trends can be distinguished. While the pair PE-11-O and PE-15-O and the pair PE-12-O and PE-13-O show the same viscosity- temperature dependence, PE-14-O seems to be slightly more sensitive to temperature.

3.2.3 Category C

A summary of the rheological properties is presented in Table 3.4. Most of the resins exhibit high values of zero shear viscosity with the exception of PE-19-H and PE-21-H. PE-21-H has a broader MWD which may account for its low viscosity. Resin PE-19-H, on the other hand, has a very narrow MWD. Furthermore, its M_w appears to be comparable to those of PE-20-O and yet, the values of zero-shear viscosity of PE-19-H and PE-20-O are not comparable at all. It can be speculated that since the molecular weight determination relies on indirect measurements the values of M_w reported for PE-19-H and PE-21-H could be only apparent values. PE-25-O, PE-26-O and PE-27-O have higher viscosity than the other resins that may be attributed to their higher M_w.

Figures 3.12 and 3.13 show the viscosity and *tan* δ curves for the resins in category C, respectively. Three different trends can be identified. The first one includes PE-19-H and PE-21-H. The resins with the highest M_w (PE-25-O, PE-26-O and PE-27-O) fall into the second trend. All the others form the trend located between the first and second trends. PE-19-H and PE-21-H attain similar values of viscosity at very low frequencies but their curves are different. While PE-19-H shows a well defined Newtonian plateau, the onset of shear thinning starts at low frequencies for PE-21-H. As mentioned before, the Newtonian plateau is characteristic of homogeneous, narrowly distributed polymers.

Table 3.4 Rheological properties of resins in Category C

Resin ID	Zero-Shear Viscosity (Pa s)[b]		Crossover ω (rad/s) at 170°C	Characteristic relaxation time (ms)[c]
	170°C	190°C		
PE-19-H	3959	2683	250	4.0
PE-20-O	9264	4939	197	5.06
PE-21-H	3969	2674	290	3.45
PE-22-O	10460	5208	184	5.43
PE-23-O	11750	5640	171	5.82
PE-24-O	10555	5485	175	5.68
PE-25-O	19265	9911	71.75	13.93
PE-26-O	16850	n.a.	98.75	10.12
PE-27-O	15020	8216	109.8	9.10

[b]Predicted by the Cross Model (Appendix A)

[c]Calculated as the inverse of crossover frequency

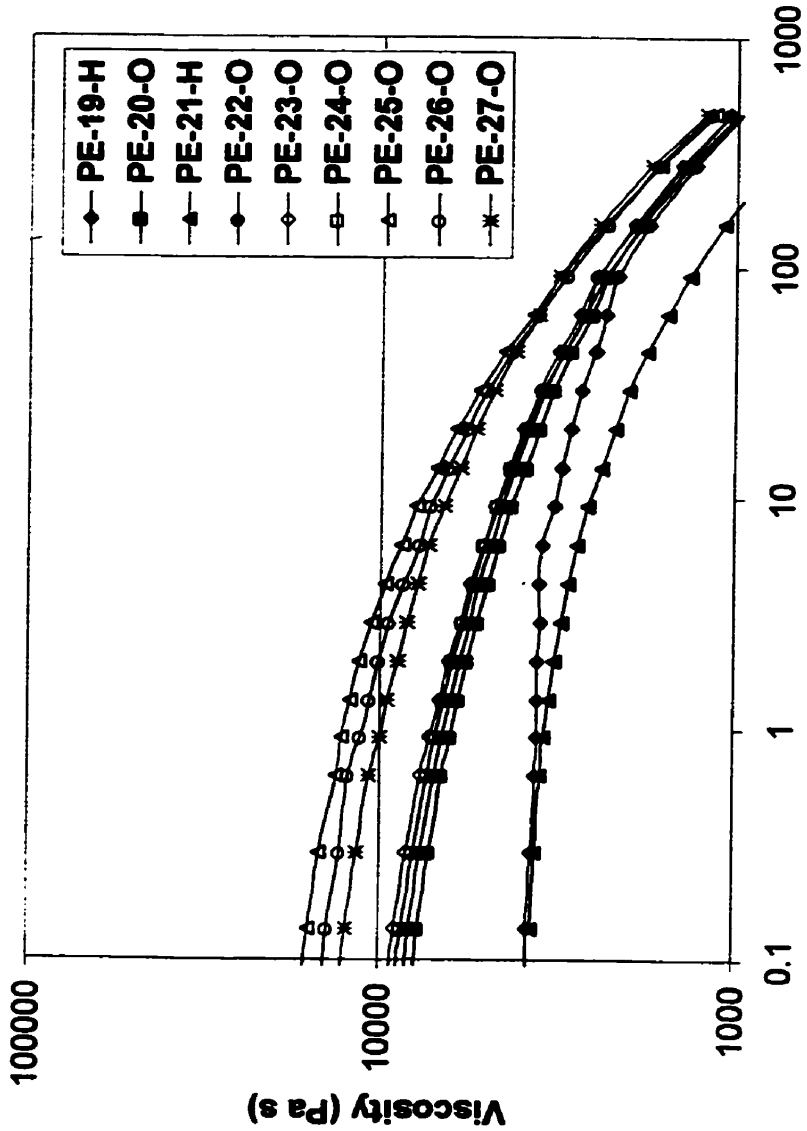

Figure 3.12 Complex viscosity for all the resins in Category C (170°C)

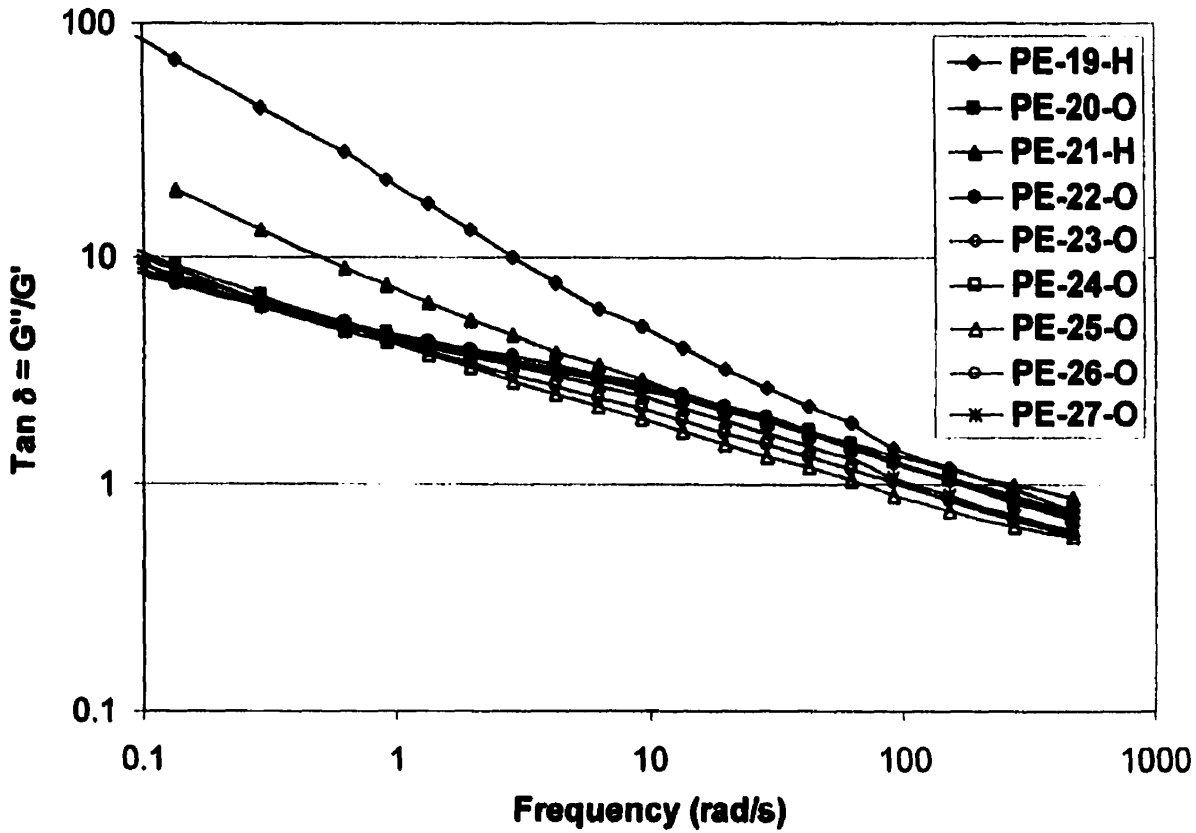

Figure 3.13 Tan δ curves for all the resins in Category C (170°C)

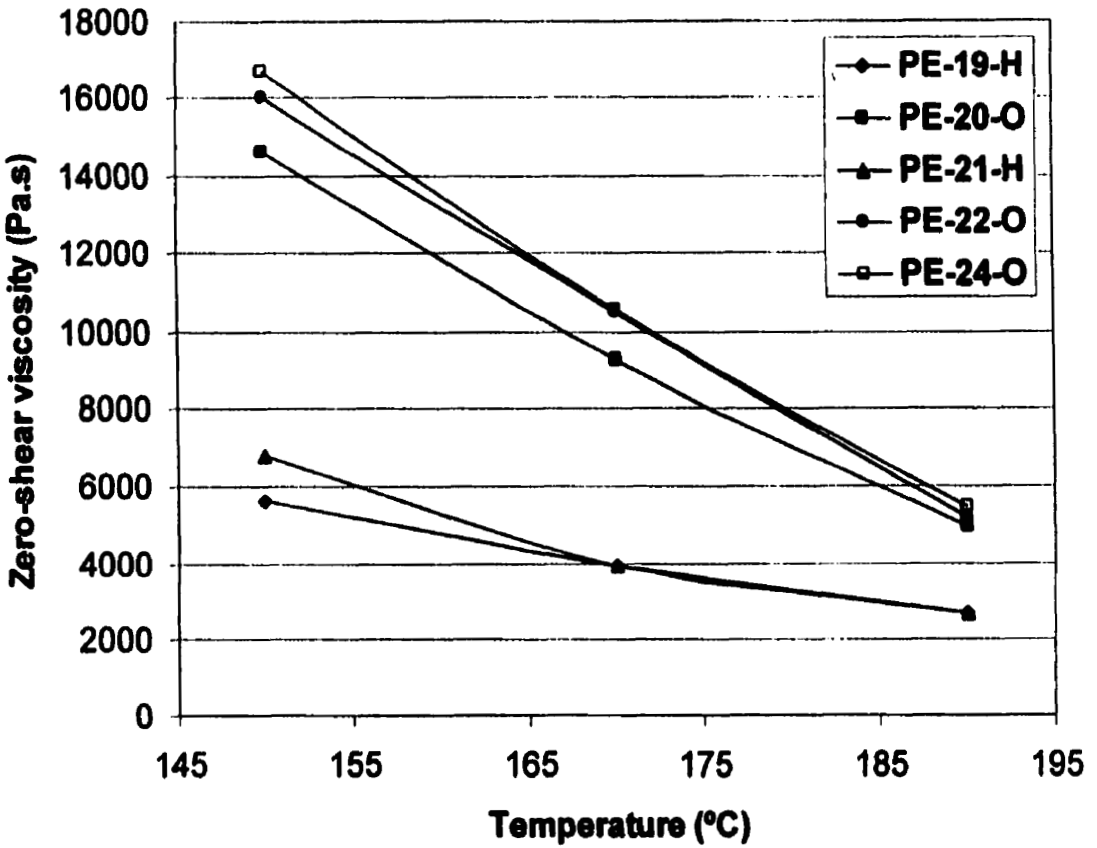

Figure 3.14 Viscosity temperature dependence for some resins in Category C

The viscosity-temperature dependence for some polymers is presented in Figure 3.14. It can be seen that PE-19-H and PE-21-H have a lower sensitivity to temperature than PE-20-O, PE-22-O and PE-24-O. PE-20-O has a higher viscosity than PE-19-H and PE-21-H but lower viscosity than PE-22-O and PE-24-O over the range of temperatures tested.

3.3 Morphology and molecular characteristics

In general, solid polymers can occur in the amorphous and the crystalline state. In the amorphous state the macromolecular chains are disordered and adopt conformations corresponding to statistical coils. The crystalline state, on the other hand, is characterized by a long-range three-dimensional order where the macromolecular chains adopt fixed conformations. The capability to crystallize depends on the structure and regularity of the chains and on the interactions between them (Riande et al., 2000). The attained level of crystallinity is usually less than 100% which means that crystalline and amorphous phases coexist. The crystallinity of a sample also depends on the conditions under which the crystallization took place and the thermal treatments applied to the sample after crystallization. Certain properties, particularly with regard to the mechanical strength and resistance to solvents, are conferred by crystallinity.

In the melting process, the order achieved during crystallization is destroyed and the chain mobility is increased. Unlike materials with low molecular weight, a single melting temperature cannot be defined. The melting process usually takes place over a range of temperatures and depends upon the rate at which the specimen is heated. Moreover, the sample's thermal history affects the melting behavior of polymeric materials. Nevertheless, a single value of melting temperature (T_m) is frequently reported in the literature. This value usually refers to the largest peak found in endotherms determined experimentally. It has been reported that the melting temperature increases with molecular weight (Hosoda, 1988). However, other material properties influence the melting temperature and thermal transitions in

a more dramatic way. For instance, the presence of a broad MWD and side branches broadens the melting range and shifts the transitions to low temperature region. This has been explained in terms of the presence of crystallites with different sizes and stabilities due to chain heterogeneity (Peeters et al., 2000; Vanden Eynde et al., 2000a).

3.3.1 Thermal analysis

Differential scanning calorimetry (DSC) was used to study the thermal transitions of all the resins used in this work. In DSC, the amount of energy withdrawn or supplied from the sample to maintain a zero differential between the sample and the reference is recorded. A METLER DSC12E calorimeter was used. This calorimeter was calibrated with Indium. The position and the areas of the endothermic peaks were determined using the software that accompanies the apparatus. In order to plot and compare different melting curves, the endotherms (originally saved in the internal units) were transformed to heat per gram following the procedure presented in APPENDIX B.

a) Melting temperature and heat of fusion

About 8 mg of powder were weighed and placed into aluminum crucibles which were loaded into the calorimeter. First, a heating/cooling run took place to ensure a homogeneous thermal history between the resins (50-150-50°C at 10°C/min). The samples were then heated from 60 to 150 °C at 10 °C/min. The measurements were repeated at least two times to ensure good reproducibility of results. The largest peak in each endotherm was then reported as melting temperature (T_m). A value of degree of crystallinity was calculated by dividing the experimental value of heat of fusion calculated as the area under the endothermic curve by the heat of fusion of an ideal completely crystalline PE sample. This value was taken as 289 J/g (Bensason et al., 1996).

b) Response to thermal treatment

The behavior of the resins after an imposed thermal treatment was studied in order to gain more information about the molecular structure, particularly the amount of branches and their distribution along the chains. After annealing, polymeric chains with different branching distributions reorganize and variations in the position of the melting peaks and in heat of fusion can be measured by DSC (Starck, 1996; Peeters et al, 2000; Zhang et al, 2001).

Approximately 5 mg of powder were weighed and placed into aluminum crucibles. The loaded crucibles were put into glass Petri dishes. As a precaution, the air in the dishes was purged with nitrogen to minimize the chances of material degradation during the thermal treatment. A convection oven was then used to anneal the samples. The oven temperature was set to temperatures 10°C above the resins' melting point. The samples were kept under these conditions for 20 hours. The temperature was then decreased by 10°C and samples were annealed for three hours. This procedure was repeated twice. Finally, the endotherms of the annealed samples were measured using the DSC apparatus. Scans were run from 60 to 150°C at 10°C/min.

3.3.2 Infrared spectroscopy

For comparative purposes, the resins were studied by infrared spectroscopy. This technique provided information related to the comonomer type and content and to some extent, degree of crystallinity.

Thin films (~300 microns) were prepared by hot pressing the different resins (as received) between two teflon® sheets. For all the resins, 2.5 g of powder were pressed using a force of 5000 lb. The press temperature was set to 204 °C (400 °F). After 2.5 minutes, the films were immediately quenched in iced water. The preparation conditions were kept as similar as possible to minimize the variation in

the film thickness. A Nexus 470 FTIR apparatus with fresh nitrogen supply from Nicolet Instruments was used. A series of 16 scans with resolution of 2 cm^{-1} were run. The collected spectra were analyzed using the absorbency units instead of transmittance because the spectra plotted in transmission mode are exponential rather than linear.

The different spectra were normalized using the band located at 2018 cm^{-1}, even though the films were prepared in such a way that great variations in thickness were not expected. By normalizing the spectra, the effect of density and thickness are removed and the resulting values are due to absorbance only. The commercial software PeakFit was used to resolve overlapped bands. This software allows the use of three different curve-fitting methods: residuals, second derivative and deconvolution. The method of residuals was selected because of its simplicity and its reduced number of mathematical treatments involved in the peak resolution. In the region between 1330 and 1390 four gaussian peaks were fitted at 1340, 1352, 1368 and 1378 cm^{-1}. The position of the peaks was assigned after the work of Rueda et al. (1978). Direct readings of absorbance intensity from the spectra were made whenever possible. A detailed example of peak resolution is presented in APPENDIX C.

a) Branching content

The absorbance at 1378 cm^{-1} (methyl deformation band) has been related to the degree of branching. The FTIR spectra of the PE-25-O, PE-26-O and PE-27-O are plotted in Figure 3.15 to illustrate the effect of relative amounts of SCB on the shoulder located at 1378 cm^{-1}. It can clearly be seen that the intensity of the shoulder increases with the number of branches. PE-25-O has more branches compared to PE-27-O. PE-26-O is the blend of these two resins (50% w/w) and therefore, the amount of branches is somewhere in between.

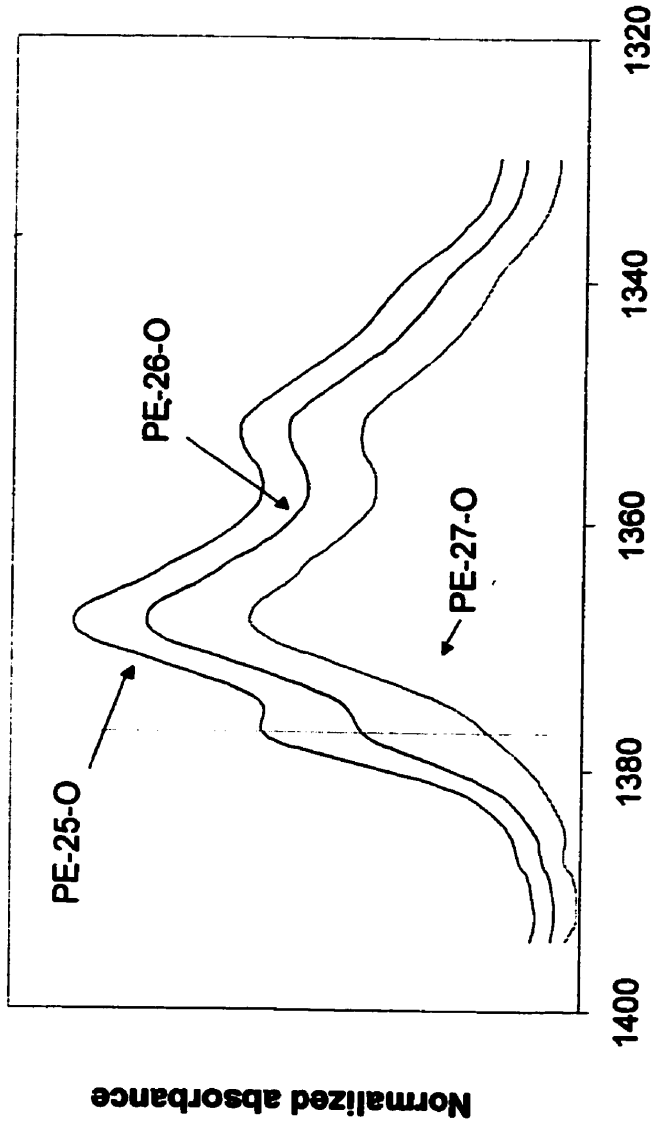

Figure 3.15 Normalized FTIR spectra of octene LLDPE with different branching content

b) Comonomer identification

The spectral region between 700 and 900 cm^{-1} provides information about the different type of comonomers. A correlation between the band at 770 cm^{-1} and ethyl branches has been established. The absorption at ~890 cm^{-1} has been attributed to branches longer than ethyl. However, this band shifts to 893 cm^{-1} in the case of butyl branches and to 888 cm-1 in the case of hexyl branches. The methyl deformation band at ~1378 cm^{-1} also shifts positions according to the branch length. For ethyl branches, for instance, the band is located at 1378-79 cm^{-1}. For butyl and hexyl branches the band moves towards 1377 cm^{-1}. The comonomer type that is present in the LLDPE resins used in this work was determined based on the presence of these bands. Some examples of comonomer determination are presented in APPENDIX C.

3.3.3 Results

3.3.3.1 Category A

The values of melting temperature and degree of crystallinity for the resins in this category are included in Table 3.5. Along with the peaks, the shape of the endotherms obtained from DSC provide information about molecular structure. The presence of higher peaks and a narrow melting range has been related to more homogeneous samples. The height of the peaks can be related to the length of the sequences that are able to crystallize. Accordingly, higher peaks indicate the presences of longer sequences which in turn correlates with the amount and distribution of branches along the chains (Zhang et al., 2001). The melting peak usually shifts to the right with increasing molecular weight, although the reverse trend has been reported for some branched polyethylenes (Alamo and Mandelkern, 1989; Peeters et al., 1997). During a DSC test, different crystallites with different stabilities are being melted and the average heat required to maintain the temperature increase is recorded. Since the perfection of the crystals is a function of

Table 3.5 Thermal and structural properties for all LLDPE resins in Category A

Resin ID	Melting Temperature (°C)[d]	Crystallinity (%)[e]	Relative Methyl Content[f]	Type of Comonomer[f]
PE-1-O	124.0	53.7	0.74	octene
PE-2-O	124.4	45.0	0.69	octene
PE-3-O	123.0	51.3	0.84	octene
PE-4-H	122.9	52.7	0.70	hexene
PE-5-H	126.7	46.5	1.87	hexene
PE-6-H	125.5	56.2	0.68	hexene
PE-7-O	124.1	47.4	0.64	octene
PE-8-B	124.7	49.1	1.89	butene
PE-9-O	124.8	43.0	1.65	octene
PE-10-H	126.4	51.1	1.88	hexene

[d]Melting peak in DSC thermogram [e]Determined by DSC [f]Determined by FTIR

Table 3.6 Thermal behavior of LLDPE resins after annealing (category A)

Resin ID	Main peak (°C)	Second peak (°C)	Crystallinity (%)
PE-1-O	126.8	112.5	52.9
PE-2-O	126.3	111.5	46.5
PE-3-O	125.5	114.1	53.7
PE-4-H	125.4	113.7	45.6
PE-5-H	128.1	110.1	47.3
PE-6-H	127.4	113.6	57.2
PE-7-O	126.3	111.6	47.8
PE-8-B	127.5	111.4	44.9
PE-9-O	124.6	120.5	29.3
PE-10-H	128.3	110.1	47.3

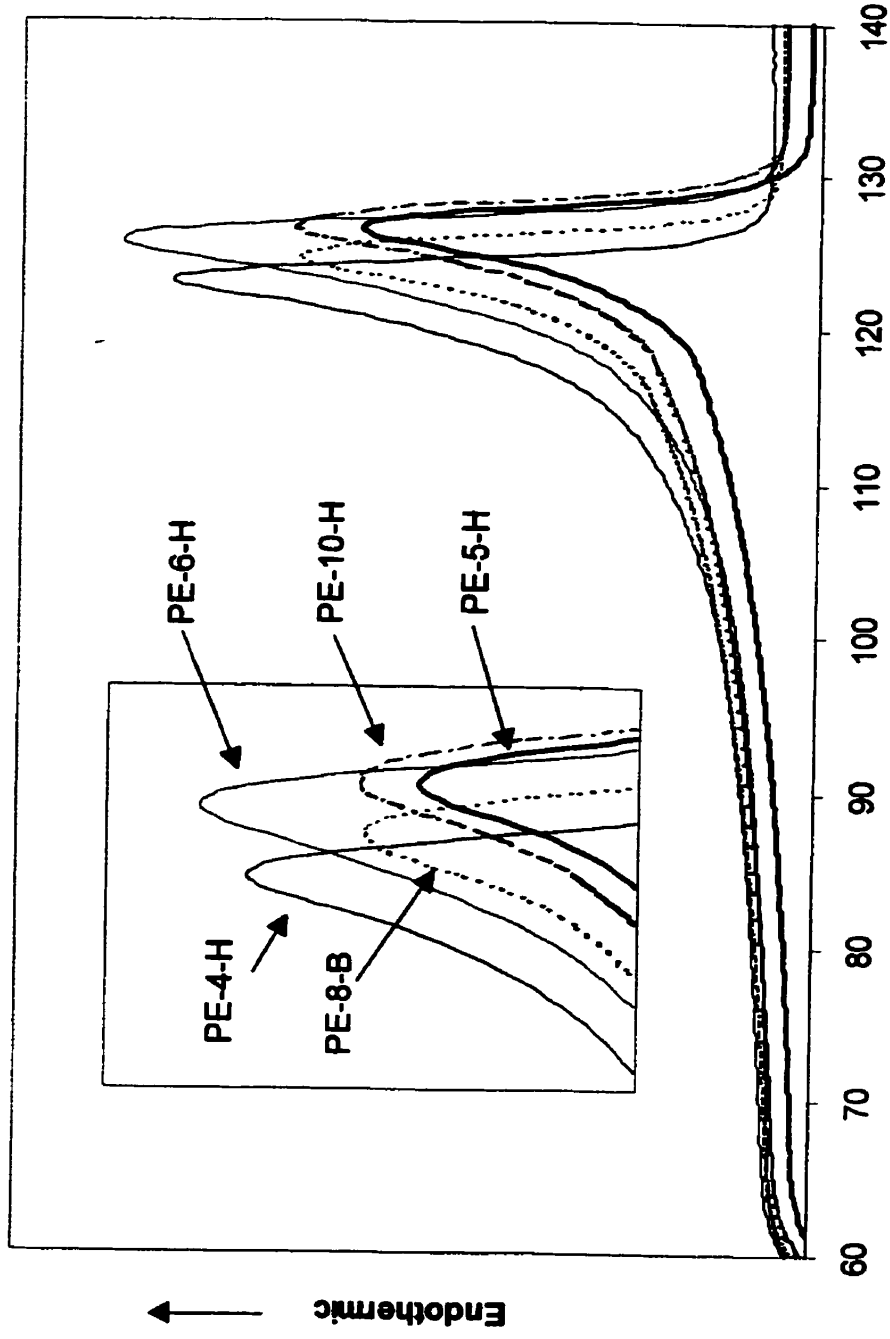

Figure 3.16 Melting endotherms of hexene LLDPE resins in Category A

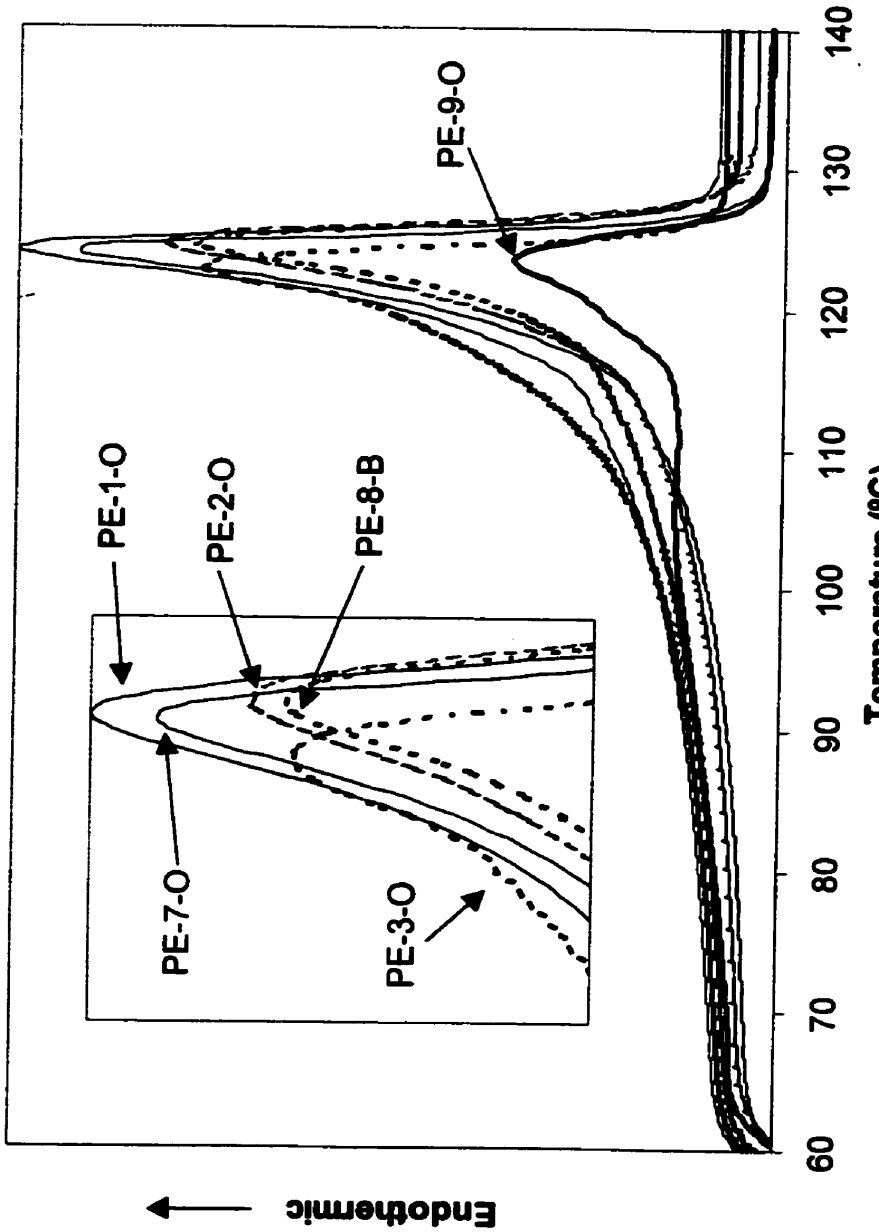

Figure 3.17 Melting endotherms of octene LLDPE resins in Category A

the type, amount and distribution of SCB different melting endotherms can be observed.

The melting endotherms for the hexene LLDPEs are presented in Figure 3.16. The melting endotherm of PE-8-B (butene) has also been included for comparison purposes. In general, narrow melting ranges can be observed. The endotherms with the higher melting peaks correspond to PE-4-H and PE-6-H, the latter being shifted to higher temperatures. This shift indicates that PE-4-H has a higher amount of SCB than PE-6-H. The endotherms for PE-5-H, PE-8-B and PE-10-H are characterized by shorter melting peaks which may be due to a more heterogeneous composition. The presence of more branches and the broadness of their MWD support this observation. It can also be seen that PE-8-B exhibits a similar endotherm as PE-10-H but it is slightly shifted to a low-temperature region. It has been reported that an increase in SCB shifts the melting peaks to the low temperature regions (Peeters et al., 2000; Vanden Eynde et al., 2000a; Vanden Eynde et al., 2000b).

The endotherm of PE-8-B was compared to those of the octene resins in Figure 3.17. PE-8-B and PE-2-O seem to have very similar endotherms, the latter with a narrower melting range. While PE-1-O and PE-7-O have sharp and high melting peaks, PE-3-O and PE-9-O show shorter peaks with a broad melting distribution which may be due to both broad MWD and high branching content. The low density and the shape of the PE-9-O endotherm are characteristic of a copolymer with high comonomer content with branches distributed heterogeneously among the chains (Starck, 1996; Starck et al, 1999).

Figures 3.18 and 3.19 show the melting behavior of hexene and octene LLDPE resins after being thermally treated. As expected, the values of T_m and degree of crystallinity increased (Table 3.6). The presence of more than one peak is observed. Usually, the secondary peaks have been related to the segregation of chains with different branching content and/or distribution (Zhang, 2001).

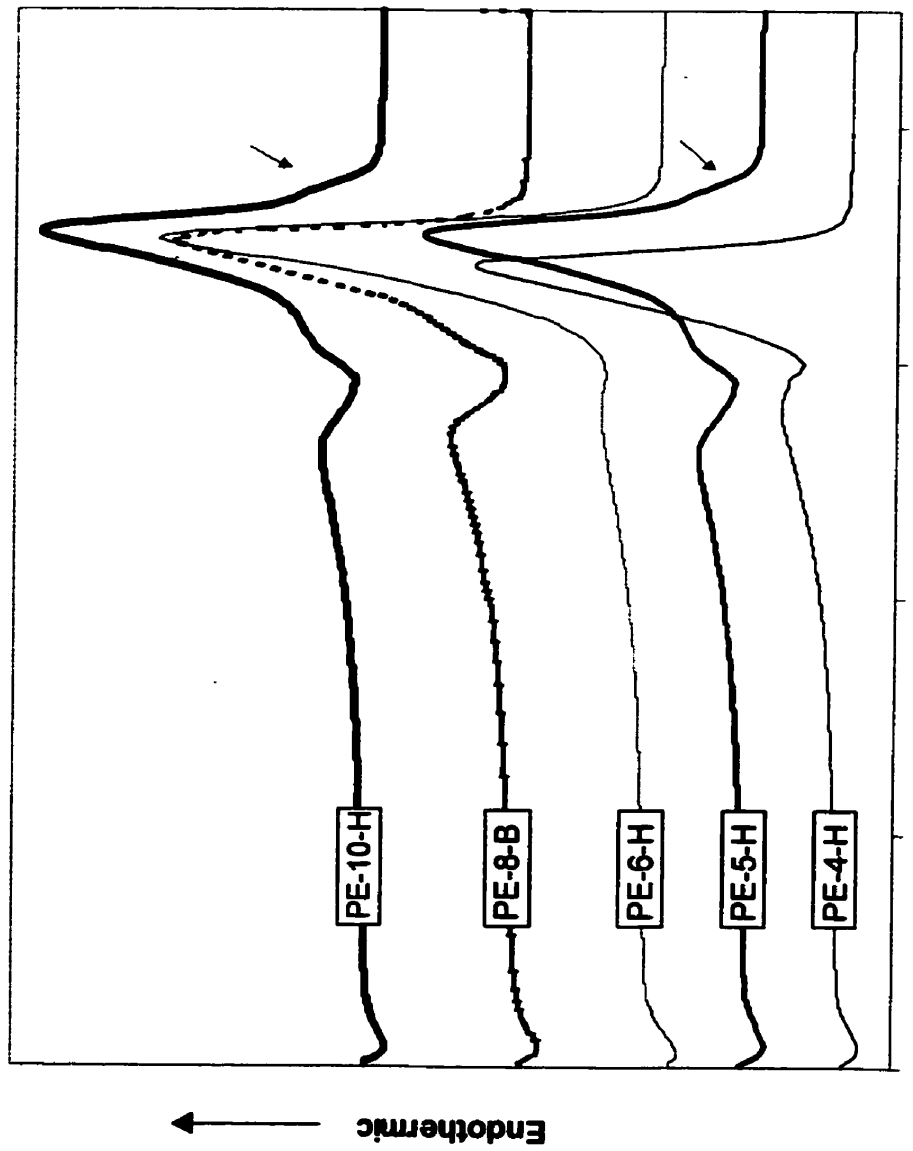

Figure 3.18 Melting endotherms of hexene and butene LLDPE resins after annealing (Category A)

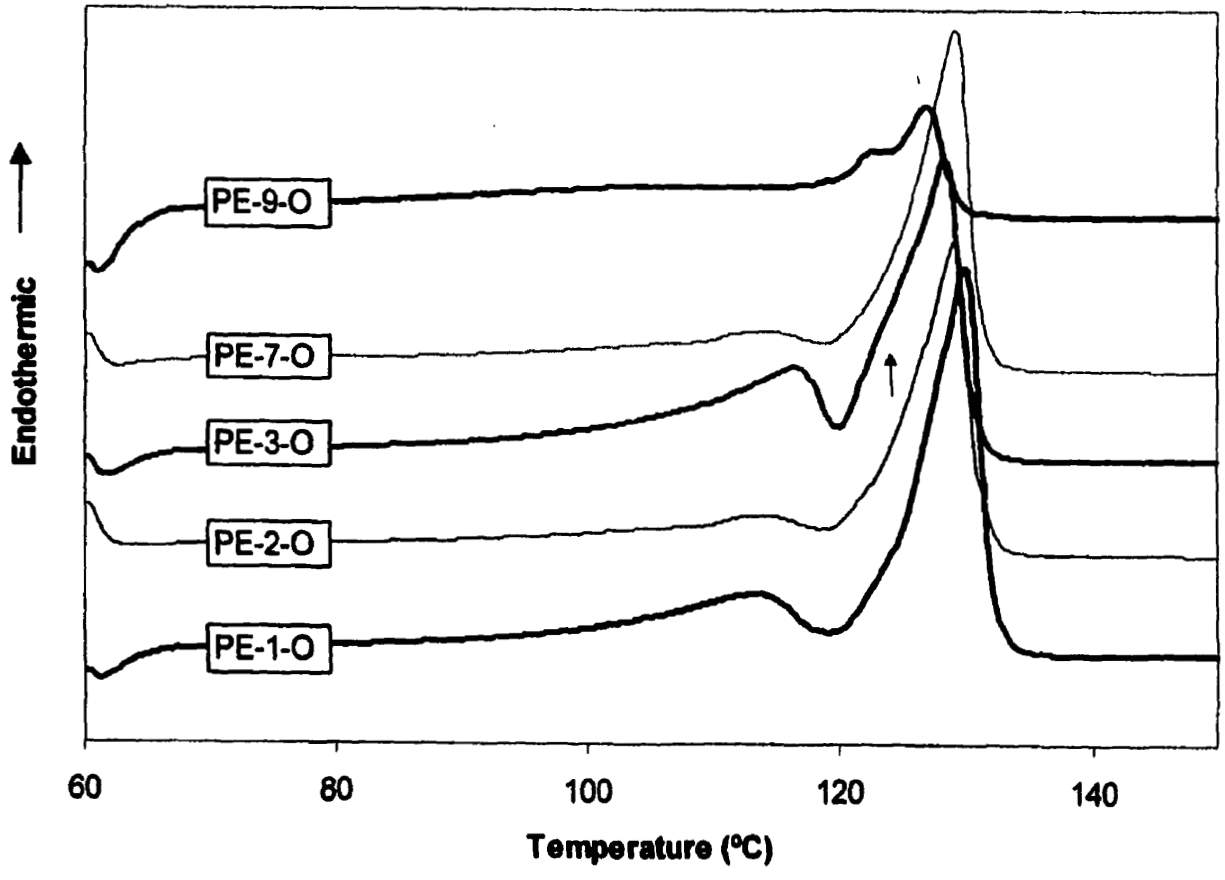

Figure 3.19 Melting endotherms of octene LLDPE resins after annealing (Category A)

PE-4-H and PE-6-H exhibit sharper melting peaks than the other hexene and butene resins (Figure 3.18). This observation together with the information gained in rheological measurements indicates that these two resins have a homogeneous composition (narrow MWD, low degree of branching, narrow branching distribution). Based on the relative importance of the secondary peak and on IR measurements, PE-4-H has a slightly higher degree of branching than PE-6-H. The presence of more SCB is known to generate chains with shorter crystallizable sequences. Shorter sequences in turn generate smaller and less stable crystals and the melting transitions shift to low temperature regions. The values of melting temperature that are reported in Tables 3.5 and 3.6 confirm this hypothesis.

PE-5-H, PE-8-B and PE-10-H show broad and short main peaks, distinctive secondary peaks and a shoulder between them indicating that these resins have a more heterogeneous composition than PE-4-H and PE-6-H. The presence of another shoulder that appears at temperatures higher than the main peak can also be observed for PE-5-H and PE-10-H. The relative importance of the secondary peak, however, is more evident for PE-8-B than the hexene resins. As mentioned before, that peak can be attributed to the presence of more branches and/or a different branching distribution The lower values of the main peak temperature and crystallinity, in addition to the IR results, support the previous statement. The heterogeneous molecular structure of PE-8-B may also explain its lower viscosity as compared to PE-5-H and PE-10-H (Table 3.2).

Three distinct trends are observed among the octene resins (Figure 3.19). PE-9-O shows a completely different melting behavior. This resin has a broad MWD and a much higher comonomer content than the other octene resins. PE-2-O and PE-7-O have comparable endotherms and seem to be more homogeneous based on the shape of the curves. The relative importance of the secondary peak is more evident for PE-1-O and PE-3-O than the other LLDPEs. Furthermore, PE-3-O shows a small shoulder between the main peak and the secondary peak, which broadens

the melting range. This indicates that PE-1-O is a less branched polymer than PE-3-O in agreement with IR measurements and the lower temperature of the main peak reported in Table 3.6. The differences exhibited by PE-1-O and PE-3-O in terms of the secondary peak temperature and heat of fusion (crystallinity) indicate that not only the branching content is different but also the distribution of SCB along the chains.

3.3.3.2 Category B

Table 3.7 summarizes the results from thermal and FTIR analysis for the resins in category B. The DSC endotherms are presented in Figure 3.20. It can be seen that PE-17-O and PE-18-H exhibit broad melting ranges with peaks that are not well defined. The melting endotherms of the other resins show narrow melting range with sharp peaks. The thermal behavior of all the resins after annealing is presented in Figure 3.21. PE-18-H shows a distinct endotherm. The presence of two peaks very close to each other and of equal importance can be observed. This resin has a broader MWD and different comonomer. The shapes of the endotherms for all the octene resins look comparable indicating similarities in microstructure (Figure 3.21). However, the information presented in Table 3.8 suggests some differences in degree of branching and/or branching distribution. PE-17-O exhibits higher degree of crystallinity (heat of fusion) and higher temperatures for both the main and the secondary peaks. These trends and the IR measurements indicate that PE-17-O has a lower amount of SCB than the other resins. PE-17-O also shows some differences in its rheological properties (Section 3.2.2). The temperatures at which the main and secondary peaks are located are slightly higher for PE-11-O and PE-14-O than for PE-12-O and PE-13-O. Interestingly, these LLDPEs also form pairs according to their viscosity temperature sensitivity (Figure 3.11). Further analysis is required to establish the differences in molecular structure and the relationship with thermal and rheological properties more precisely.

Table 3.7 Thermal and structural properties for all LLDPE resins in Category B

Resin ID	Melting Temperature (°C)[d]	Crystallinity (%)[e]	Relative Methyl Content[f]	Type of Comonomer[f]
PE-11-O	125.9	46.2	0.48	octene
PE-12-O	125.8	44.6	0.61	octene
PE-13-O	125.8	44.9	0.52	octene
PE-14-O	126.0	49.6	0.48	octene
PE-15-O	125.9	44.7	0.54	octene
PE-16-O	126.1	48.6	0.41	octene
PE-17-O	127.0	49.0	0.38	octene
PE-18-H	129.6	55.7	0.72	hexene

[d]Melting peak in DSC thermogram [e]Determined by DSC [f]Determined by FTIR

Table 3.8 Thermal behavior of LLDPE resins after annealing (Category B)

Resin ID	Main peak (°C)	Second peak (°C)	Crystallinity (%)
PE-11-O	128.8	112.8	48.2
PE-12-O	127.9	112.1	46.1
PE-13-O	128.2	112.3	51.9
PE-14-O	129.1	112.9	51.6
PE-15-O	128.5	112.3	50.4
PE-16-O	128.9	113.2	47.1
PE-17-O	129.5	114.1	53.7
PE-18-H	130.3	126.2	53.4

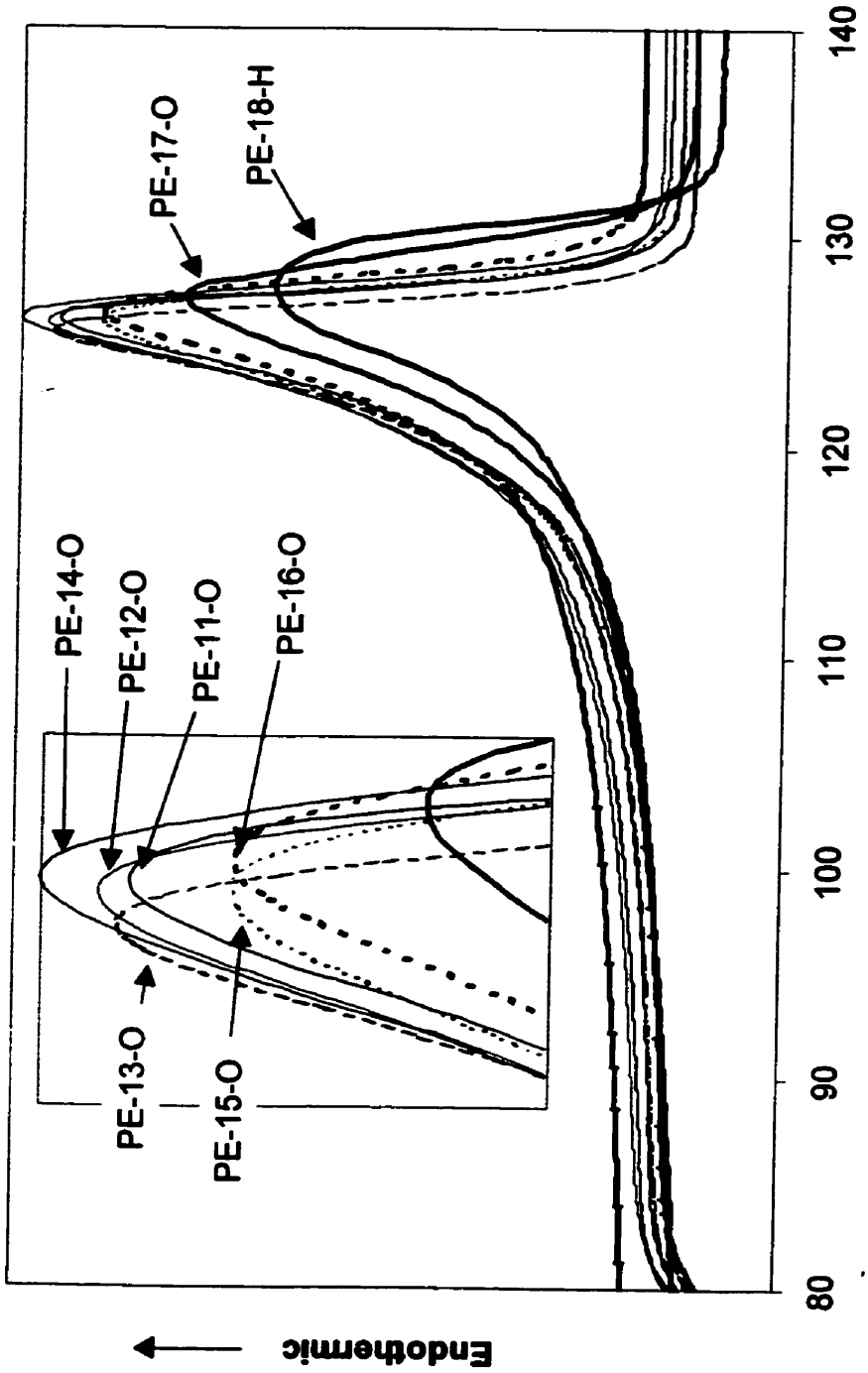

Figure 3.20 Melting endotherms of all LLDPE resins in Category B

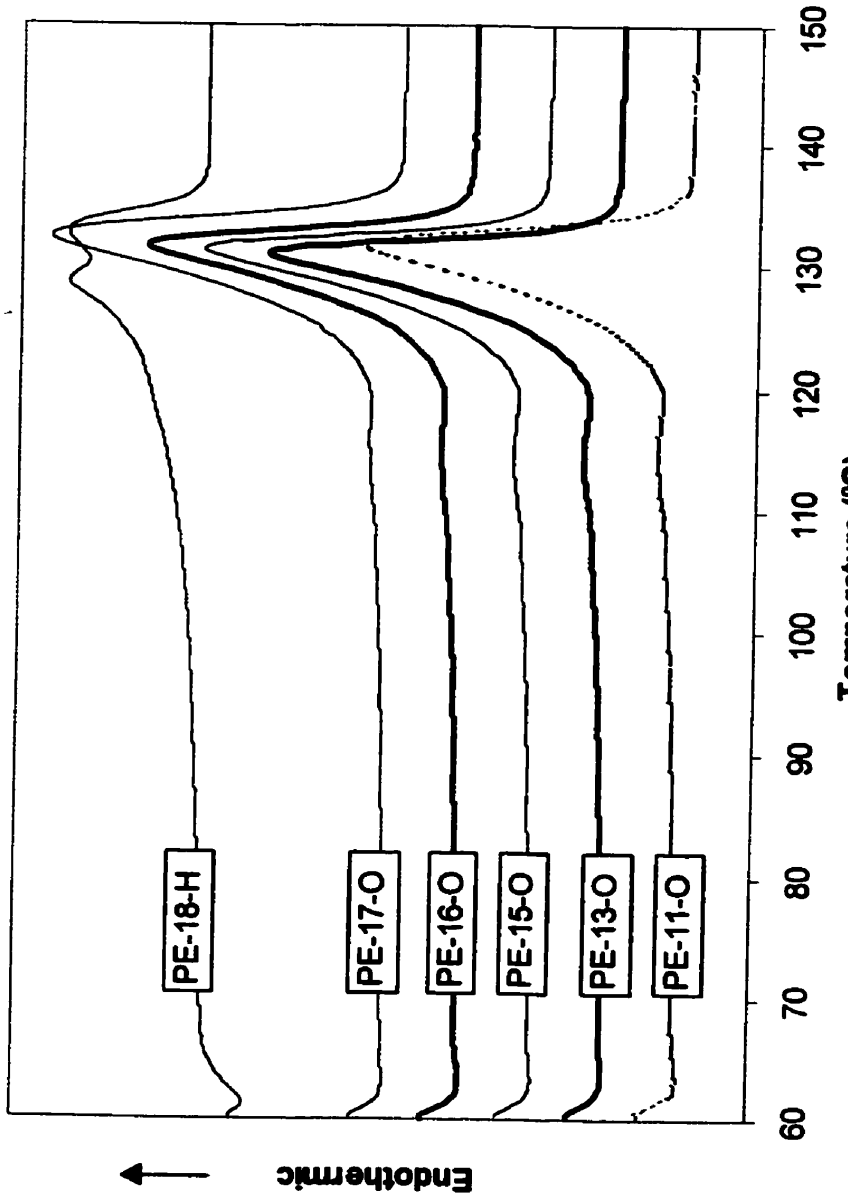

Figure 3.21 Melting endotherms of LLDPE resins after annealing (Category B)

3.3.3.3 Category C

Three different groups of endotherms can be seen in Figure 3.22 based on the melting range as well as the melting peak position. The endotherms of PE-22-O, PE-23-O and PE-24-O are similar to that of PE-20-O. This suggests that besides the small differences in M_w and degree of branching (Table 3.9) these resins must have comparable branching distributions. The melting peaks of PE-22-O and PE-27-O are slightly shifted to higher temperatures, which may indicate that these two resins have a slightly lower amount of SCB than PE-20-O, PE-23-O and PE-24-O. On the other hand, PE-19-H and PE-21-H seem to have a higher comonomer content based on the shift of their endotherms to lower temperatures as compared to that of PE-20-O. The low melting temperature of PE-25-O has been attributed to the higher amount of hexyl branches than the other resins in this category.

After annealing (Figure 3.23), only PE-19-H, PE-21-H and PE-26-O show more than one peak confirming their higher comonomer content. PE-21-H also has a broader MWD, which is reflected in the melting endotherm. At low temperatures, the presence of a distinctive region can be clearly seen. PE-19-H, on the other hand, only shows a very small peak that is difficult to detect using the plotted scale. The rheological and thermal differences between PE-19-H and PE-21-H have been attributed to their particular molecular structure. While PE-19-H appears to be very homogeneous, PE-21-H exhibits a higher level of heterogeneity (MWD, branching content and branching distribution).

PE-25-O has the highest degree of branches and yet, only one peak is detected after annealing (Figure 3.23). A possible explanation of this phenomenon is that the branches are distributed in such a way that only small and unstable crystals are formed. The very low value of the main peak temperature and degree of crystallinity (heat of fusion), despite the large value of M_w, supports the hypothesis. It is also interesting to note that the shape of the main peak for PE-27-O is unusually broad and unresolved. This suggests a population of crystals with different

Table 3.9 Thermal and structural properties for all LLDPE resins in Category C

Resin ID	Melting Temperature (°C)[d]	Crystallinity (%)[e]	Relative Methyl Content[f]	Type of Comonomer[f]
PE-19-H	126.8	59.7	0.40	hexene
PE-20-O	129.7	57.6	0.19	octene
PE-21-H	126.6	53.7	1.25	hexene
PE-22-O	131.1	57.8	0.22	octene
PE-23-O	130.8	57.8	0.18	octene
PE-24-O	130.1	58.1	0.21	octene
PE-25-O	115.0	33.5	0.95	octene
PE-26-O	127.7	47.5	0.56	octene
PE-27-O	131.6	60.6	0.15	octene

[d]Melting peak in DSC thermogram [e]Determined by DSC [f]Determined by FTIR

Table 3.10 Thermal behavior of LLDPE resins after annealing (Category C)

Resin ID	Main peak (°C)	Second peak (°C)	Crystallinity (%)
PE-19-H	128.5	115.5	57.8
PE-20-O	131.1	--	63.0
PE-21-H	128.8	110.3	56.5
PE-22-O	132.3	--	68.0
PE-23-O	132.2	--	62.6
PE-24-O	132.2	--	57.5
PE-25-O	114.6	--	30.7
PE-26-O	131.0	117.6	52.8
PE-27-O	129.2	--	57.1

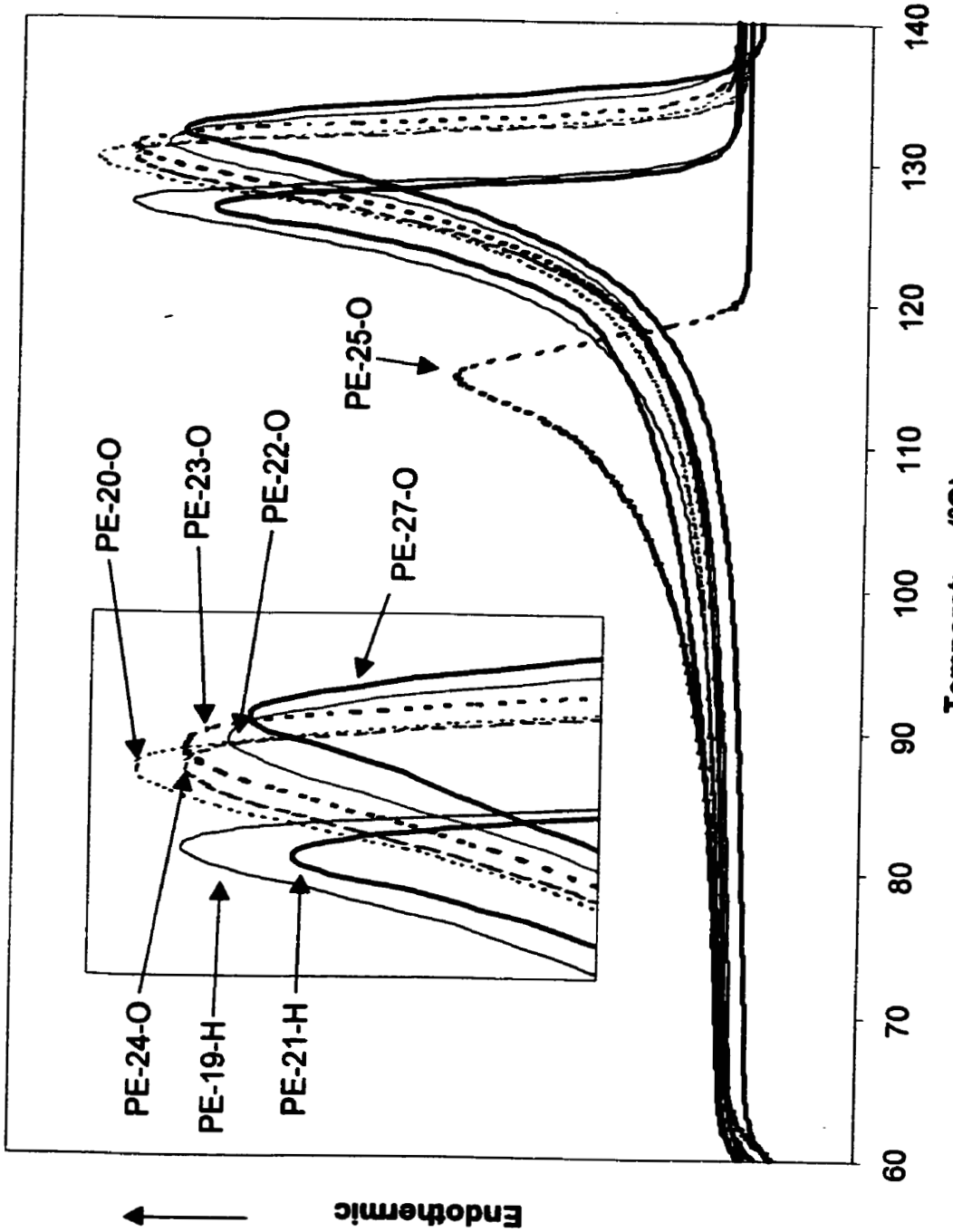

Figure 3.22 Melting endotherms of all LLDPE resins in Category C

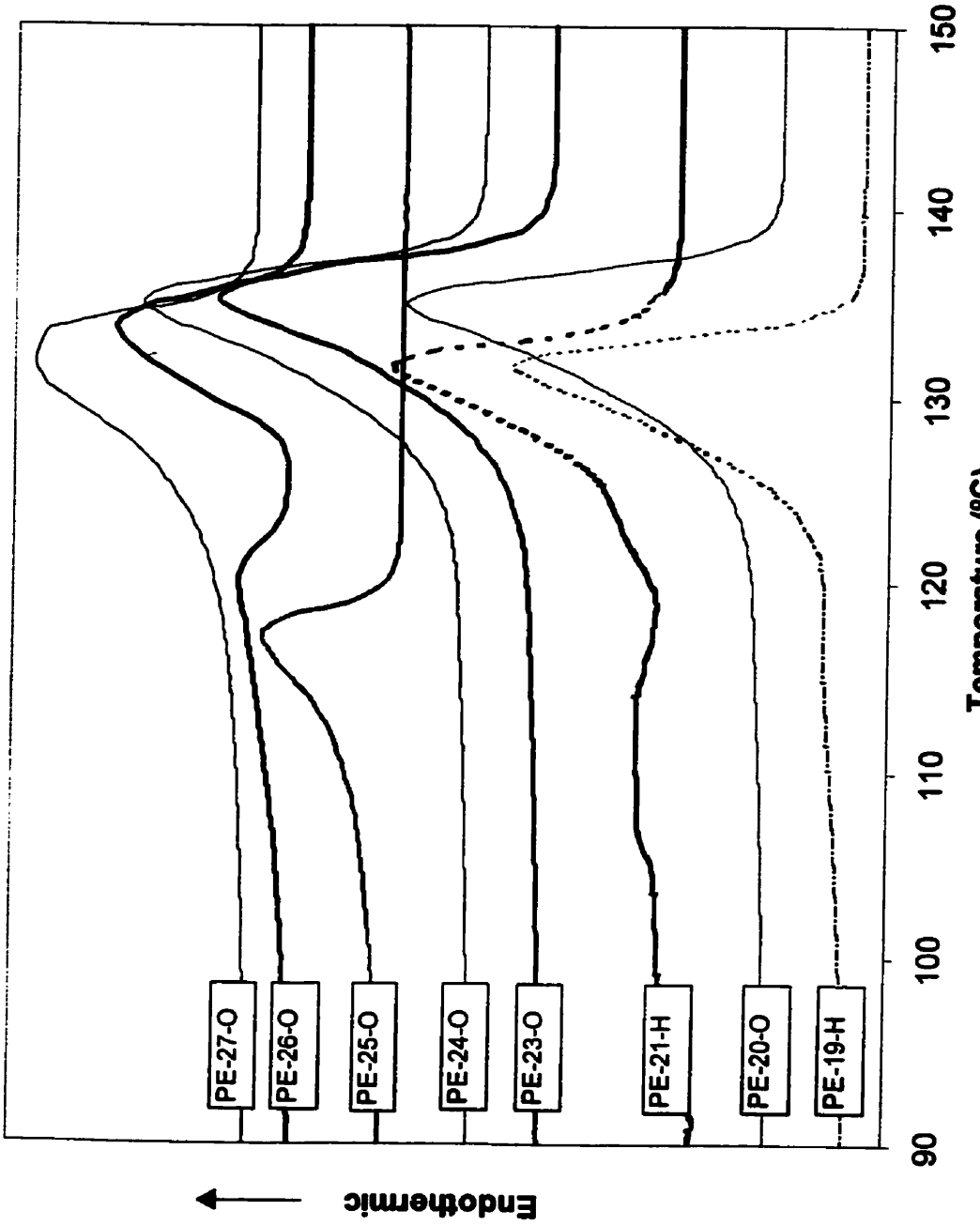

Figure 3.23 Melting endotherms of LLDPE resins after annealing (Category C)

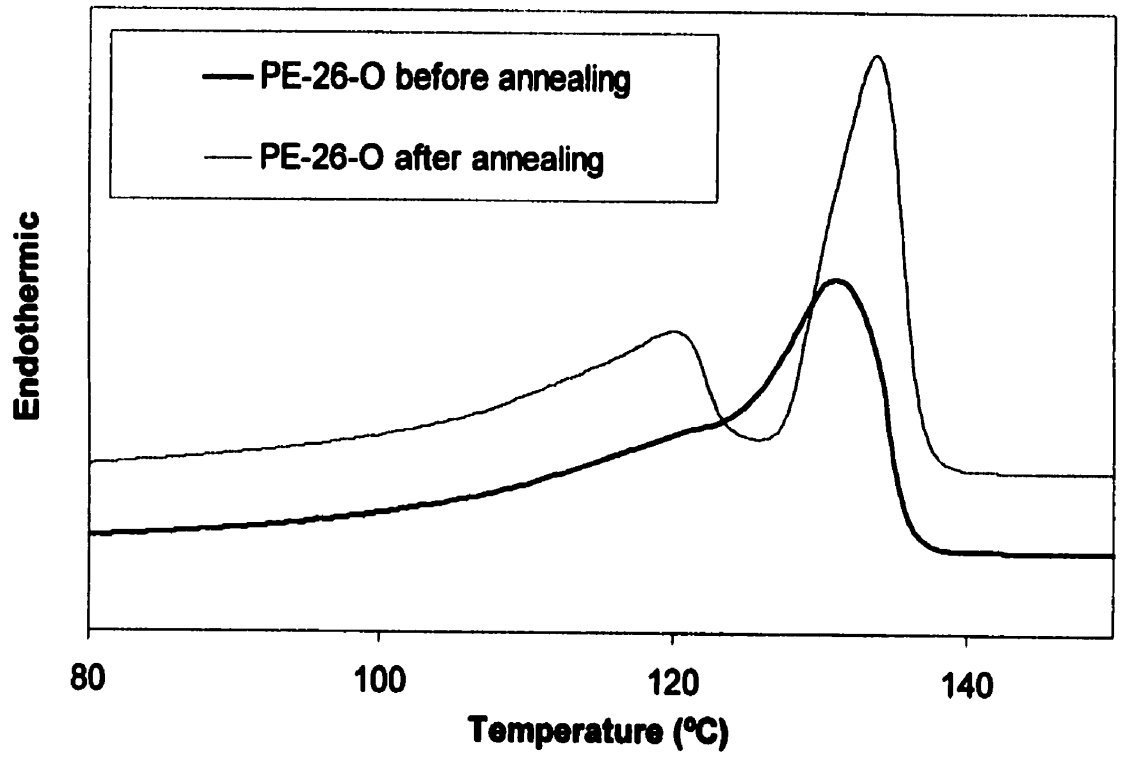

Figure 3.24 Melting endotherms before and after a thermal treatment for PE-26-O

stabilities. Linear chains with high M_w form large and stable crystals. The presence of hexyl branches, which are not included in the crystal lattice, disrupts the methylene sequence which is able to crystallize resulting in a range of crystal sizes (Peeters et al., 1997; Zhang et al., 2001). It is therefore speculated that PE-27-O has different populations of relatively large crystals.

PE-26-O is the blend of PE-25-O and PE-27-O (50% w/w). Figure 3.24 shows that before annealing, a phase separation cannot clearly be observed. After annealing, chains with different branching content and distribution segregate and the presence of two peaks located at approximately the same position as the virgin resins is detected (Table 3.10).

3.4. Summary

The results presented in this chapter clearly show that the properties of ethylene/α-olefins are a function of the chemical composition i. e. comonomer content, and of the chemical composition distribution i.e. inter- and intra-molecular heterogeneity. Homogeneous resins can be described as resins with narrow MWD and uniform composition, which means that the comonomer is distributed evenly along the macromolecular chains. It was found that homogeneous resins exhibit low values of viscosity and elasticity and their shear thinning behavior starts at high frequencies. As the molecular microstructure becomes more heterogeneous, the elasticity of the resins increases and the shear thinning behavior becomes more apparent. Subtle variations in the type of heterogeneity, however, were not detected solely based on the linear viscoelastic responses of the materials.

The thermal properties of ethylene copolymers are very sensitive to both the molecular structure and the thermal treatment imposed on the material. Results from the thermal analysis, in conjuction with the IR measurements and the rheological characterization, were related to the comonomer content and its distribution. In general, it was observed that as the comonomer content increases the melting

temperature decreases and the melting range broadens and shifts to lower temperature regions. It was also observed that after a prolonged thermal treatment, chains with different structures tend to segregate thus showing multiple peaks in the melting endotherms. It is very difficult, however, to establish a general theory as resins from different polymerization processes were used in this study. It is possible that some of the observed trends have been the result of coupled effects of the molecular microstructure on the response of these materials to the thermal treatment.

Rheological measurements, thermal analysis and infrared spectroscopy were found to be useful in determining the chemical composition and the chemical composition distribution of the resins used in this study. None of the above techniques, when used alone, would have provided conclusive results. The inference on the molecular structure resulted from the combined analysis of the results obtained from these characterization techniques. Despite the fact that advanced techniques such as TREF or NMR can be used to characterize molecular structure of polymers, the results presented in this chapter suggest that ethylene/α-olefin copolymers can be characterized using alternative techniques that have the advantages to be rapid, economic and environmentally sound.

Sintering of ethylene/α-olefin copolymers

Chapter 4

4.1 Sintering experiments

Sintering experiments were performed using a METLER FP82 hot stage, controlled by a METLER FP90 central processor. The sintering process was followed using a CCD camera coupled to an Olympus optical microscope. Pictures were taken at fixed time intervals and directly saved in electronic format. Each sample consisted of two particles of approximately equal diameter (~500 μm) placed on a glass slide. The sintering experiments were carried out at two different conditions: constant temperature and ramped temperature. Under isothermal conditions, the materials' viscosity and surface tension are not expected to vary during the experiment and the results can be compared more easily. Experiments conducted at ramped temperature are, however, more representative of situations encountered in the actual rotomolding process.

Isothermal experiments were conducted at 170 °C. At this temperature, useful information can be obtained on the sintering behavior of the resins used in this work within reasonable experimental time. Furthermore, the measurement of properties such as viscosity can be easily performed. The hot stage was pre-heated to 120 °C and the sample was placed inside. The temperature was then rapidly increased to 170 °C. For non-isothermal experiments, the temperature ranged from 111 to 226.5 °C. The heating rate was set at 11 °C/min. These conditions were determined based on data obtained during the molding cycle of polyethylenes (Bellehumeur, 1997).

Figure 4.1 shows a typical sintering evolution of a low-viscosity resin. The projected area of the particles and the diameter of the neck formed between them

were measured using the image analysis software ImagePro®. The shape of the particles was idealized as schematically represented in Figure 4.2. The dimensionless quantity *y/a* represent the ratio between the neck radius and the particle's radius. Thus, a value of *y/a* approaching one indicates that these two quantities are the same and a single particle has been formed. The procedure used to calculate the dimensionless sintering neck growth was similar to that presented by Bellehumeur et al. in 1996. An example of such a calculation is presented in APPENDIX D.

4.1.1 Effect of particle size and shape

It is well established in the literature that the sintering rate is affected by the size of the particles. As reviewed by Mazur (1995), Newtonian sintering models predict sintering rates that are inversely proportional to the particles' diameter. Some experimental results have shown, however, that this effect was more pronounced for high viscosity resins (Bellehumeur et al., 1996). The effect of particle size has not been considered in the present study and only particles of comparable size have been used. For clarity and completeness, the average diameter of the particles used in sintering experiments has been always reported.

In addition to the size, the shape of the particles plays a very important role in the study of polymer sintering. Powder particles have very irregular shapes and, as a result, the initial contact between them varies from one experiment to another. Figure 4.3 illustrates the effect of the particles' initial contact on the sintering neck growth. It can be seen that a large initial contact enhances the sintering rate. To ensure good reproducibility of the results, a minimum of three experiments were carried out in an effort to minimize the effect of particle shape on the sintering rate. Another alternative was the conduction of experiments using cylindrical particles. The use of cylindrical particles offers a better control of the initial contact formed between the particles. Complete information about the preparation of cylinders can be found in APPENDIX E.

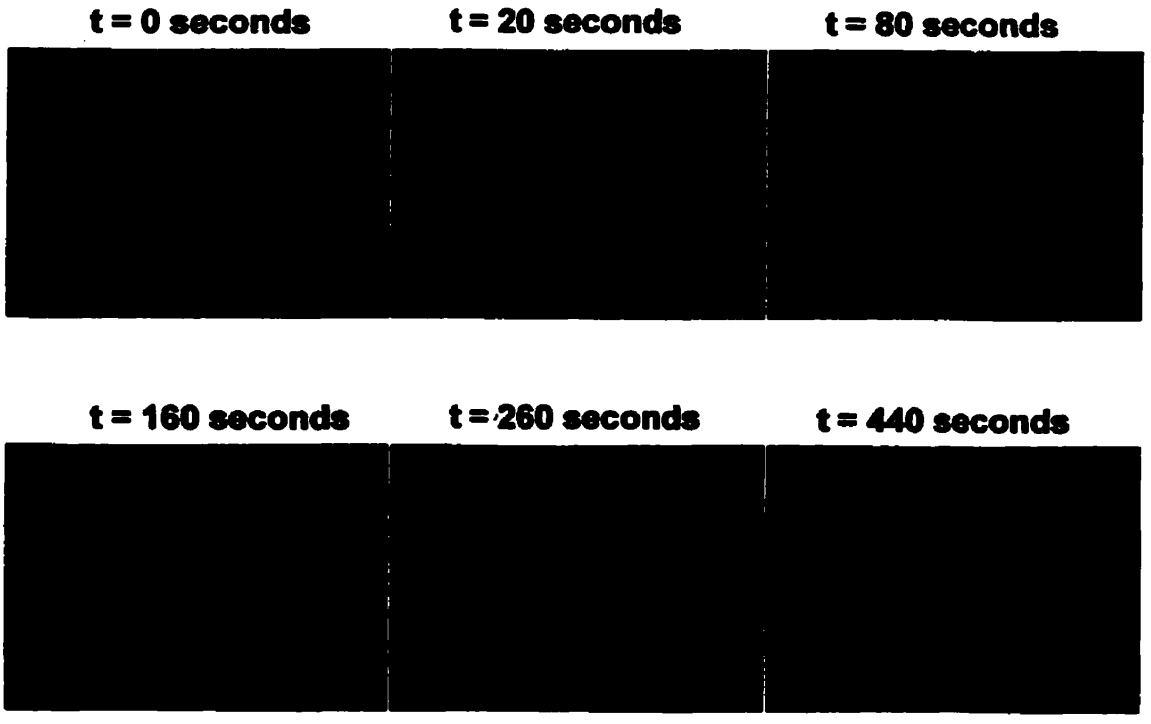

Figure 4.1 Typical sintering evolution of a LLDPE resin in powder form at 170 °C

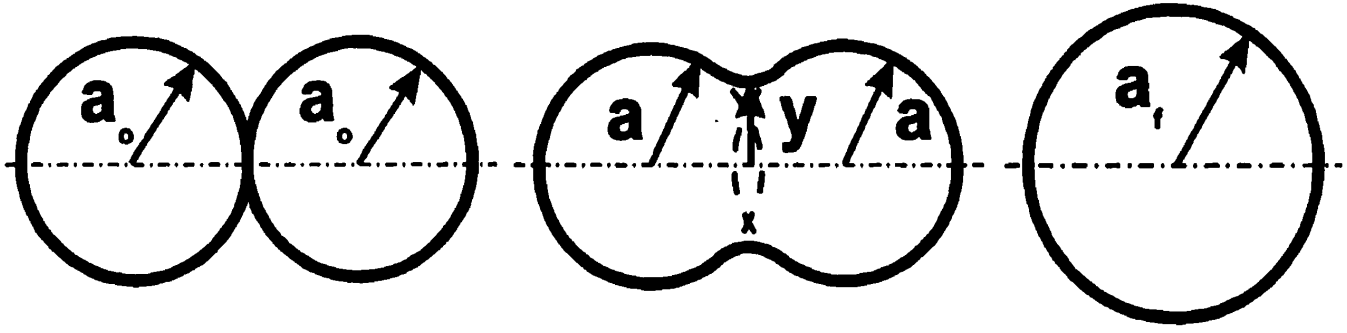

Figure 4.2 Schematic sintering sequence for two particles, where *a*, a_o, a_f and *y* are the particle radius, initial particle radius, final particle radius, and neck radius

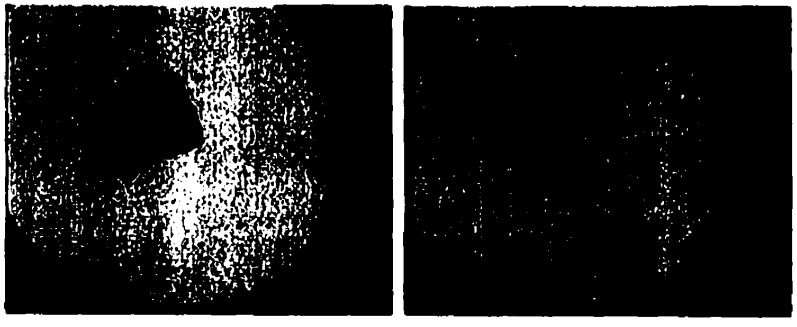

Experiment 1
2ao = 438 microns

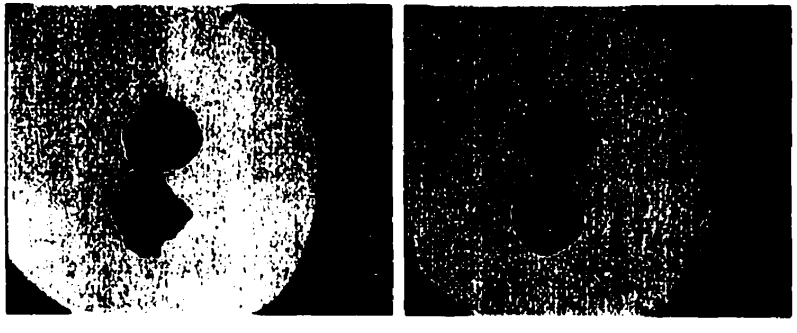

Experiment 2
2ao = 452 microns

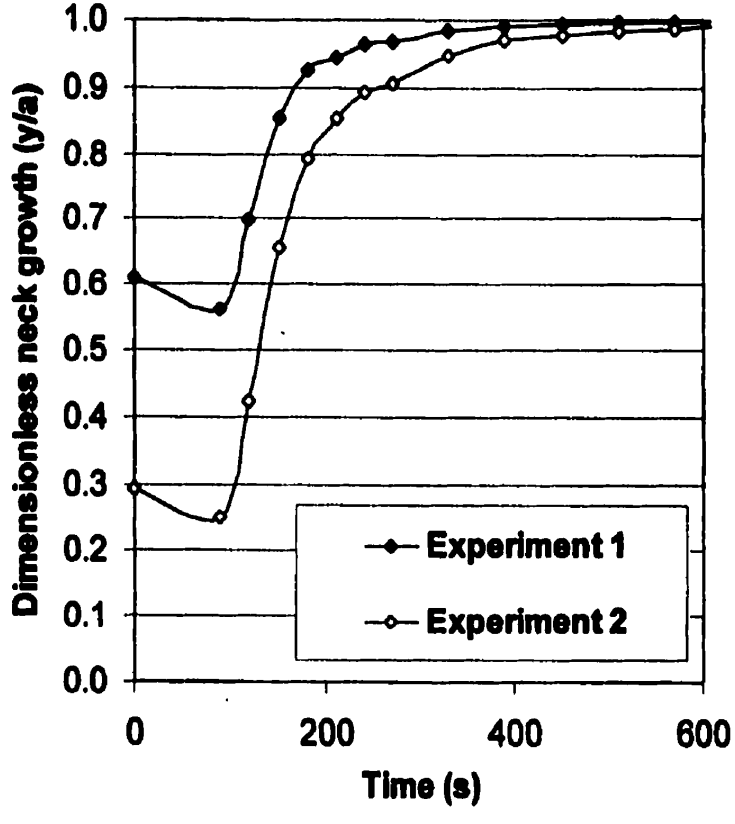

Figure 4.3 Effect of initial contact between powder particles on the sintering of PE-16-O. Experiments at ramped temperature (111 to 226.5° at 11°C/min)

The curves presented in Figure 4.3 also show that the neck growth between the sintering particles is preceded by an initial decrease in the value of the dimensionless neck radius (y/a). The following observation, typical of sintering experiments carried out using powder, explains this phenomenon. Immediately after melting, the contour of the particles becomes regular which causes some variations in the initial contact.

In general, the standard deviation of the dimensionless neck radius was found to be more important for powder particles than for cylindrical particles, particularly at the early stages of coalescence with values that ranged from 0.05 to 0.2. By using cylindrical particles, the standard deviation of the results was usually less than 0.15. After the initial stages of the sintering process, however, the standard deviation of the sintering results for both powder and cylinders were small with values that seldom reached 0.05.

4.1.2 Effect of material pretreatment

During the grinding process of the LLDPE resins, high temperatures and shearing stresses are frequently encountered (McDaid and Crawford, 1998). It is reasonable to expect that the pretreatment imposed on the resins during the pulverization process may influence their sintering behavior. The magnitude of these effects is nevertheless difficult to quantify. Experiments using both powder particles (as received) and cylindrical particles are conducted in this work to obtain a general overview of the effect of pulverization on the sintering process.

Cylindrical particles were prepared by hot pressing the different resins on a perforated metallic plate (APPENDIX E). They were either quenched in iced water (fast-cooled cylinders) or cooled slowly in air (slow-cooled cylinders). Sintering results from experiments using fast-cooled and slow-cooled cylinders are presented in Figures 4.4 and 4.5, respectively. It can be seen that the variability of the sintering

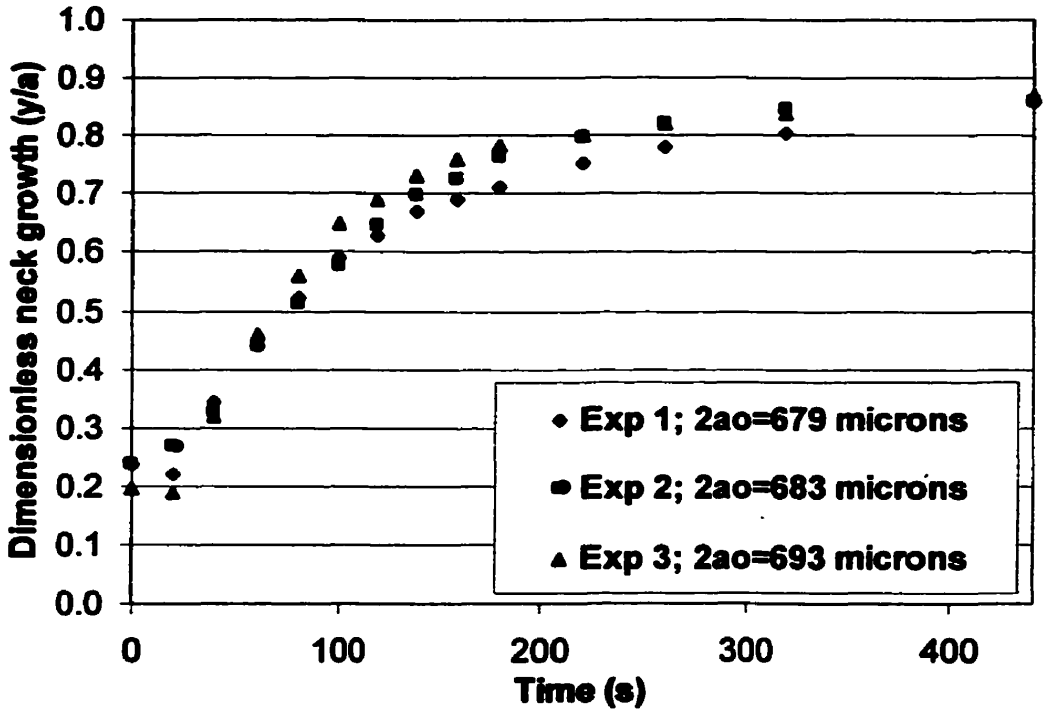

Figure 4.4 Dimensionless neck growth for slow-cooled cylinders. Experiments at constant temperature (170°C)

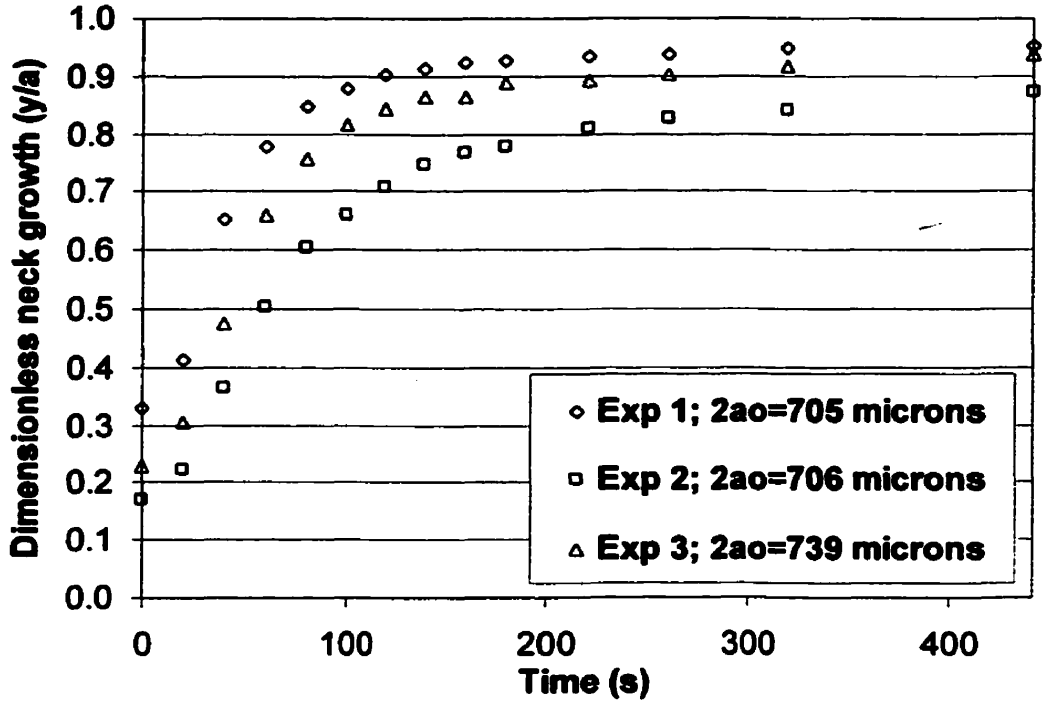

Figure 4.5 Dimensionless neck growth for fast-cooled cylinders. Experiments at constant temperature (170 °C)

results is more important when fast-cooled cylinders were used. This behavior has been partly attributed to the effect of quenching on thermal properties of the materials. For LLDPE, it has been found that besides molecular structure, thermal history also influences the thermal transitions (Peeters et al., 1997; Peeters et al., 2000). Different populations of crystallites with different sizes and stabilities may originate from rapid cooling because of the short crystallization times. It was decided to use slow-cooled cylinders in this study since those experiments provided more consistent results.

4.1.3 Other effects

In all sintering experiments, the molten particles are in contact with the substrate and adhesion forces may be important. Previous studies, however, have shown that the type of substrate does not significantly affect the sintering results (Siegman et al.,1986; Bellehumeur, 1997). Based on this information it was decided to conduct the sintering experiments on glass slides only. These transparent substrates facilitate the observation of the process under transmittance illumination mode.

Variations in the type and the amount of additives present in the resins may have an impact on the sintering process. Experiments were performed on a resin with two different additive packages and the results are presented in Figure 4.6. Important differences can be observed in the particles' contour evolution. In general, different substances are added to decrease the rate of thermal oxidation/degradation. Additives, however, may also act as nucleating agents during crystallization and modify the polymer thermal behavior. Specific interactions in a molecular level could take place as well, thus resulting in variations of surface energy or adhesion properties. The additive package for most of the resins used in this work was more or less the same. Some exceptions are PE-11-O to PE-15-O and PE-17-O. The amount of additives for these resins was approximately half that of a regular package.

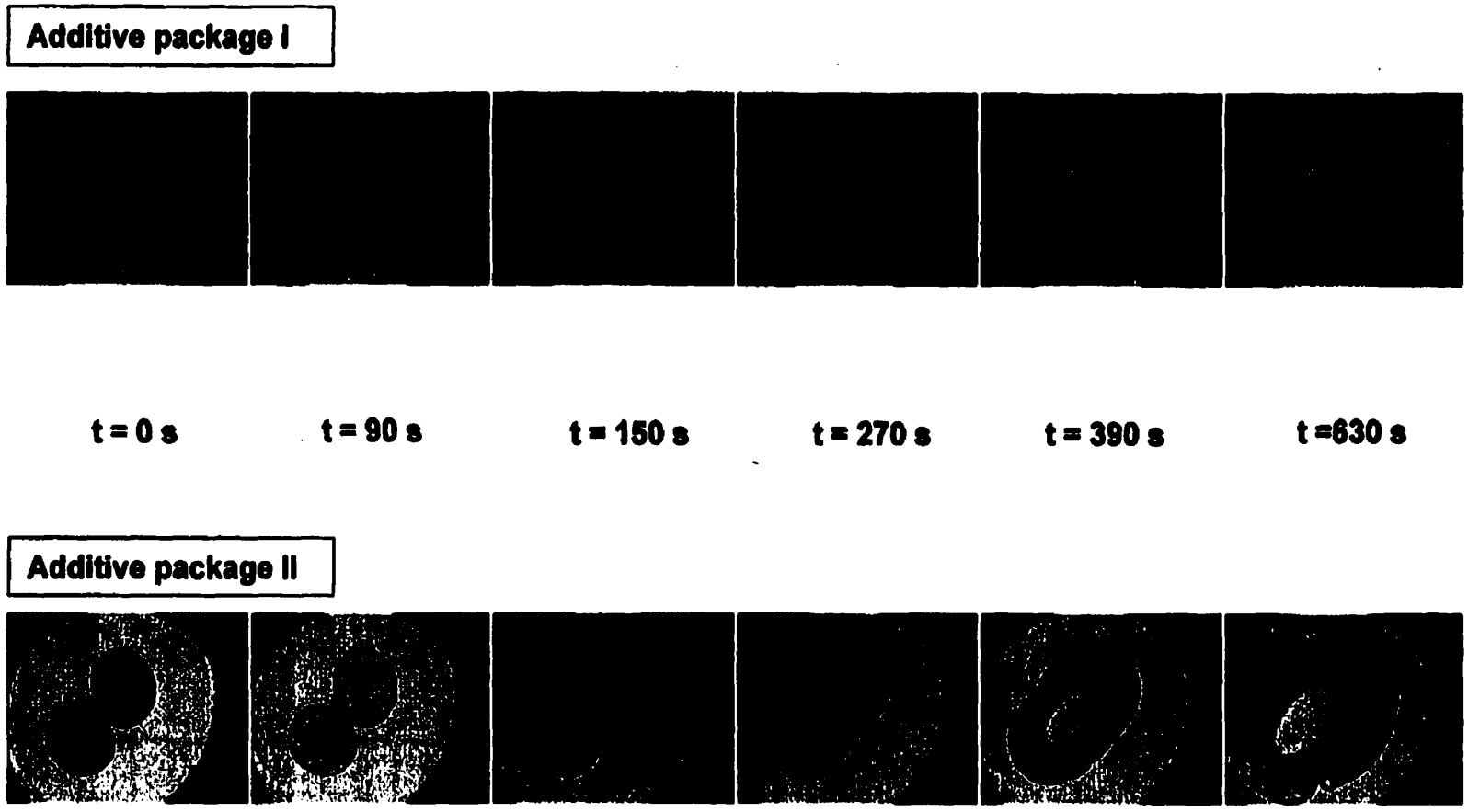

Figure 4.6 Effect of additive package on sintering. Experiments conducted with cylinders at ramped temperature (111 to 226.5°C at 11°C/min)

4.2 Sintering results and discussion

4.2.1 Molecular weight

The effect of molecular weight on the sintering rate is investigated in this section. It has been reported that in general, both viscosity and melting temperature increase with increasing molecular weight if other material properties remain the same. Moreover, the diffusion theories (e. g. reptation theory) predict slower diffusion with longer chains (de Gennes, 1971). It is thus expected that sintering will be negatively affected by the molecular weight.

The sintering behavior at 170 °C of octene copolymers with different M_w has been plotted in Figures 4.7 to 4.10. The selected resins all have similar and very narrow MWD as well as relatively low comonomer content. It can be observed that the sintering curves are ordered according to molecular weight, as expected. The resin with the highest M_w (PE-22-O) is also the one with highest zero-shear viscosity and melting temperature while PE-2-O exhibits the lowest values of both viscosity and melting temperature. Similar results were reported by Bellehumeur et al. in 1996. The sintering curves for PE-11-O, PE-12-O and PE-16-O overlap and lie in between that of PE-2-O and PE-22-O.

The results of experiments carried out at 170°C using slow-cooled cylinders are presented in Figure 4.8. The sintering behavior of PE-27-O under the same conditions has also been plotted in this graph. The sintering trends remain similar to those seen using powder particles. While the sintering curves of powder particles are closer to each other (Figure 4.7), the curves for slow-cooled cylinders are more separated (Figure 4.8). The differences seen in the sintering results using powder and cylinders are not consistent with results presented in the literature (Bellehumeur et al., 1996). A possible explanation of a slower sintering rate using cylinders rather than powder for PE-16-O and PE-22-O could be related to the differences in the

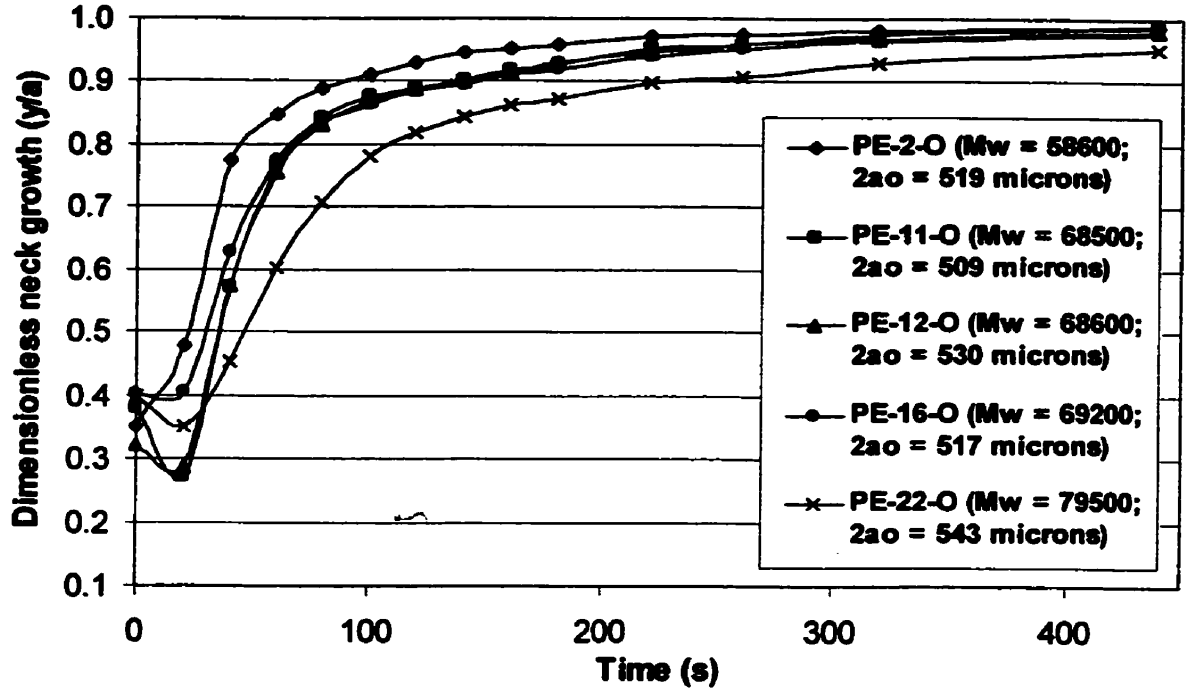

Figure 4.7 Neck growth evolution for octene resins in powder form. Experiments at constant temperature (170 °C)

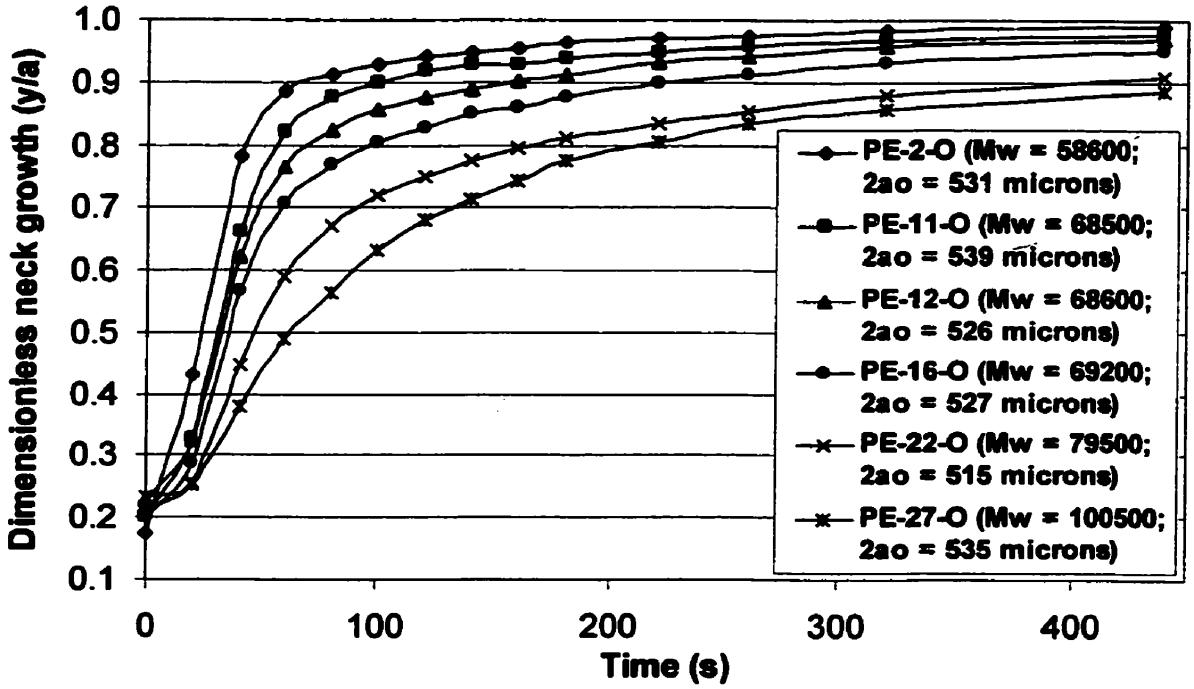

Figure 4.8 Neck growth evolution for octene resins. Experiments with cylinders at constant temperature (170 °C)

surface area of the particles. Powder particles have a much larger surface area compared to cylindrical particles. The reduction of surface area by the action of surface tension is one of the main driving forces of the coalescence of polymers.

When cylinders are used, the reduced surface area may also help to resolve the effect of small variations in the zero-shear viscosity and of other parameters such as the material elasticity and thermal properties. PE-11-O, PE-12-O and PE-16-O have slightly different values of zero-shear viscosity at 170 °C. Moreover, based on the relaxation time presented in Table 3.3, PE-16-O has a higher elasticity than PE-11-O and PE-12-O. The results presented using cylinders (Figure 4.8) reflect the differences between these three resins while the results obtained using powder (Figure 4.7) are unaffected by them.

The results of experiments carried out under non-isothermal conditions are presented in Figures 4.9 and 4.10. For these experiments, it is expected that the slow heating rates enhance the importance of thermal transitions on the sintering rate. In experiments conducted at constant temperature the particles are being melted very quickly and they rapidly gain mobility in the early stages of the sintering process. At a ramped temperature, on the other hand, heat is transferred very slowly to the particles modifying the patterns of chain mobility and interactions. PE-2-O seems to sinter faster than the other resins in accordance to M_w in the experiments using powder at ramped temperature (Figure 4.9). PE-22-O, however, seems to sinter more slowly than in experiments at constant temperature (Figure 4.7). This can be partly explained in terms of thermal properties. PE-22-O exhibits a much higher value of melting temperature. Hence, the onset of the sintering neck growth for PE-22-O is delayed as compared to the other resins. When slow-cooled cylinders are used in experiments at ramped temperature (Figure 4.10), the effect of melting temperature can be clearly seen with PE-22-O and PE-27-O as they start sintering later that the other LLDPEs.

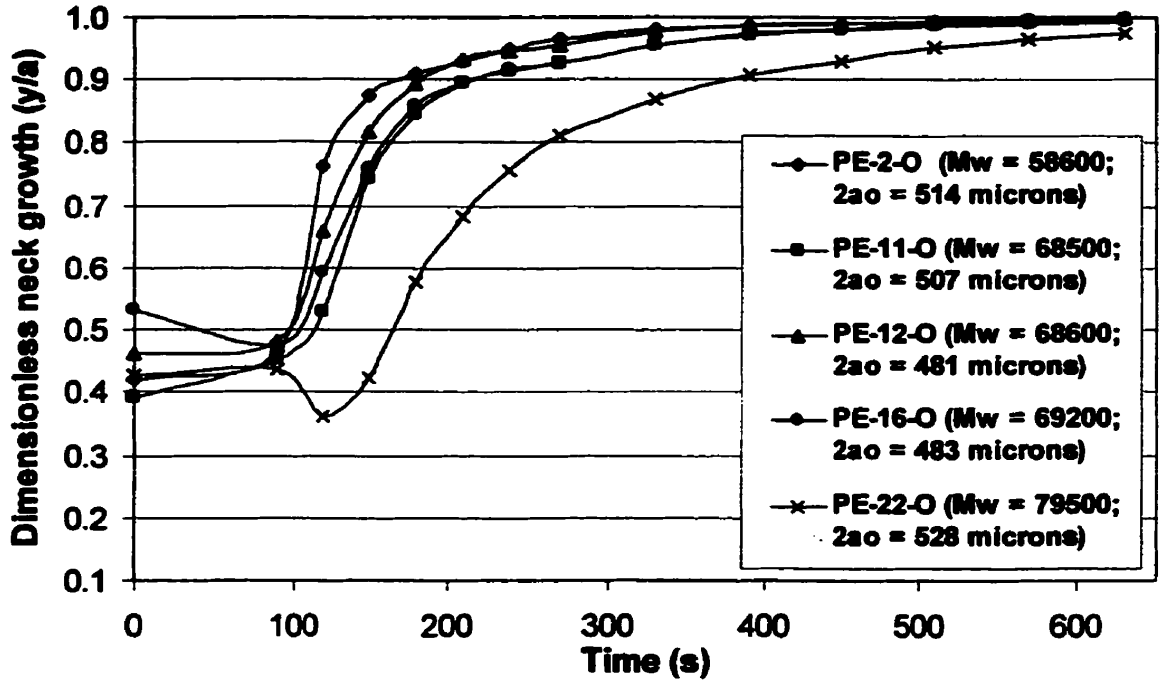

Figure 4.9 Neck growth evolution for octene resins in powder form. Experiments at ramped temperature (111 to 226.5 °C at 11°C/min)

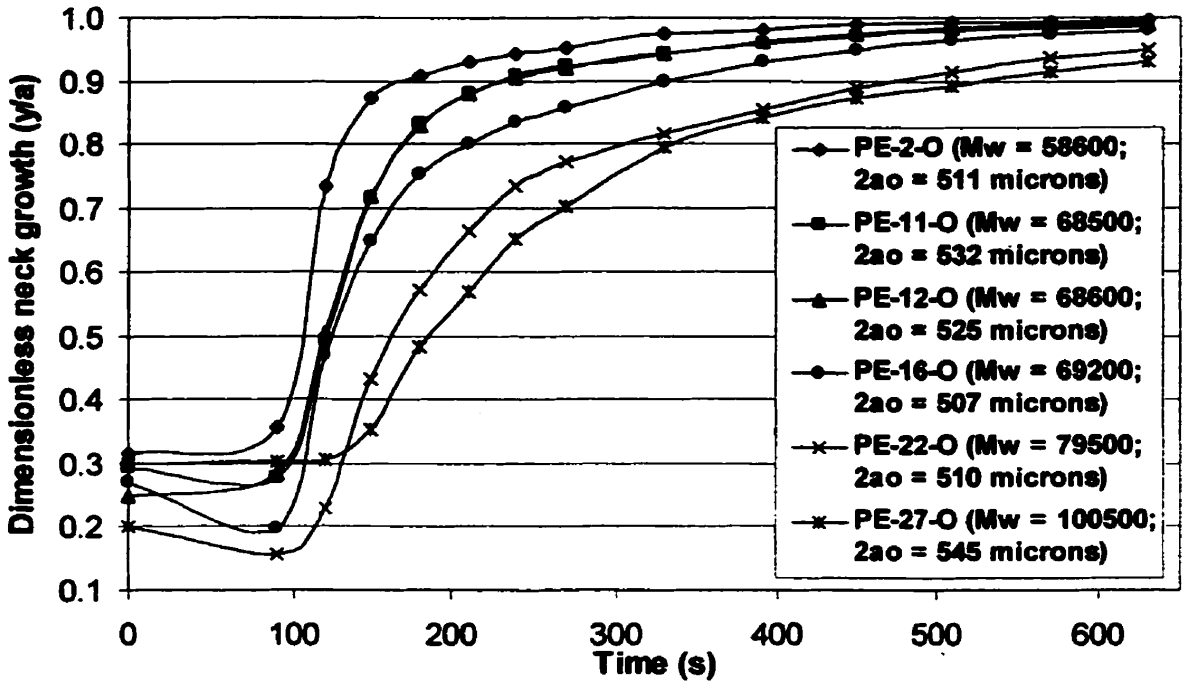

Figure 4.10 Neck growth evolution for octene resins. Experiments with cylinders at ramped temperature (111 to 226.5 °C at 11°C/min)

4.2.2 Molecular weight distribution

The molecular weight of polymers is not a unique value but a distribution of different values. The polydispersity index or PDI (M_w/M_n) gives an indication of the broadness of such distribution. The smaller the PDI, the narrower the distribution. The MWD is a consequence of the type of polymerization and the conditions under which the reactions took place. A broader MWD influences the rheological properties in that the shear-thinning behavior is enhanced and the elastic properties increased. The thermal properties are also affected by MWD. The low molecular weight chains, usually highly branched in the case of LLDPE, tend to segregate forming amorphous regions or less stable crystallites. The melting range broadens as a result. Moreover, those amorphous regions can seriously affect interdiffusion according to the experimental evidence found by Qureshi et al. (2001) and Poon et al. (2001).

Figure 4.11 compares the sintering behavior of PE-2-O and PE-3-O using powder at 170 °C. The results obtained using cylinders under the same conditions are nearly identical to those presented in Figure 4.11. The non-isothermal sintering results using cylinders are presented in Figure 4.12. Even though these two resins have comparable values of M_w and zero-shear viscosity, they have different molecular structure, as discussed in the previous chapter. It appears that the differences in the resins' molecular structure cannot be detected in the sintering results obtained at constant temperature (Figure 4.11). The results obtained at ramped temperature using cylinders, on the other hand, show that PE-2-O sinters at a faster rate than PE-3-O. The faster sintering rate of PE-2-O over that of PE-3-O could be due to their different MWD. The influence of the MWD on the sintering behavior of these two resins is probably seen through its effect on the heat of fusion, which is lower for PE-2-O than for PE-3-O rather than through its effect on the resin elasticity.

The sintering behavior of three low viscosity hexene copolymers is presented in Figures 4.13 to 4.16. The characterization of these three resins has clearly shown

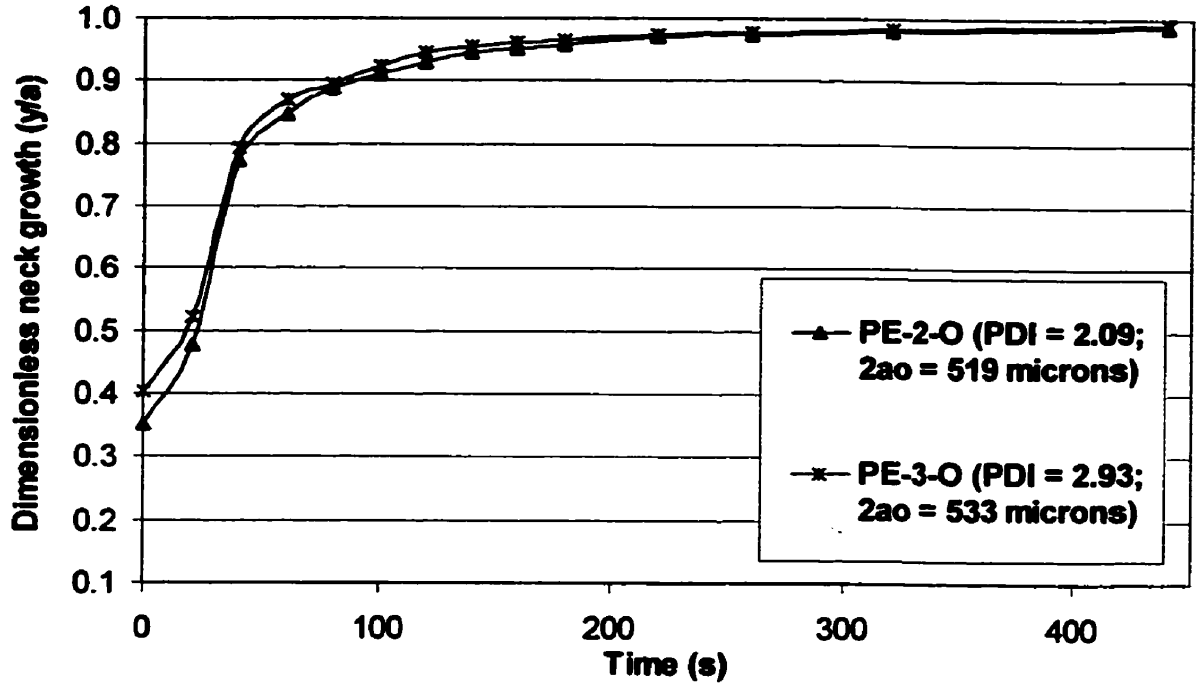

Figure 4.11 Neck growth evolution for octene resins in powder form. Experiments at constant temperature (170°C)

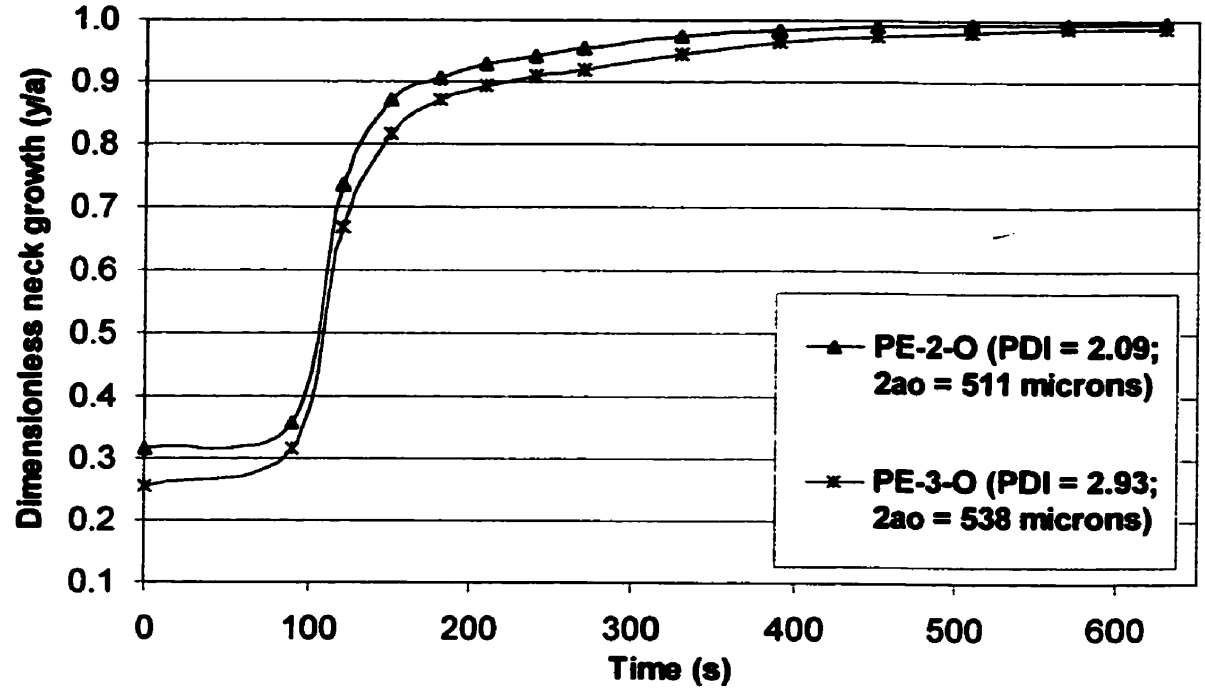

Figure 4.12 Neck growth evolution for octene resins. Experiments with cylinders at ramped temperature (111 to 226.5 °C at 11°C/min)

that while the M_w of PE-5-H is comparable to that of PE-4-H and PE-6-H, it has a broader MWD and a much broader SCB distribution than PE-4-H and PE-6-H. The sintering curves obtained at constant temperature (Figures 4.13 and 4.14) do not show any difference between these three resins but the sintering curves obtained for the experiments conducted at ramped temperature are separated (Figures 4.15 and 4.16). As expected, PE-4-H is found to sinter at a faster rate than PE-5-H. This result can be explained based on the differences in the viscosity temperature dependence (Figure 3.4). In the early stages of the experiments conducted at ramped temperature, PE-5-H has a much higher viscosity than both PE-4-H and PE-6-H. While the results with powder particles show that PE-6-H sinters at a faster rate than PE-5-H, the two resins have comparable sintering rates when cylinders are used. The results obtained with cylinders (Figure 4.16) may be explained by the fact that the lower viscosity of PE-6-H at low temperatures compared to PE-5-H is being counteracted by its greater heat of fusion.

4.2.3 Comonomer type and content

It has been reported that neither the type of comonomer nor its amount have an effect on the rheological properties measured in the linear viscoelastic region (Wood-Adams et al., 2000). However, it has also been reported that the type and distribution of LLDPE branches influence the melt strength (Goyal, 1995). The melt strength is related to extensional viscosity, a material property that is not easy to measure but which is relevant to sintering due to the nature of the flow. It is well known, on the other hand, that the presence of SCB strongly impacts the thermal properties and crystalline structure. In very general terms, the melting temperature and degree of crystallinity decrease with increasing SCB. Nevertheless, it is still unclear whether the branch length also influences the thermal properties.

Of all the twenty-six resins, PE-6-H and PE-7-O are the two with comparable molecular structures while having different types of comonomers. The results of sintering experiments carried out at constant temperature with powder particles are

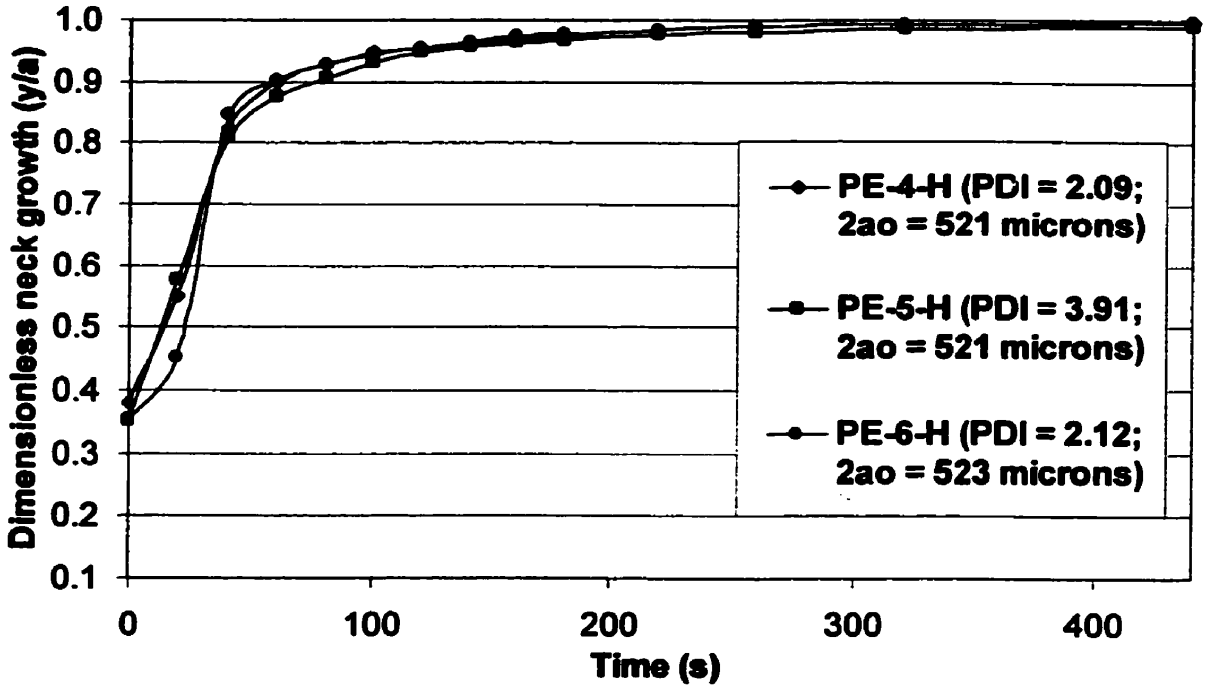

Figure 4.13 Neck growth evolution for hexene resins in powder form. Experiments at constant temperature (170°C)

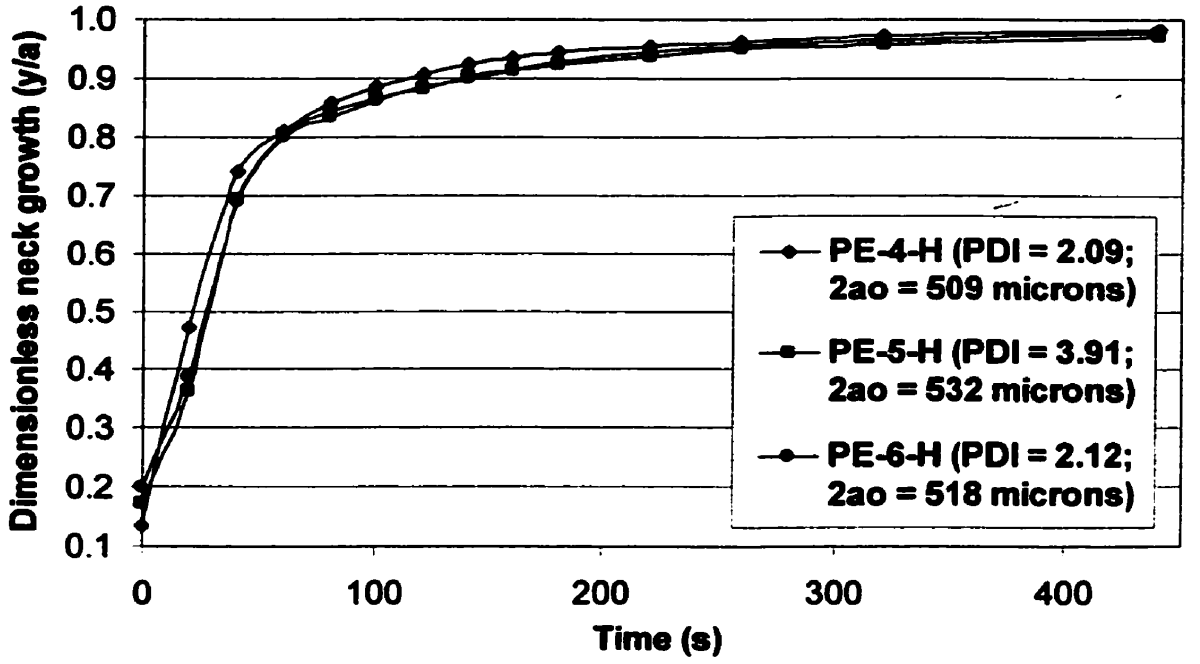

Figure 4.14 Neck growth evolution for hexene resins. Experiments with cylinders at constant temperature (170°C)

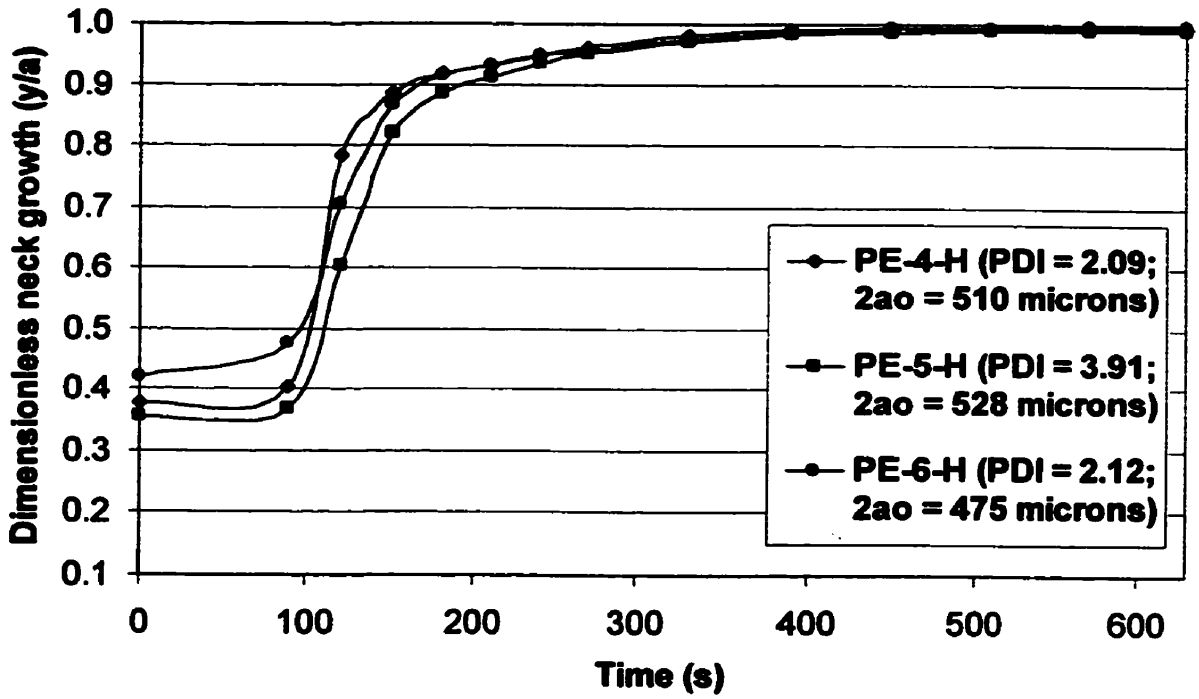

Figure 4.15 Neck growth evolution for hexene resins in powder form. Experiments at ramped temperature (111 to 226.5 °C at 11°C/min)

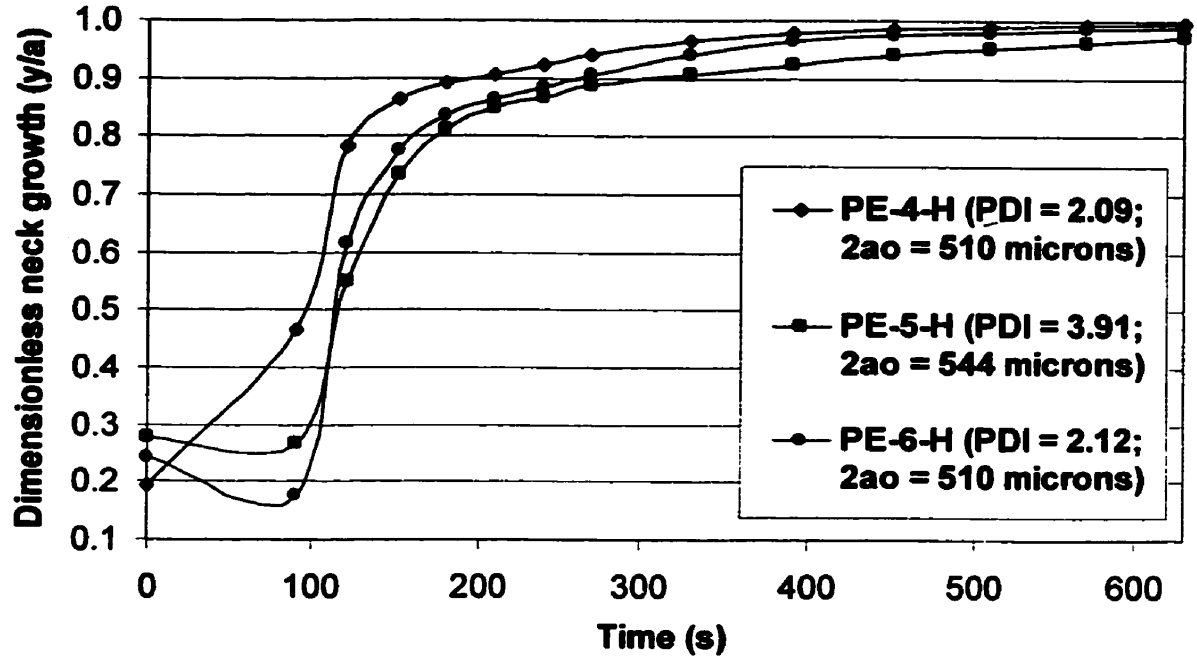

Figure 4.16 Neck growth evolution for hexene resins. Experiments with cylinders at ramped temperature (111 to 226.5 °C at 11°C/min)

presented in Figure 4.17. The curves are very close and similar results were obtained using cylinders. Those trends were also observed in experiments conducted at ramped temperature (Figure 4.18). Nonetheless, these two resins have different rheological and thermal properties that most likely have arisen from differences in branching distribution and copolymerization conditions. PE-6-H is less viscous and less elastic than PE-7-O, but it has a higher melting temperature and heat of fusion (crystallinity). Those effects may have counteracted each other. It is difficult to say whether the length of the SCB have an effect on sintering or not.

The sintering behavior of PE-25-O, PE-26-O and PE-27-O at constant temperature is presented in Figure 4.19. These three resins have comparable M_w and MWD but their comonomer content is completely different. As a result, variations in the values of melting temperature and degree of crystallinity are observed. The values of degree of crystallinity, related to heat of fusion, are presented to give the reader a perspective of the comonomer content. It can be seen that PE-27-O, the resin with fewer branches, sinters fastest. PE-27-O is closely followed by PE-26-O and PE-25-O, respectively. The sintering curves are ordered according to comonomer content. According to Wu (1982) there are important differences in surface tension between amorphous and crystalline regions. He mentioned that the values of the crystalline surface tension could be almost twice the values of the amorphous surface tension. A polymer with a higher degree of branching is less crystalline because the SCB are usually excluded from the crystal lattice. Since surface tension is the one of the main driving forces of the sintering process, it is then expected that an increasing number of SCB will generate more amorphous regions and as a result the sintering rate will be decreased. This effect is consistent with the observations made in Figure 4.19.

The effects of SCB on the sintering process are also evident for the results obtained at ramped temperature (Figure 4.20). It can be seen that as the comonomer content increases the onset of sintering neck growth occurs at lower temperatures. This effect is however counteracted by a slower sintering rate. An

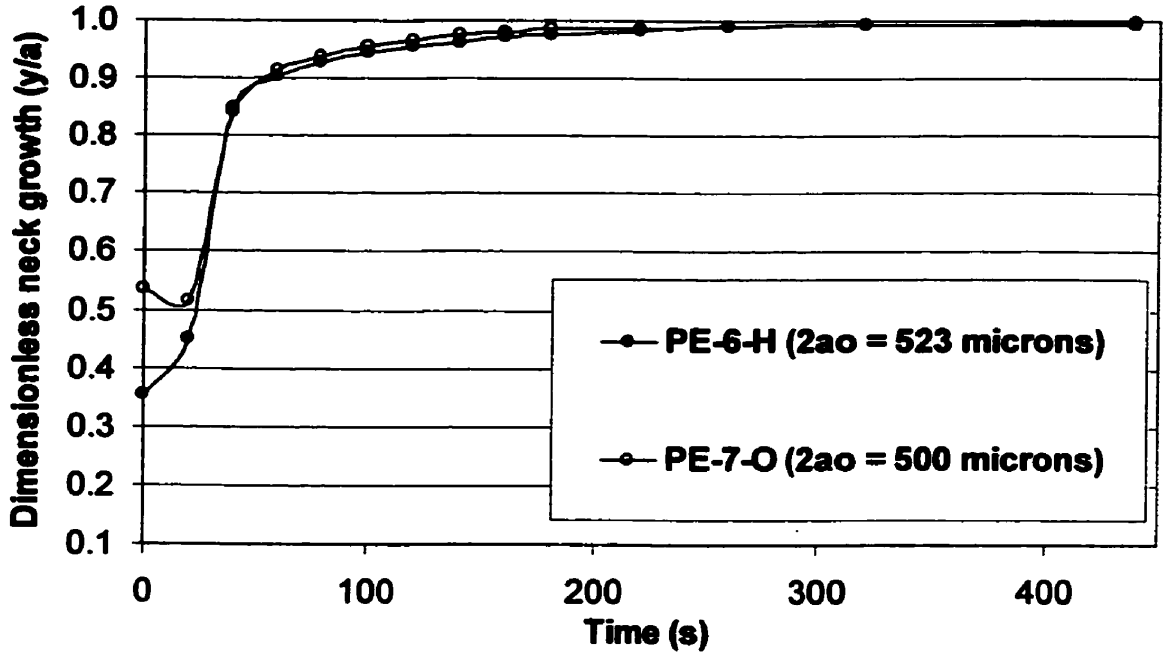

Figure 4.17 Neck growth evolution for LLDPE resins in powder form. Experiments at constant temperature (170°C)

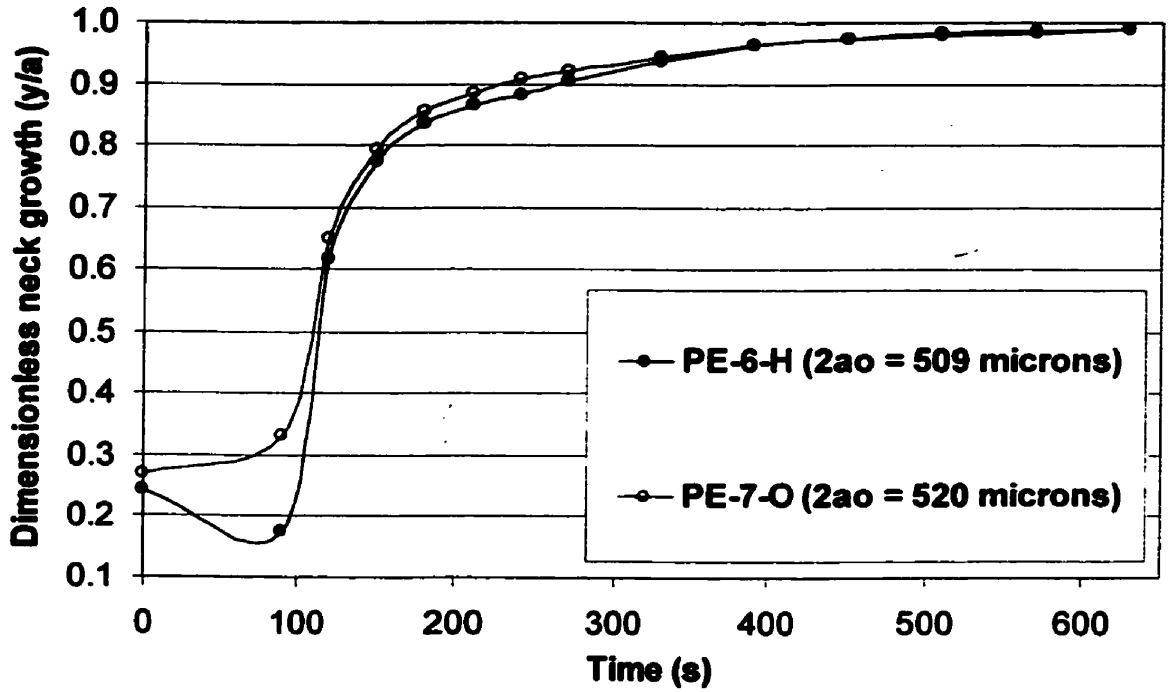

Figure 4.18 Neck growth evolution for LLDPE resins. Experiments with cylinders at ramped temperature (111 to 226.5 °C at 11°C/min)

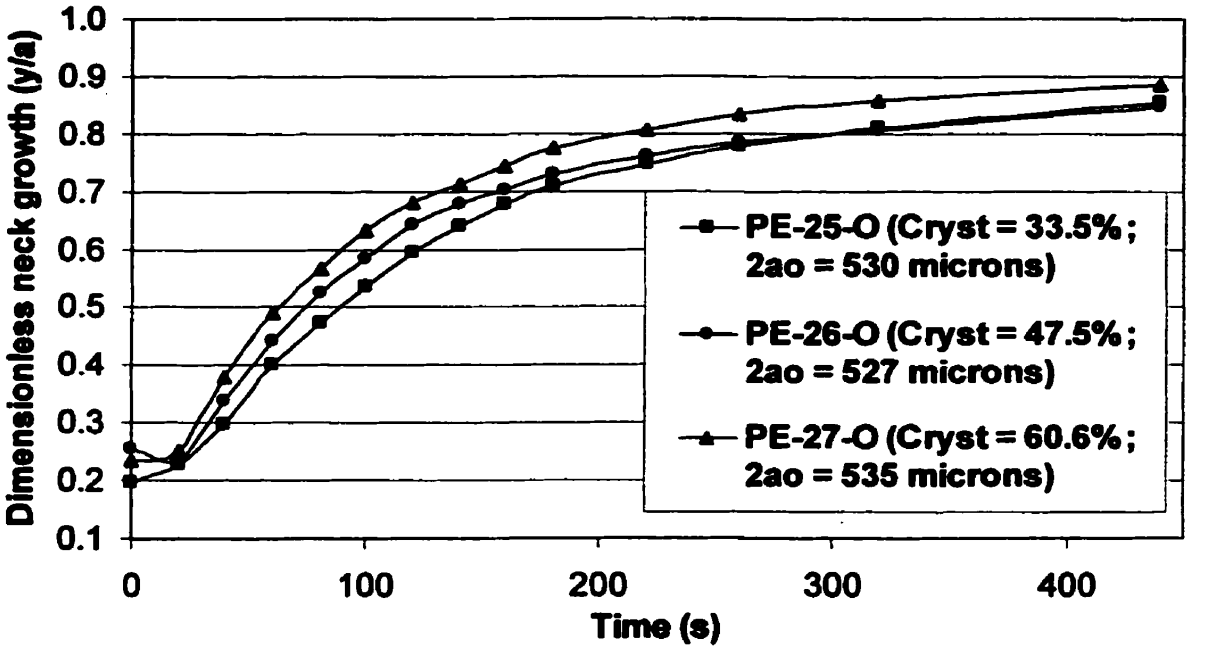

Figure 4.19 Neck growth evolution for octene resins. Experiments with cylinders at constant temperature (170°C)

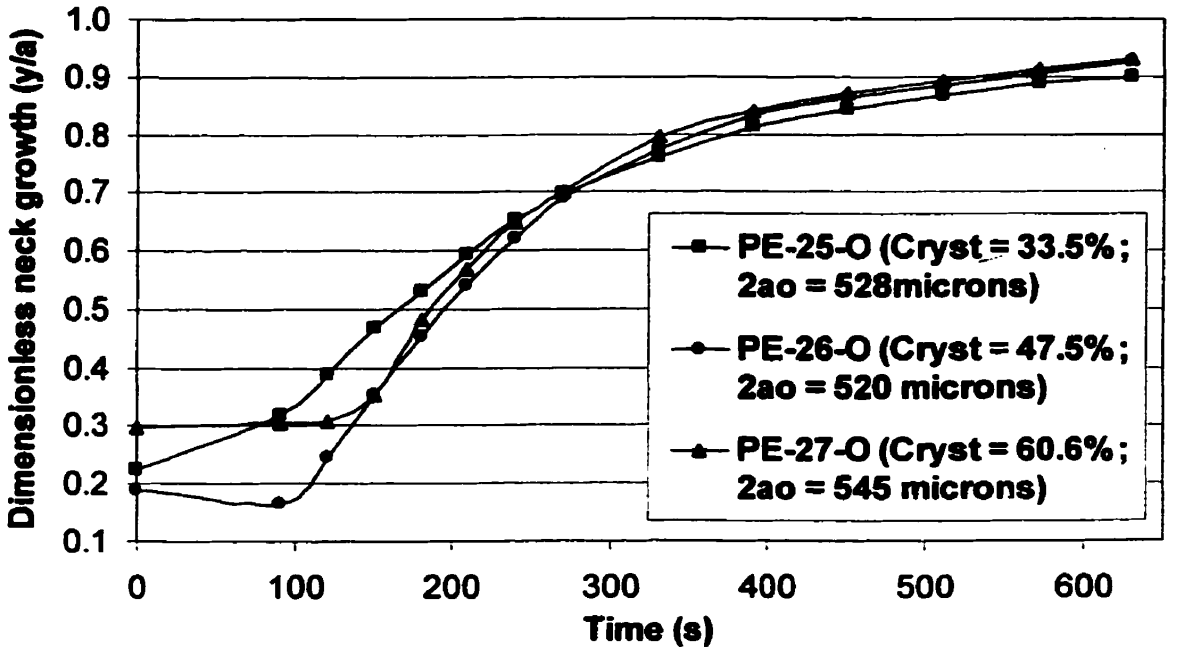

Figure 4.20 Neck growth evolution for octene resins. Experiments with cylinders at ramped temperature (111 to 226.5 °C at 11°C/min)

increase in comonomer content generally results in a decrease of the heat of fusion and the melting temperature. This effect is observed with PE-25-O, PE-26-O and PE-27-O and can explain the variations in the temperatures at which the sintering process starts between the three resins. The differences seen in the sintering rates may also originate by the differences in the chain mobility due to variations of the chain linearity. The more linear the chains, the faster they should diffuse (Riande et al, 2000). Moreover, there is evidence that UHMWPE, which is usually highly crystalline, exhibits sintering rates much higher than expected (Siegman et al, 1986; Barnetson, and Hornsby, 1995). This has been partly explained in terms of crystallite morphology and chain mobility. Rastogi et al. (1998) studied the sintering of ultrahigh molecular weight polyethylene crystallized under special conditions. Such crystallization process allowed the formation of a highly mobile chain conformation which, according to these researchers, significantly improves the sintering process.

4.2.4 Rheological properties

It has been recognized that the materials' viscosity and elasticity play a major role in polymer sintering (Mazur, 1995; Bellehumeur et al., 1996). Since both viscosity and elasticity represent resistances to the sintering neck growth, their increase translates into slower sintering rates. In the following sections the resins are divided according to zero-shear viscosity and their sintering behavior is compared.

4.2.4.1 Low viscosity

The sintering neck growth of four low-viscosity resins (PE-1-O, PE-4-H, PE-6-H and PE-8-B) are presented in Figures 4.21 to 4.24. While the four resins have comparable values of zero-shear viscosity at 170°C, their viscosity-temperature dependence varies from one resin to another. The results obtained from the material characterization indicate that both PE-4-H and PE-6-H have a slightly more homogeneous chemical composition that PE-1-O. They also show that the molecular

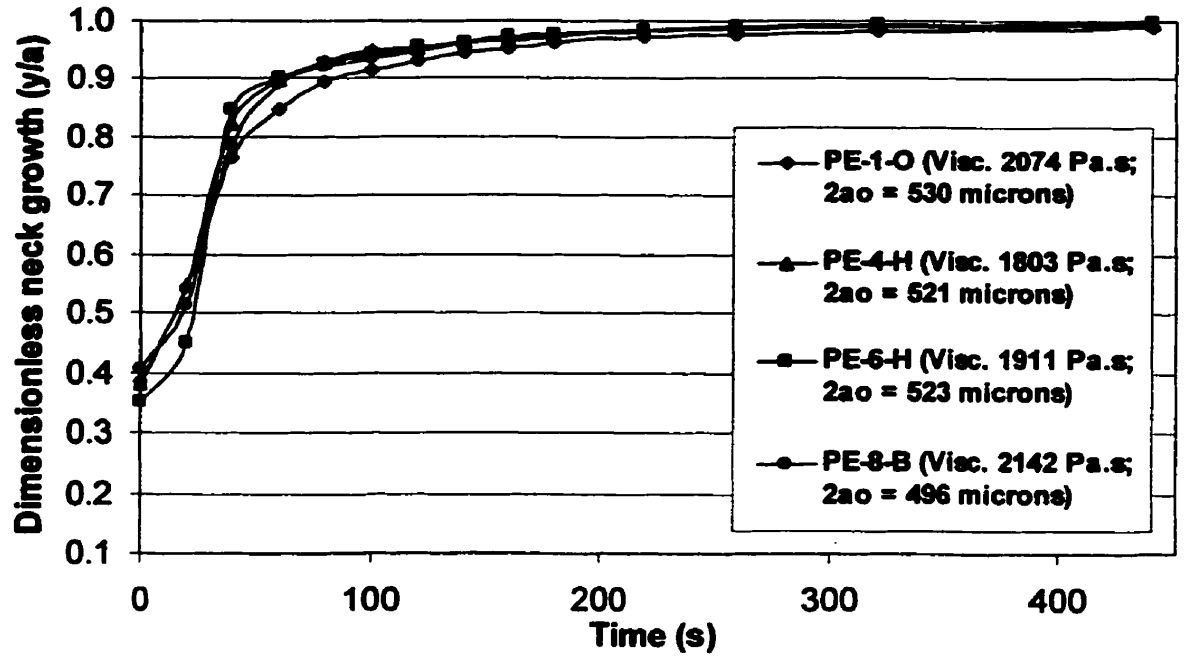

Figure 4.21 Neck growth evolution for low-viscosity resins in powder form. Experiments at constant temperature (170°C)

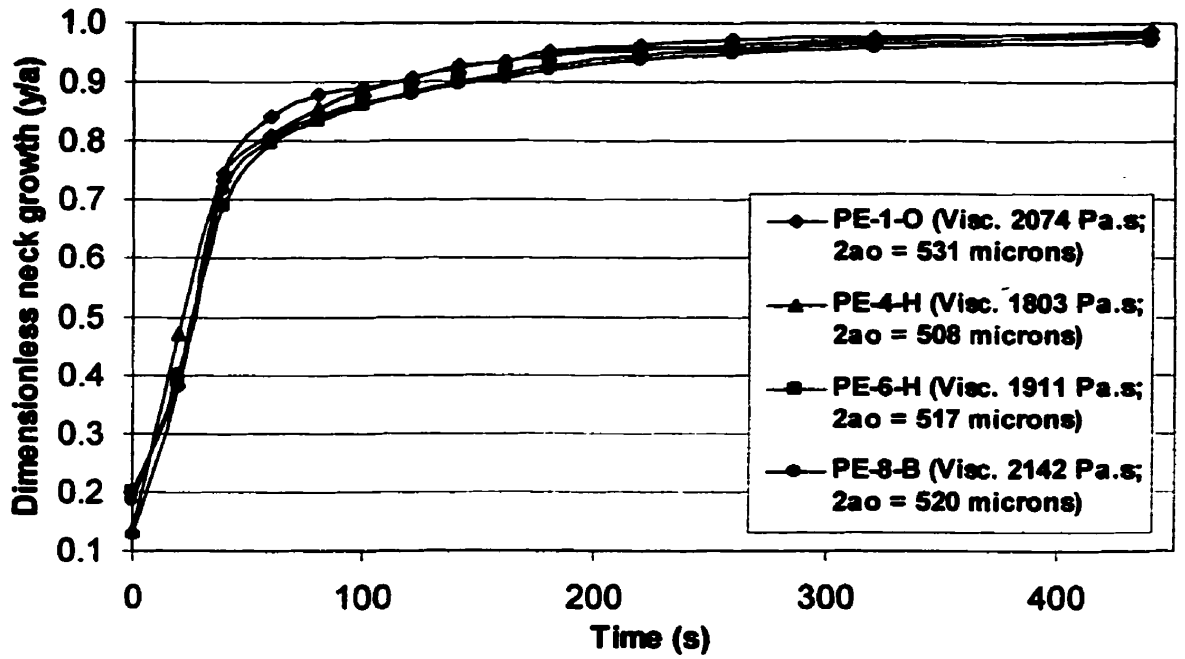

Figure 4.22 Neck growth evolution for low-viscosity resins. Experiments with cylinders at constant temperature (170°C)

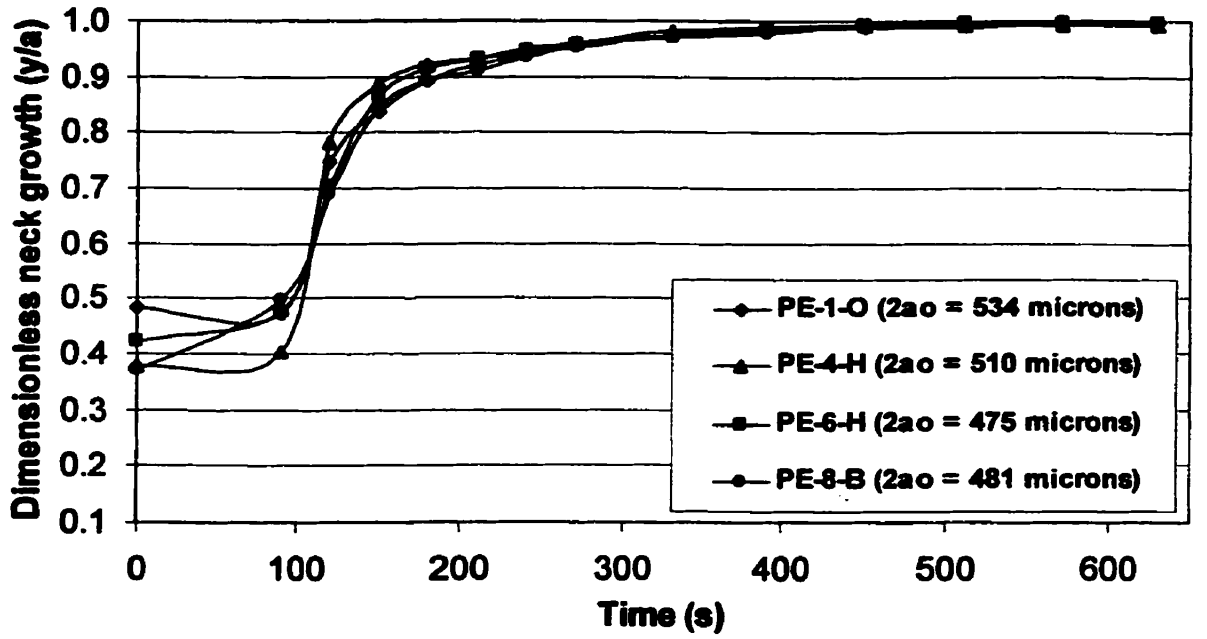

Figure 4.23 Neck growth evolution for low-viscosity resins in powder form. Experiments at ramped temperature (111 to 226.5 °C at 11°C/min)

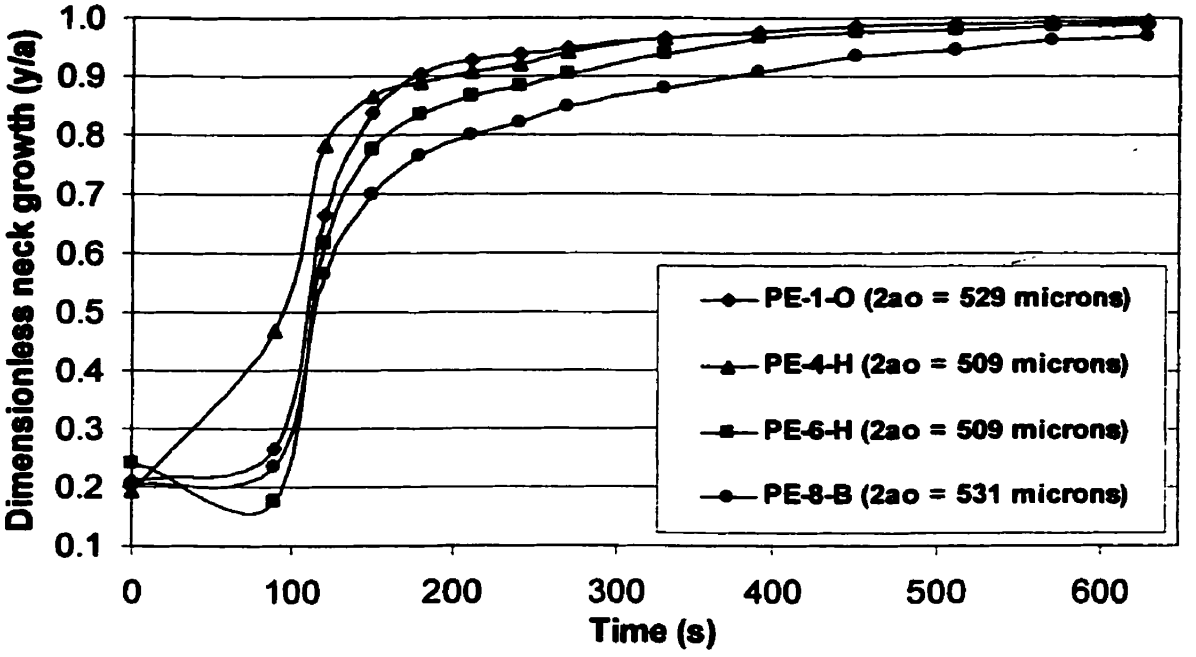

Figure 4.24 Neck growth evolution for low-viscosity resins. Experiments with cylinders at ramped temperature (111 to 226.5 °C at 11°C/min)

structure (MWD, SCB distribution) of PE-8-B is altogether different than PE-1-O, PE-4-H and PE-6-H probably due to differences in the catalyst and conditions used in the polymerization process. Figure 4.21 shows that the sintering rate and the required time to complete the coalescence are very similar for all the resins. Results obtained using cylinders (Figure 4.22) are similar to those presented in Figure 4.21. Despite the differences in the molecular structure, the sintering behavior at constant temperature for these resins is consistent with the expected trends based on viscous flow mechanism models.

Results from non-isothermal experiments obtained with powder particles differ from those obtained with cylinders. The sintering curves for powder particles are very close to one another in spite of the differences in the viscosity-temperature dependence exhibited by the four resins (Figure 4.23). This observation confirms the hypothesis that the large surface area of powder particles somewhat reduces the relative impact of the other properties on the sintering rate.

The results obtained with cylinders under non-isothermal conditions follow, to some extent, the trends expected based on the thermal and rheological properties of these resins. Accordingly, the effect of the low melting temperature of PE-4-H on sintering is evident in Figure 4.24. PE-6-H and PE-8-B have a melting temperature 3 °C above that of PE-4-H and as a result, they sinter at a slower rate. The only exception is the sintering behavior of PE-1-O, which remains close to that of PE-4-H, despite the fact that PE-1-O has a higher melting point and higher zero-shear viscosity at low temperature. PE-1-O has, however, a lower M_w which may have enhanced the chain diffusion in the sintering process.

The sintering behavior of PE-2-O, PE-3-O and PE-5-H are compared in Figures 4.25 and 4.26 (constant temperature) and Figures 4.27 and 4.28 (ramped temperature). It can be observed that PE-5-H sinters more slowly than PE-2-O and PE-3-O under all conditions with the exception of the isothermal experiments using powder particles in which the trends are not well resolved. Although the three resins

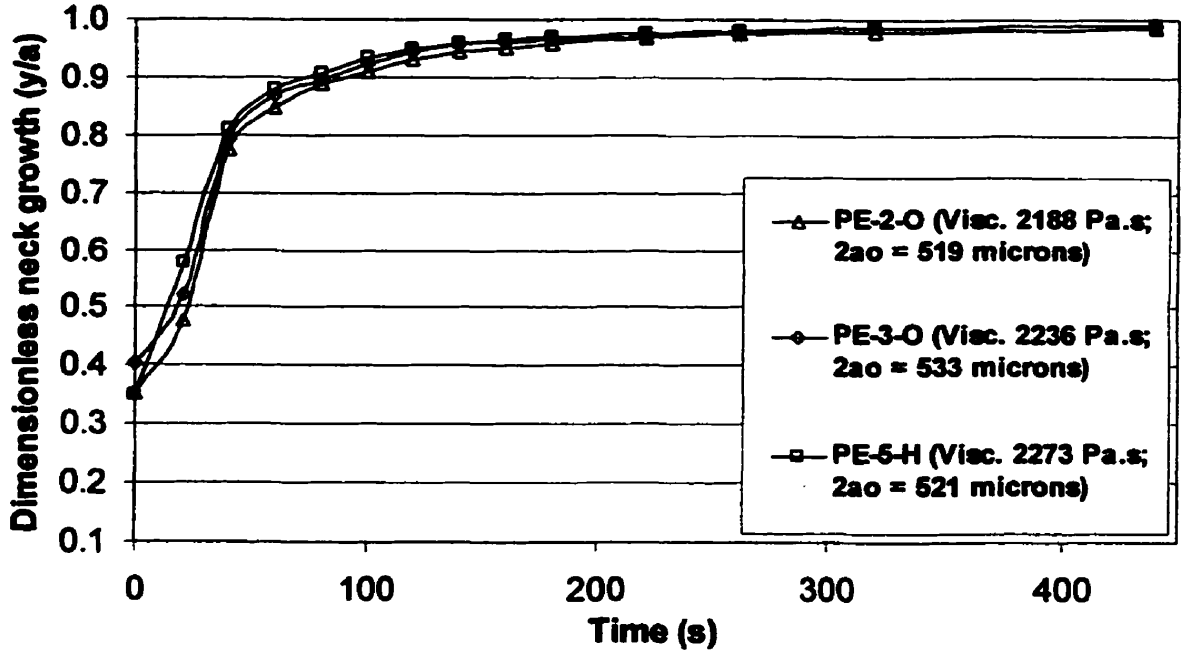

Figure 4.25 Neck growth evolution for low-viscosity resins in powder form. Experiments at constant temperature (170°C)

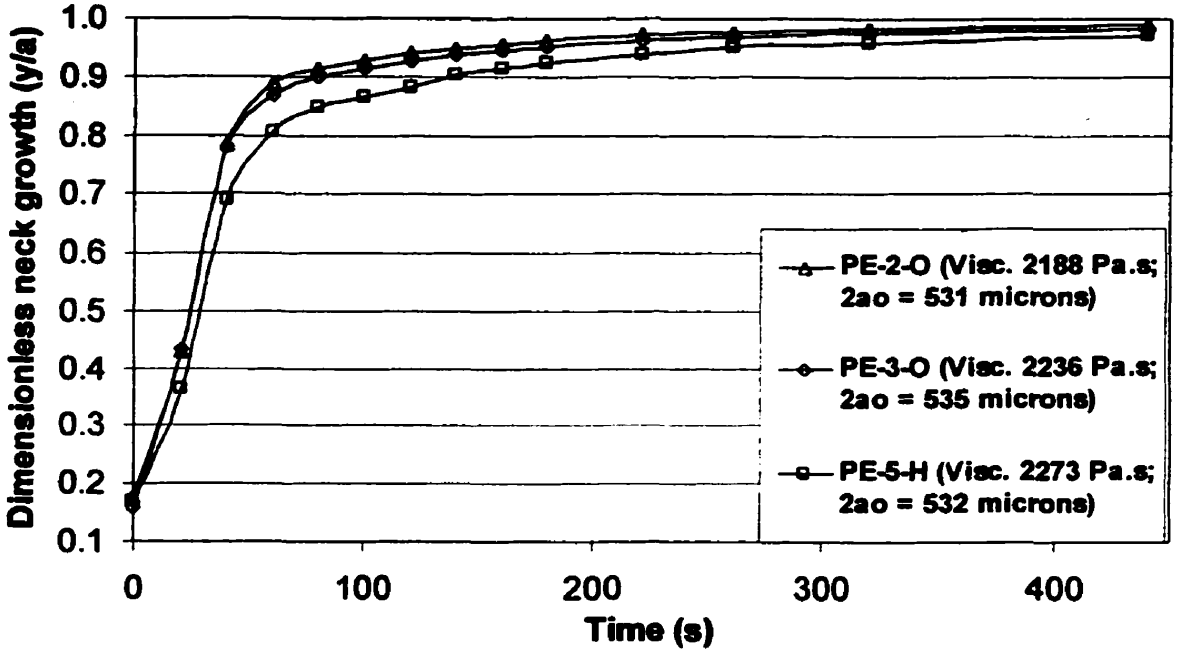

Figure 4.26 Neck growth evolution for low-viscosity resins. Experiments with cylinders at constant temperature (170°C)

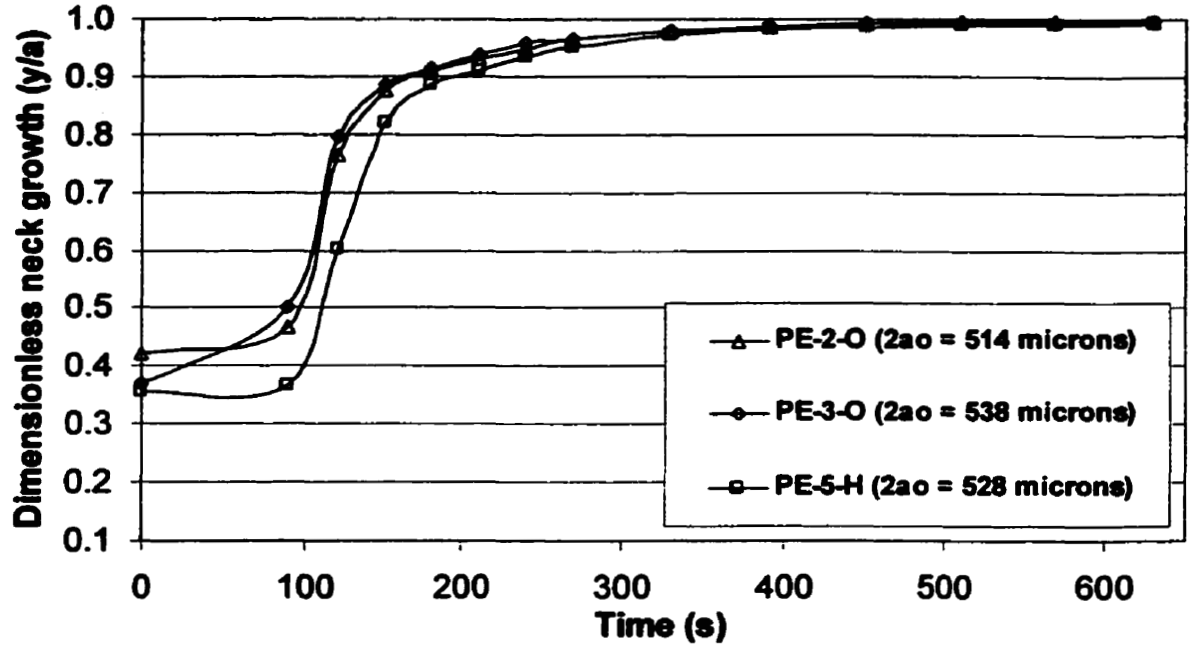

Figure 4.27 Neck growth evolution for low-viscosity resins in powder form. Experiments at ramped temperature (111 to 226.5 °C at 11°C/min)

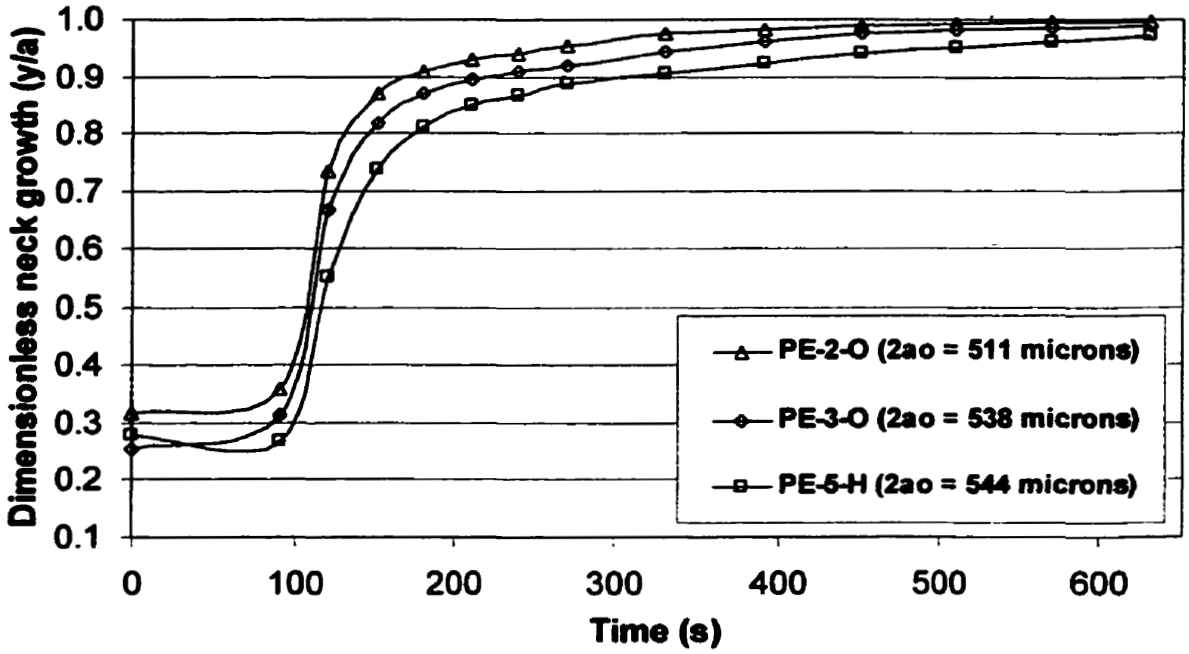

Figure 4.28 Neck growth evolution for low-viscosity resins. Experiments with cylinders at ramped temperature (111 to 226.5 °C at 11°C/min)

exhibit comparable values of zero-shear viscosity at 170 °C, there are many differences between them including type, amount and distribution of branches, molecular weight distribution. These differences in microstructure alter both the elastic and thermal properties. For the non-isothermal experiments using cylinders (Figure 4.28), the sintering curves seem to be organized according to MWD. PE-2-O, the resin with the narrowest MWD, sinters fastest. It is followed by PE-3-O and PE-5-H, the latter being the resin with the broadest MWD. Based on the thermal analysis presented in Chapter 3, PE-5-H has a higher amount and broader distribution of SCB than PE-2-O and PE-3-O. These differences in the chemical composition distribution in addition to the MWD may explain the differences in the sintering behavior seen in Figure 4.26 and 4.27.

Experimental results obtained with PE-7-O and PE-10-H, two resins with zero-shear viscosity of 3000 Pa.s, are presented in Figures 4.29 and 4.30 (constant temperature) and Figures 4.31 and 4.32 (ramped temperature). When powder particles are used, similar trends are observed. On the other hand, the sintering curves for the two resins separate when slow-cooled cylinders are used. This separation between the curves is more dramatic for experiments conducted at ramped temperature than those at constant temperature. In Figure 4.32, PE-9-O has been included for comparison. While this resin has a comparable value of viscosity, it is more elastic than PE-7-O and PE-10-O. PE-7-O sinters at a faster rate than PE-9-O, which is expected based on the differences in elasticity of these two resins. PE-10-H, however, shows similar elastic properties as PE-7-O, and yet it behaves as PE-9-O in the sintering process. The differences in the sintering behavior of the three resins when cylinders are used can be attributed to the fact that the molecular structure of PE-9-O is different to that of PE-10-H. Furthermore, PE-10-H has a molecular structure (MWD, SCB) that is more heterogeneous than that of PE-7-O.

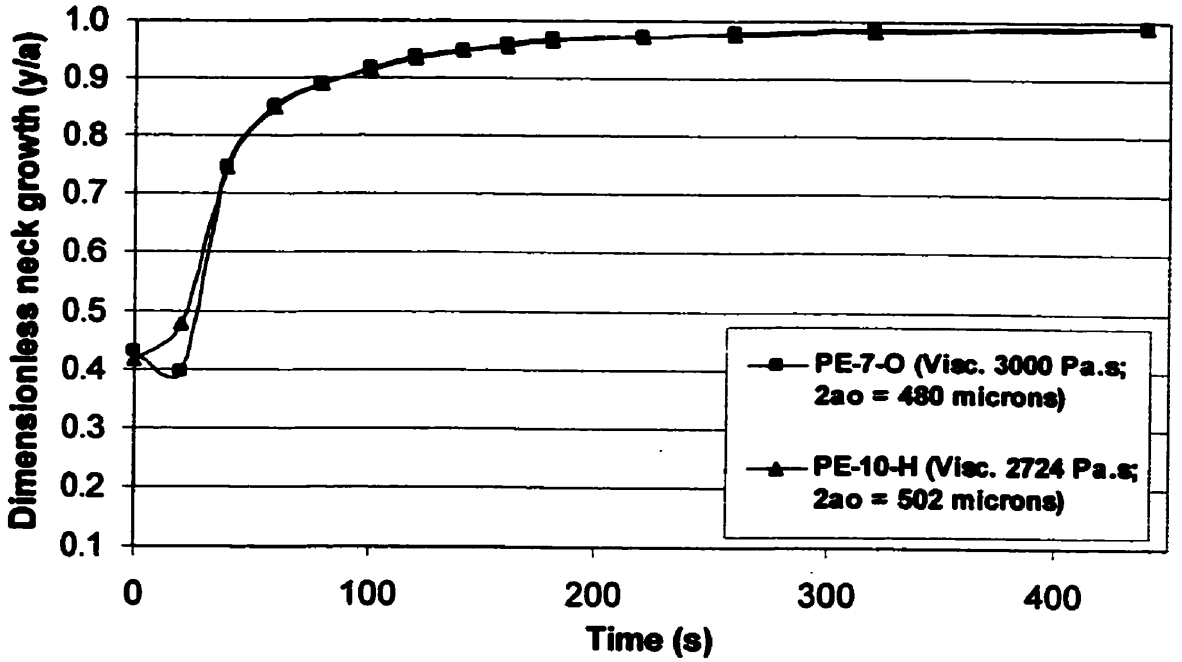

Figure 4.29 Neck growth evolution for low-viscosity resins in powder form. Experiments at constant temperature (170°C)

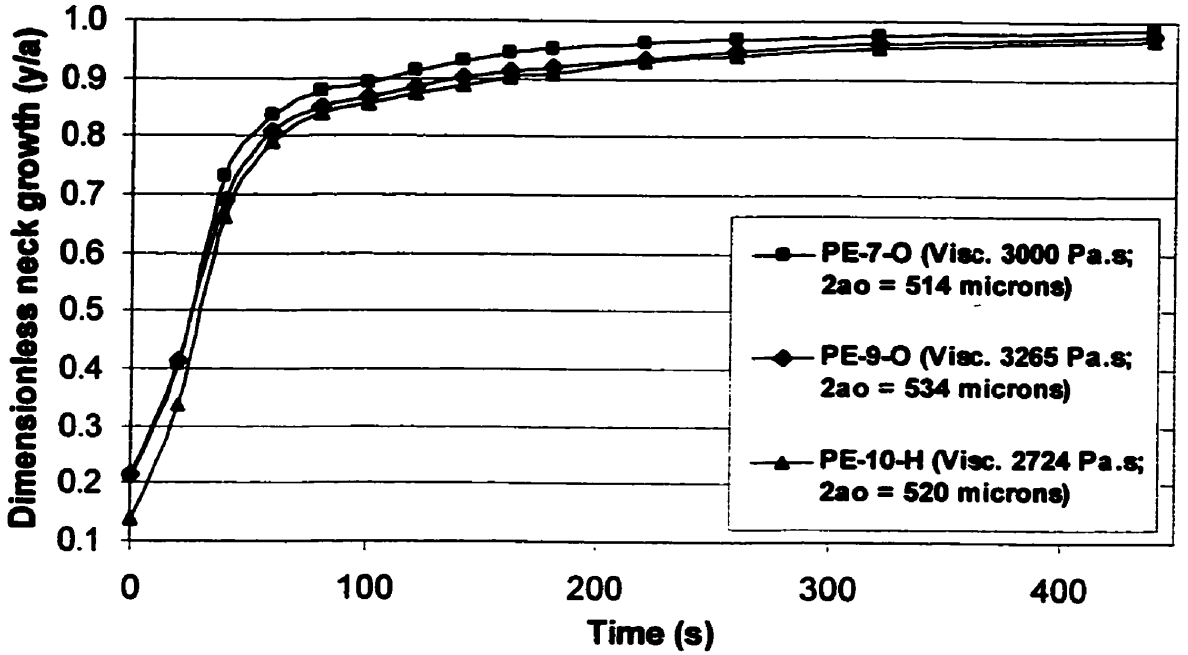

Figure 4.30 Neck growth evolution for low-viscosity resins. Experiments with cylinders at constant temperature (170°C)

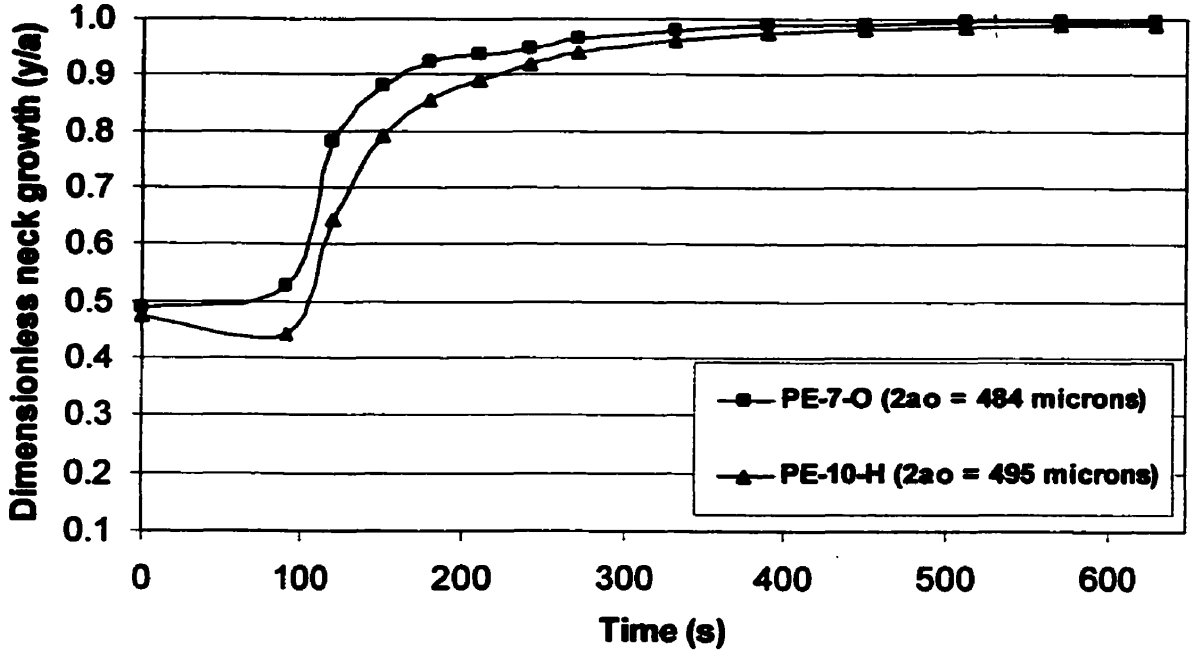

Figure 4.31 Neck growth evolution for low-viscosity resins in powder form. Experiments at ramped temperature (111 to 226.5 °C at 11°C/min)

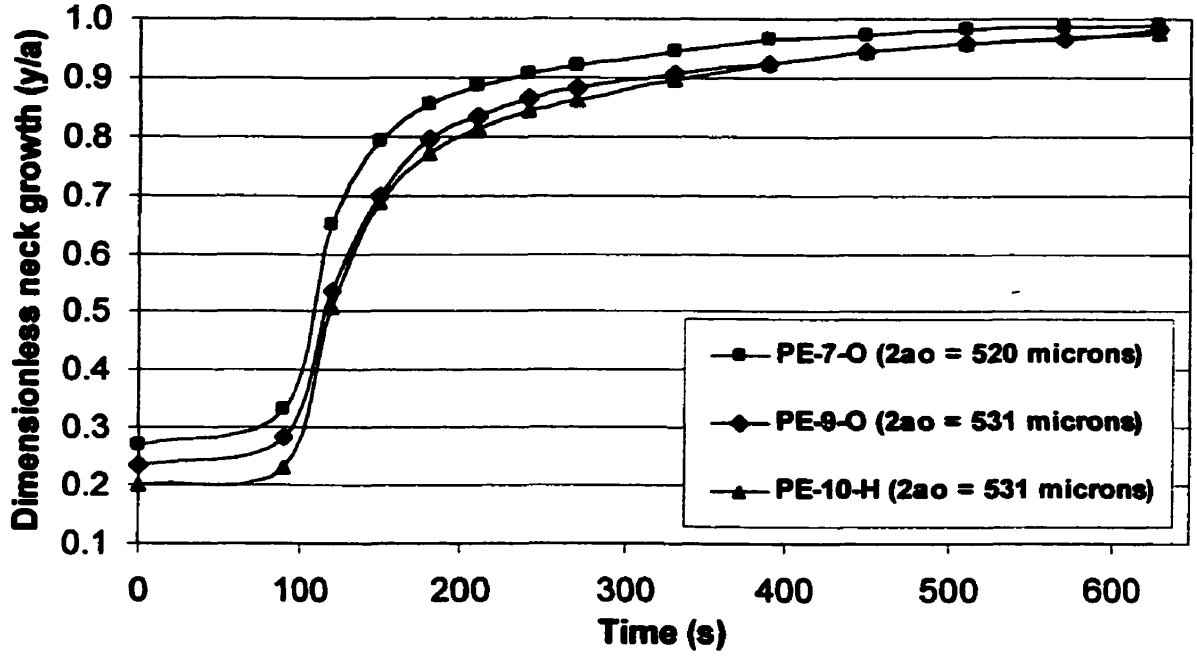

Figure 4.32 Neck growth evolution for low-viscosity resins. Experiments with cylinders at ramped temperature (111 to 226.5 °C at 11°C/min)

4.2.4.2 Medium viscosity

The sintering results for PE-16-O and PE-17-O are compared in Figures 4.33 and 4.34 (constant temperature) and Figures 4.35 and 4.36 (ramped temperature). PE-18-H has been included in Figures 4.34 and 4.36 for comparison. Apart from experiments using cylinders at constant temperature, PE-16-O sinters slightly faster under all conditions. This resin has lower viscosity and is less elastic as indicated by its larger value of *tan* δ.

Figures 4.37 and 4.38 compare the sintering rates of PE-13-O, PE-15-O, PE-19-H and PE-21-H which have similar zero-shear viscosity at 170 °C. In terms of elasticity, only PE-19-H exhibits high values of *tan* δ (Figure 3.13) i. e. low elasticity. It can be seen that all the resins sinter in a very similar way regardless of their different elasticity. The results from experiments conducted under non-isothermal conditions are presented in Figures 4.39 and 4.40 for powder and cylindrical particles, respectively. Neither with powder nor cylinders can significant differences in the sintering behavior for these four resins be observed. The exception is PE-15-O which shows a slower sintering rate (Figure 4.40). It is difficult to determine why the resins behave the way they do. PE-19-H clearly shows lower elastic properties than its counterparts. Both PE-19-H and PE-21-H have comparable values of zero-shear viscosity and viscosity-temperature dependence but they have a much larger apparent Mw than PE-13-O and PE-15-O. This higher Mw may have had a negative impact on the chain diffusion which would appear to be more important during ramped temperature experiments using cylinders.

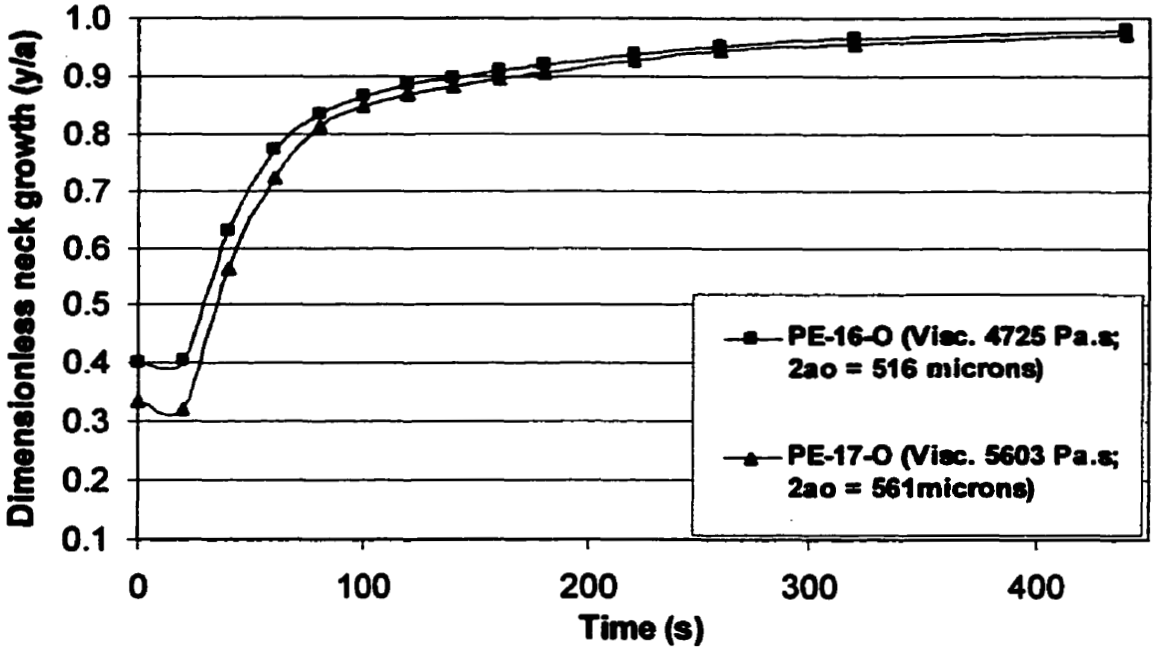

Figure 5.33 Neck growth evolution for medium-viscosity resins in powder form. Experiments at constant temperature (170°C)

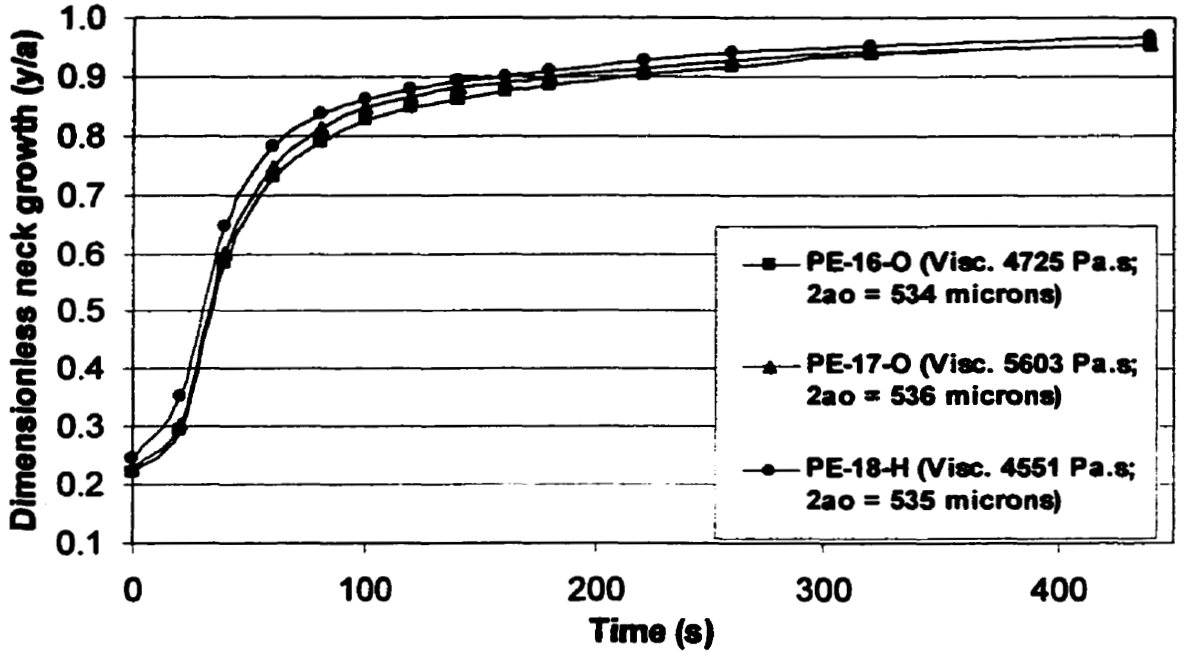

Figure 4.34 Neck growth evolution for medium-viscosity resins. Experiments with cylinders at constant temperature (170°C)

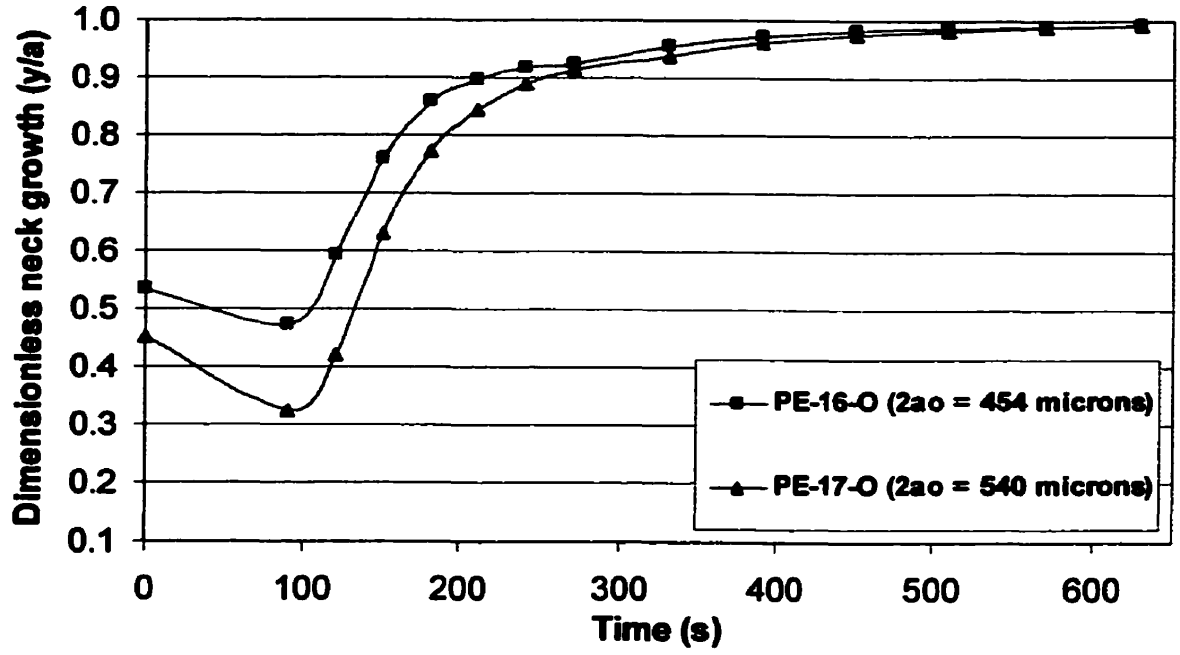

Figure 4.35 Neck growth evolution for medium-viscosity resins in powder form. Experiments at ramped temperature (111 to 226.5 °C at 11°C/min)

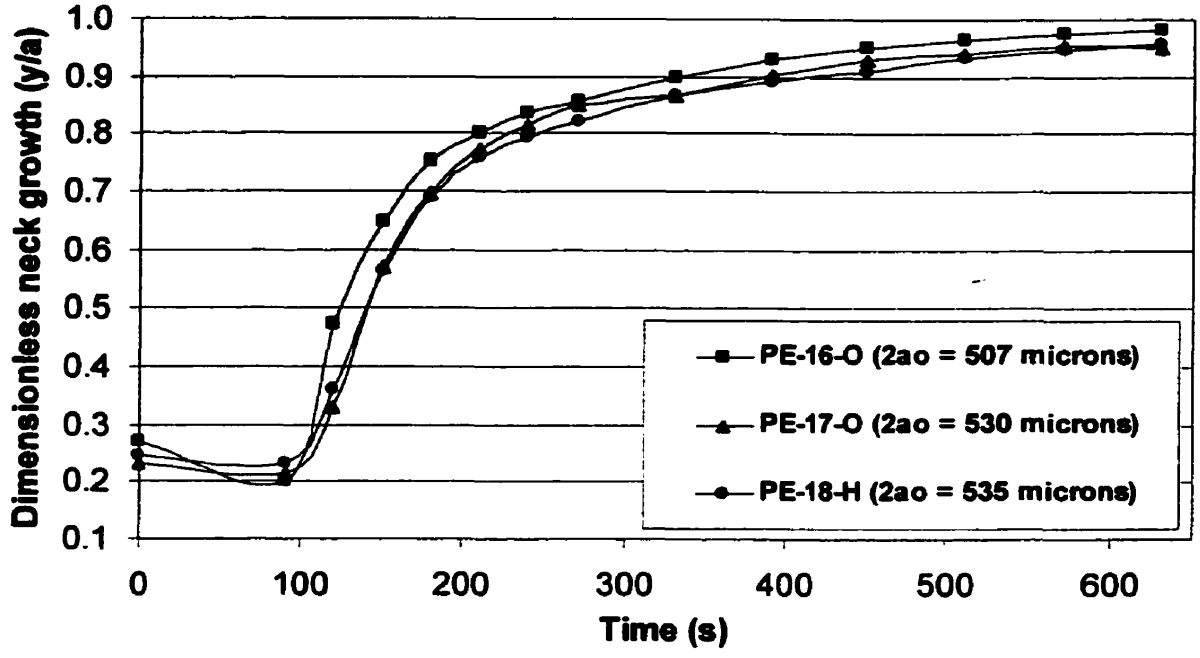

Figure 4.36 Neck growth evolution for medium-viscosity resins. Experiments with cylinders at ramped temperature (111 to 226.5 °C at 11°C/min)

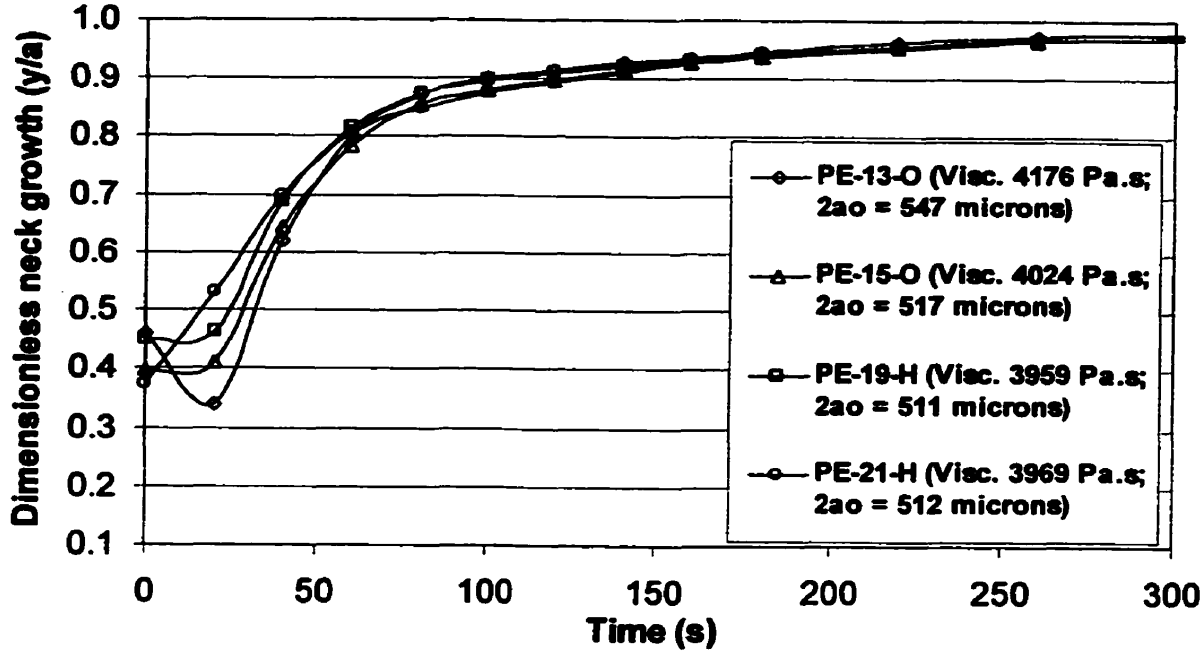

Figure 4.37 Neck growth evolution for medium-viscosity resins in powder form. Experiments at constant temperature (170°C)

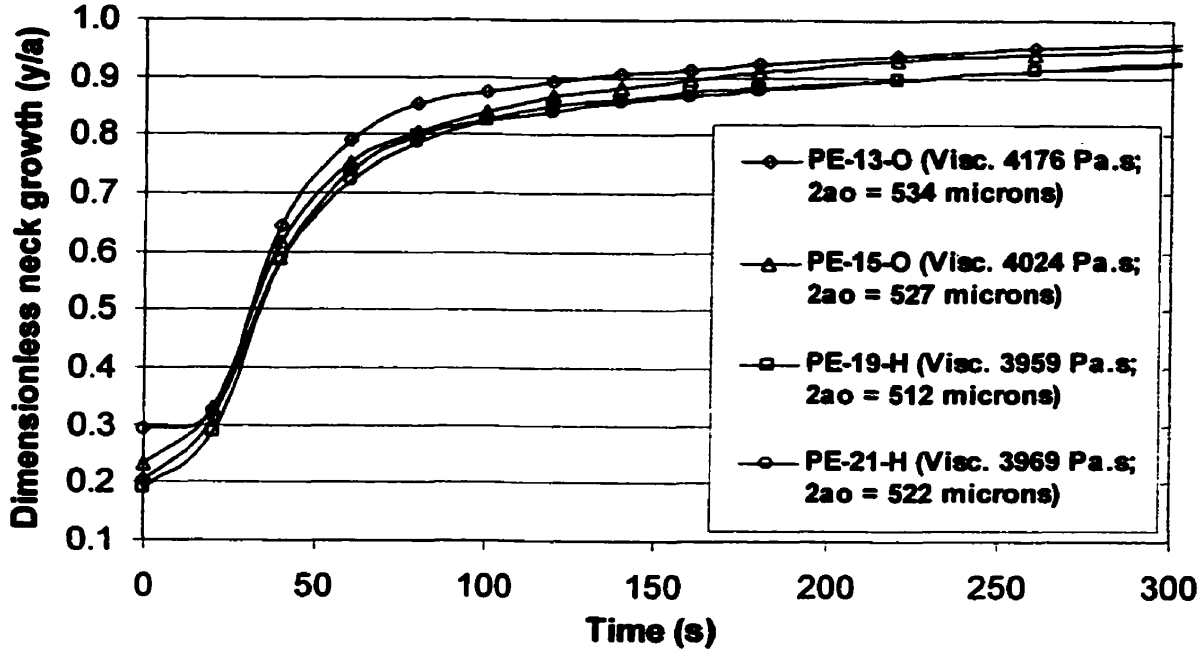

Figure 4.38 Neck growth evolution for medium-viscosity resins. Experiments with cylinders at constant temperature (170°C)

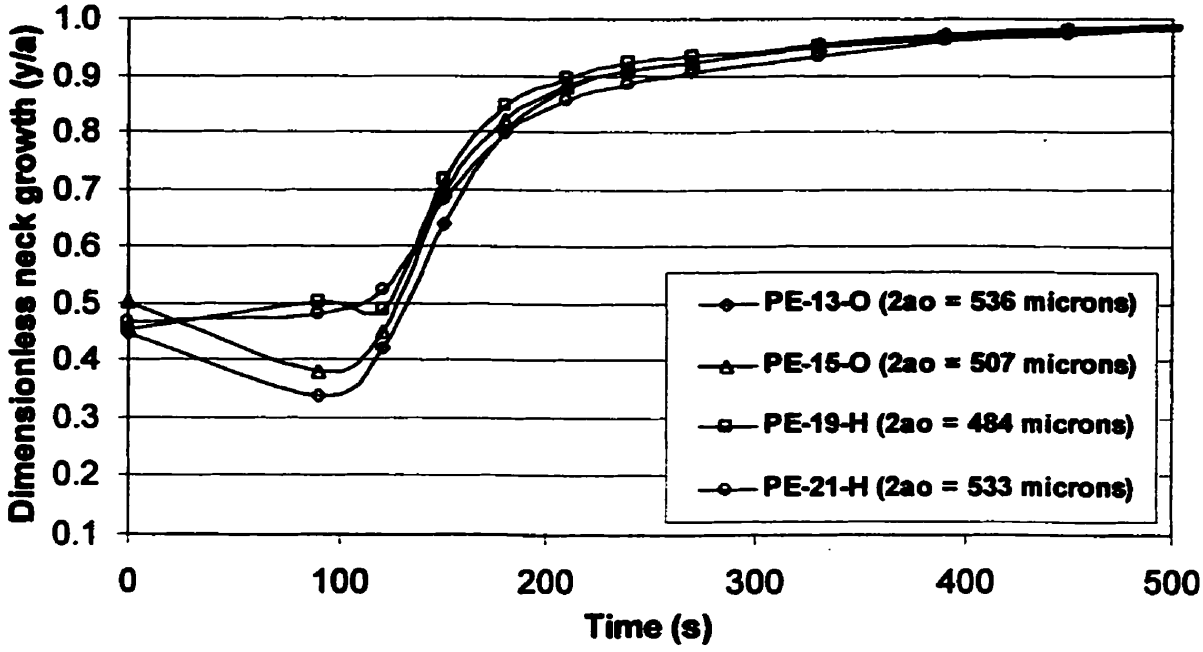

Figure 4.39 Neck growth evolution for medium-viscosity resins in powder form. Experiments at ramped temperature (111 to 226.5 °C at 11°C/min)

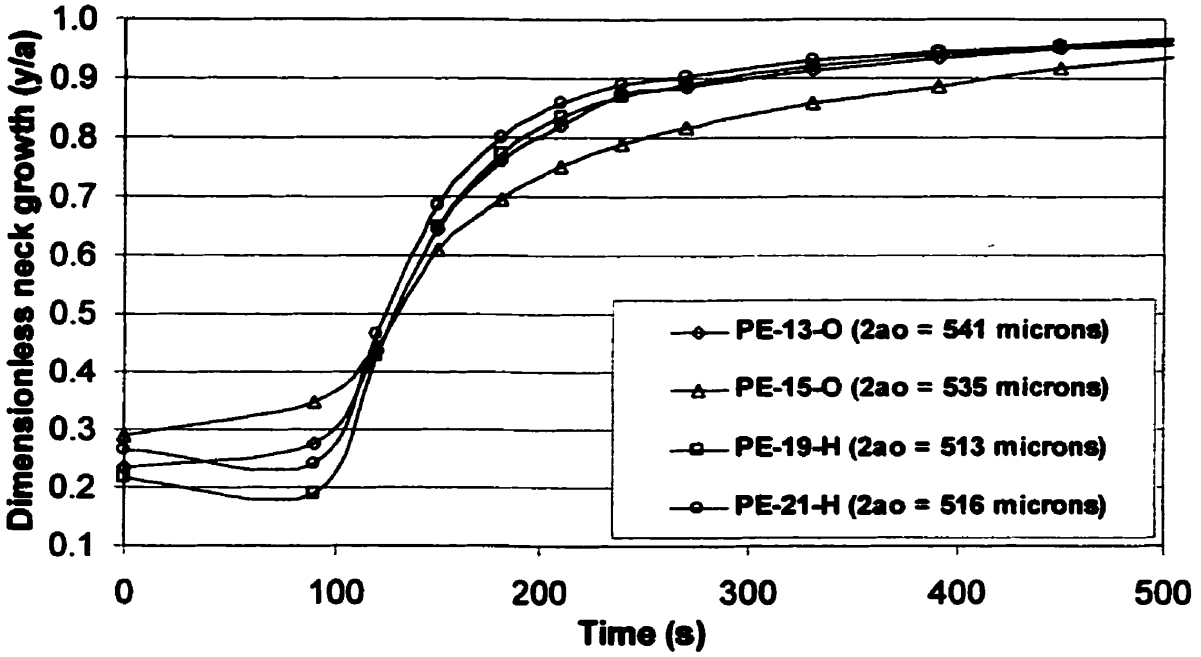

Figure 4.40 Neck growth evolution for medium-viscosity resins. Experiments with cylinders at ramped temperature (111 to 226.5 °C at 11°C/min)

4.2.4.3 High viscosity

PE-23-O and PE-24-O are compared in Figures 4.41 and 4.42 (constant temperature) and Figures 4.43 and 4.44 (ramped temperature). This time, the trends are very close to each other in the case of cylinders and slightly separated in the case of powder. This may indicate that the resins were ground under different conditions and the different thermal/shear treatments imposed during grinding are visible under these experimental conditions. PE-27-O is also included in Figures 4.42 and 4.44. This resin exhibits high values of both viscosity and elasticity originating mainly from its higher value of molecular weight. Accordingly, its sintering rate is low.

4.3 Summary

It was shown in this chapter that the experimental conditions at which sintering experiments are conducted may help to resolve the effect of material properties other than viscosity on the sintering process. In particular, the use of cylindrical particles and non-isothermal conditions seems to enhance the importance of the thermal transitions and the viscosity temperature dependence. The sintering results of experiments conducted with powder particles showed closer trends and slightly higher sintering rates than those conducted with cylinders. Those observations were attributed to the differences in surface area between powder and cylindrical particles.

The experimental results showed that the resins' molecular structure is an important factor in the sintering of ethylene/α-olefin copolymers. It was observed that the molecular weight has a negative influence on the sintering rate. This effect was expected since as the M_w increases, properties such as viscosity and elasticity also increase. High values of viscosity and elasticity represent a resistance to the sintering process. Moreover, as the M_w increases, so does the length of the

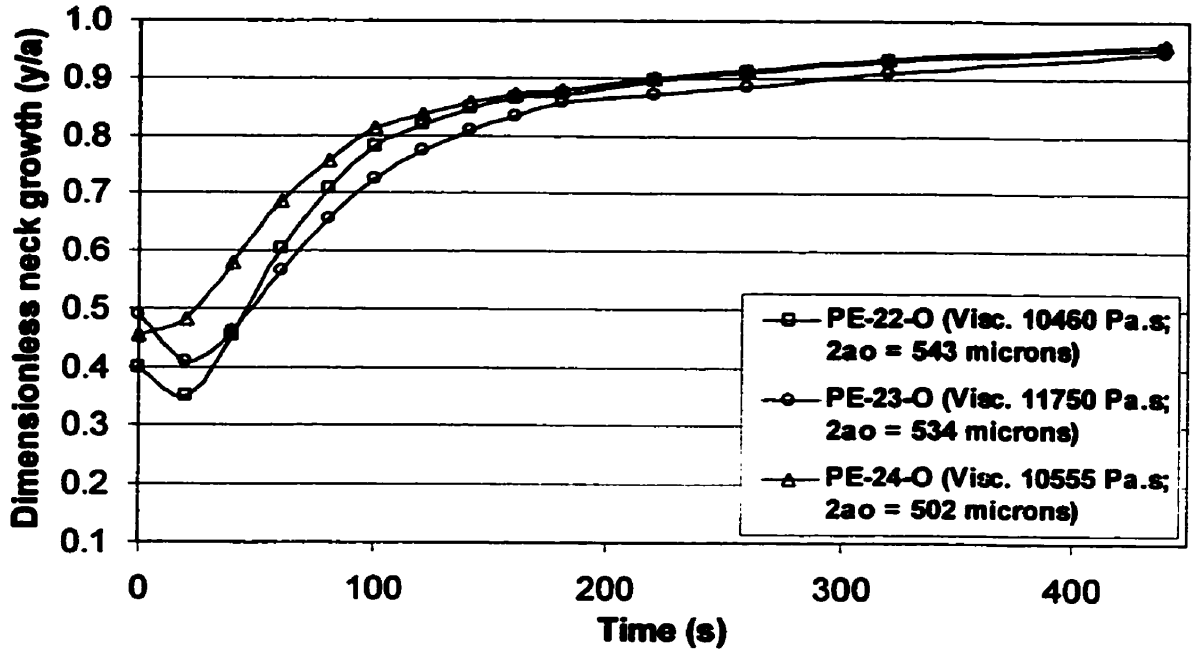

Figure 4.41 Neck growth evolution for high-viscosity resins in powder form. Experiments at constant temperature (170°C)

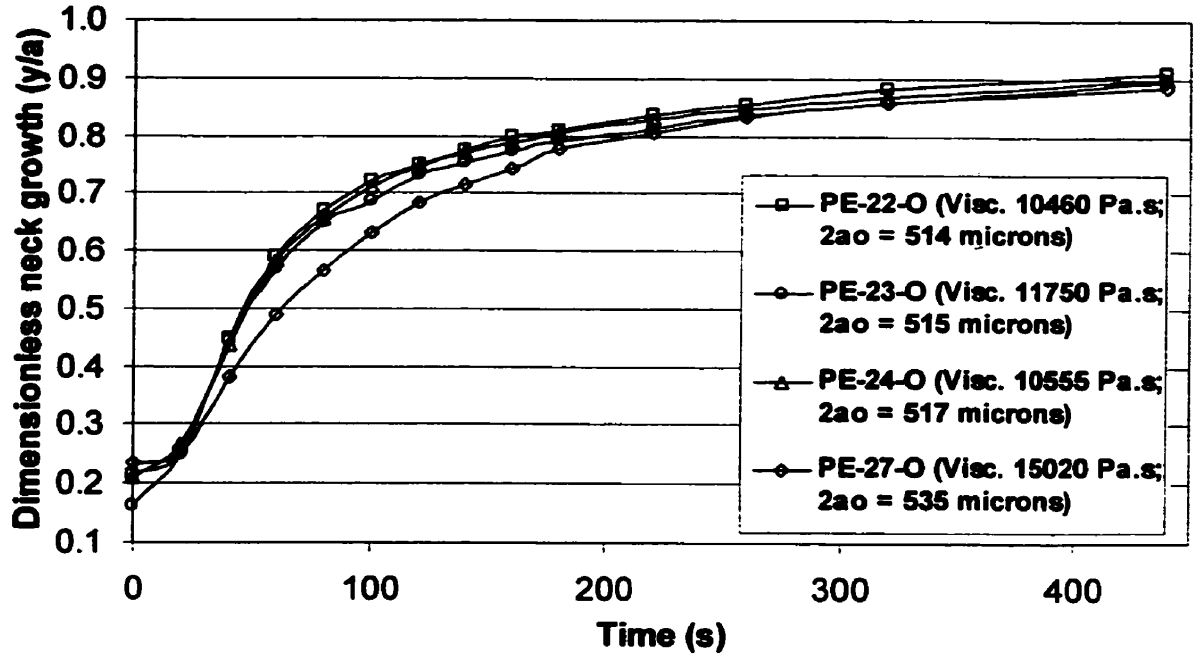

Figure 4.42 Neck growth evolution for high-viscosity resins. Experiments with cylinders at constant temperature (170°C)

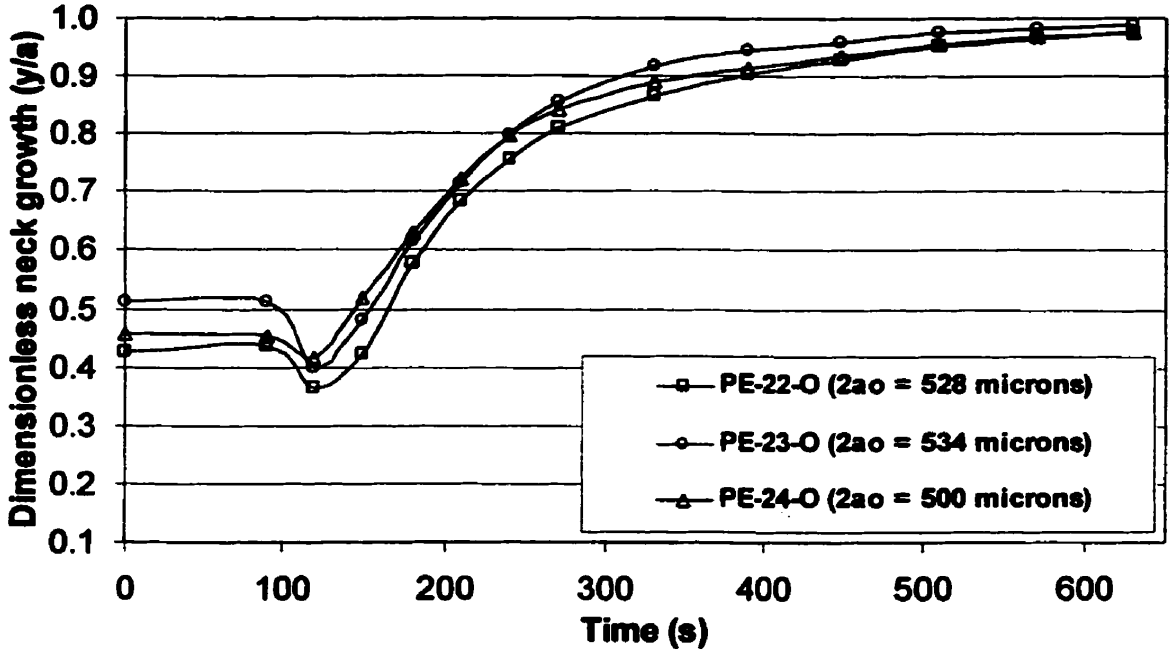

Figure 4.43 Neck growth evolution for high-viscosity resins in powder form. Experiments at ramped temperature (111 to 226.5 °C at 11°C/min)

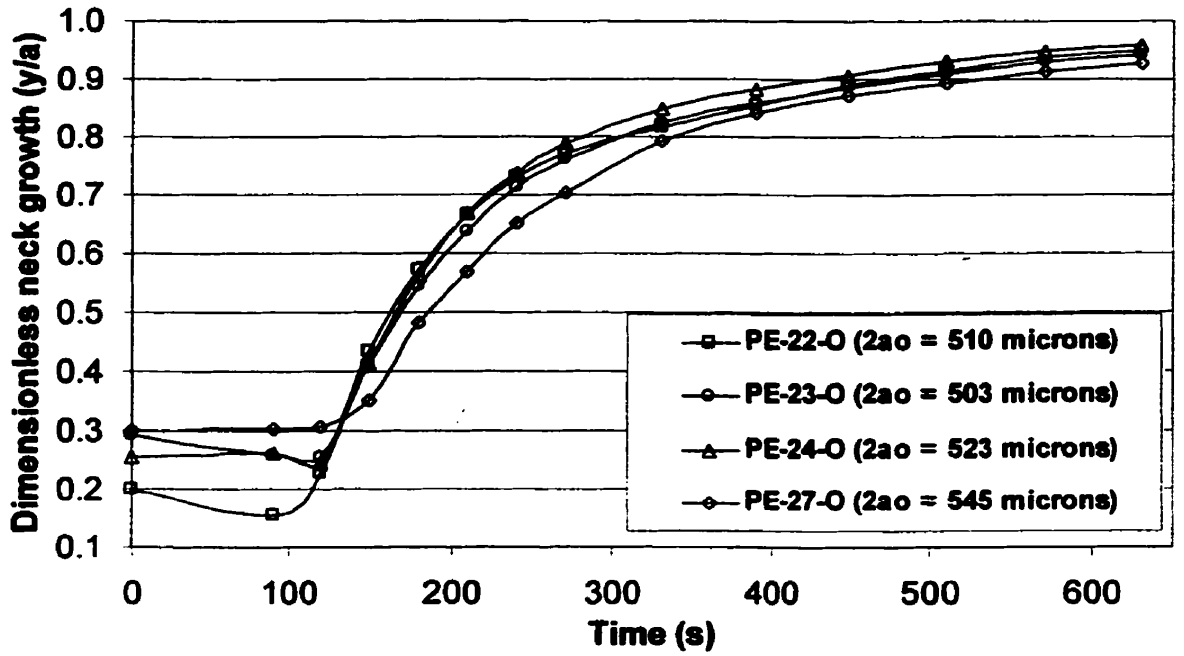

Figure 4.44 Neck growth evolution for high-viscosity resins. Experiments with cylinders at ramped temperature (111 to 226.5 °C at 11°C/min)

macromolecular chains, which is also associated with the interdiffusion phenomenon.

It was difficult to evaluate the influence of MWD, type and distribution of SCB on the sintering process. For the resins used in this study it was not possible to isolate the effect of one variable from another with the experimental results. It was observed, on the other hand, that as the comonomer or SCB content increases, the sintering rate decreases. This observation was explained in terms of morphology and thermal properties. Side branches are excluded from the crystal lattice generating amorphous regions which can represent an obstacle to self-diffusion. Furthermore, amorphous regions exhibit smaller values of surface tension, one of the driving forces in the sintering process. Nevertheless, the melting temperature and heat of fusion decrease with increasing comonomer content, which in turn favors an early start of the sintering neck growth under non-isothermal conditions. Experimental evidence suggests that copolymers with a more homogeneous structure may sinter faster than their heterogeneous counterparts, which are more elastic and have a broad melting range.

Conclusions and recommendations

Chapter 5

The aim of this study was to determine the effect of molecular structure on the sintering of ethylene/α-olefin copolymers. Since this work is part of a larger project focused on the rotational molding process, most of the resins studied were rotational molding grades. Other resins were also included in order to support and verify some of the hypotheses that arose during this research. Prior to conducting the sintering experiments, the different resins were characterized using rheological, thermal and spectroscopic techniques. Results obtained from these characterization techniques, combined with GPC measurements, were found to be very useful in determining the molecular structure of the resins. The results showed that the rheological and thermal behaviors of ethylene/α-olefin copolymers are related to their chemical composition and chemical composition distribution. No simple trend could be identified and a general conclusion could not be drawn. Nevertheless, interesting observations were made and the results from the molecular characterization were used in the analysis of the sintering behavior of the different resins used in this work.

The rheological properties that are of interest for polymer sintering are the zero-shear viscosity and the elasticity. Past studies have shown that they represent the resistance in the sintering process. It was observed that along with the molecular weight dependence, the homogeneity of the molecular structure also influences the rheological properties. Resins with narrow MWD, low comonomer content and evenly distributed SCB, exhibit a well-defined Newtonian plateau and low elasticity. As the resin becomes more heterogeneous, the onset of the shear-thinning behavior shifts to low frequencies and the elasticity increases. In spite of the usefulness of the observations made during rheological testing, often only small differences were detected and other techniques were needed to elucidate the

chemical microstructure. The thermal studies reflected the differences in molecular structure to a better extent. The thermal transitions of ethylene copolymers are not only sensitive to molecular architecture but to thermal history as well. The inter- and intra-molecular differences were studied using differential scanning calorimetry before and after a thermal treatment. It was observed that the presence of heterogeneities (broad MWD, high comonomer content, broad SCB distribution) usually broadened the melting range and shifted the melting endotherms to regions of lower temperature. Moreover, the presence of short and rounded peaks was detected. After a thermal treatment (annealing) the chains tended to segregate based on chain length and branching content, resulting in multiple peaks in the melting endotherms. The results obtained from thermal analysis were in relatively good agreement with the results obtained using FTIR, making it possible to differentiate between the types of heterogeneities present in the material microstructure.

Sintering experiments were conducted under isothermal and non-isothermal conditions using powder and cylindrical particles. It was found that the sintering rate for the resins used in this work, when in powder form, followed the trends predicted by Newtonian models. Variations in the sintering rate were observed when cylinders were used, which could not be explained based on the resins' viscosity and elasticity. It is speculated that when the resins are processed in powder form the effect of properties other than viscosity and elasticity become less important due to geometrical considerations. One important difference between powder and cylindrical particles is the value of surface area. The reduction of surface area by surface tension is one of the driving forces of the sintering phenomenon. Sintering experiments conducted under non-isothermal conditions were found to provide information that can be more easily related to actual processes. Furthermore, under such conditions the importance of the thermal transitions and the viscosity temperature dependence were studied. The sintering experiments provided information about the effects of molecular structure on the coalescence process. The molecular weight was found to have a negative impact on the sintering

phenomenon. It was, however, difficult to evaluate the effect of other molecular characteristics on the sintering rate mostly due to the narrow range of resins used in this work. The effects of MWD, type of comonomer and comonomer distribution on sintering were not clearly established due to the fact that the influence of each variable could not be isolated. The comonomer content, on the other hand, seemed to negatively impact the sintering process. The presence of more branches generates more amorphous regions which in turn affect self-diffusion and decrease the surface tension. Increasing the comonomer content, however, generally results in a reduction of the melting temperature and of the heat of fusion, which can be beneficial to the sintering process.

The importance of the material viscosity and elasticity on sintering was verified. Other parameters, however, must be considered in the study of sintering of ethylene copolymers. The experimental evidence suggested that copolymers which are more homogeneous in terms of molecular structure may sinter faster than heterogeneous polymers. Faster sintering does not necessarily translate into good processability in rotational molding. Other properties associated with morphology, namely warpage and impact performance, must be studied in conjunction with sintering.

The use of only two particles might not represent the behavior of multiple particles during sintering. Future work in this project should include the comparison between the information provided by the sintering experiments against the information collected in the actual processes, i. e. rotomolding. It is of particular importance to relate the information gained on molecular structure to impact properties of the molded parts.

The effect of the different additives on sintering is covered very briefly in this thesis. The relevance of the grinding process has been also discussed. Therefore, a thorough investigation of the role of additives and pulverization in the sintering phenomenon is suggested.

References

Adisson, E., Ribeiro, M., Deffieux, A. and Fontanille, M., *Evaluation of the heterogeneity in linear low-density polyethylene comonomer unit distribution by differential scanning calorimetry characterization of thermally treated samples,* Polymer, Vol. 33, No. 20, pp. 4337-4342, (1992).

Alamo, R. G. and Mandelkern, L., *Thermodynamic and structural properties of ethylene copolymers*, Macromolecules, Vol. 22, pp. 1273-1277, (1989).

Alizadeh, A., Richardson, L., Xu, J., McCartney, S., Marand, H., Cheung, Y. W. and Chum, S., *Influence of structural and topological constraints on the crystallization and melting behavior of polymers. 1. Ethylene/1-octene copolymers,* Macromolecules, Vol. 32, pp. 6221-6235, (1999).

Baker, C. and Maddams, W. F., *Infrared spectroscopic studies of polyethylene, 1. The measurement of low levels of chain branching*, Die Makromolekulare Chemie, Vol. 177, pp. 437-448, (1976).

Balta Calleja, F. J. and Rueda, D. R., *Study of the interlamellar folded structure of polyethylene as revealed by melting point and crystallinity*, Polymer Journal, Vol. 6, No. 3, pp 216-221, (1974).

Barnetson, A. and Hornsby, P. R., *Observations on the sintering of ultra-high molecular weight polyethylene,* Journal of Materials Science Letters, Vol. 14, pp. 80-84, (1995).

Bellehumeur, C. T., Bisaria, M. K., and Vlachopoulos J., *An experimental study and model assessment of polymer sintering*, Polymer Engineering and Science, Vol. 36, No. 17, pp. 2198-2207, (1996).

Bellehumeur, C. T., *Polymer sintering and its role in rotational molding*, PhD. Thesis, McMaster University, (1997).

Bensason, S., Minick, J., Moet, A., Chum, S., Hiltner, A. and Baer, E., *Clasification of homogeneous ethylene-octene copolymers based on comonomer content,* Journal of Polymer Science: Part B: Polymer Physics, Vol. 34, pp. 1301-1315, (1996).

Bin Wadud, S. E. and Baird, D. G., *Rheology of metallocene-catalyzed polyethylenes: the effect of branching*, Proc. SPE ANTEC, pp. 1200-1204, New York City, NY, (1999).

Blitz, J. P. and McFaddin, D. C., *The characterization of short chain branching in polyethylene using FTIR*, Journal of Applied Polymer Science, Vol. 51, pp. 13-20, (1994).

Crist, B. and Claudio, E. S., *Isothermal crystallization of random ethylene-butene copolymers: Bimodal kinetics*, Macromolecules, Vol. 32, pp. 8945-8951, (1999).

Defoor, F., Groeninckx, G., Schouterden, P. and Van der Heijden, B., *Molecular, thermal and morphological characterization of narrowly branched fractions of 1-octene LLDPE: 2. Study of the lamellar morphology by transmission electron microscopy,* Polymer, Vol. 33, No. 24, pp. 5186-5190, (1992).

De Genes, P. G., *Reptation of a polymer chain in the presence of fixed obstacles*, Journal of Chemical Physics, Vol. 55, No. 2, pp. 572-579, (1971).

Frenkel, J., *Viscous flow of crystalline bodies under the action of surface tension*, Journal of Physics (USSR), No. 9, pp. 385-391, (1945).

Fu, Q., Chiu, F. C., McCreight, K. W., Guo, M., Tseng, W. W., Cheng, S. Z. D., Keating, M. Y., Hsieh, E. T. and DesLauriers, P. J., *Effects of the phase-separated melt on crystallization behavior and morphology in short chain branched metallocene polyethylenes*, Journal of Macromolecular Science – Physics, B36(1), pp. 41-60, (1997).

Gartner, C., Sierra, J. D. and Avakian, R., *New polyolefins characterization by instrumental analysis*, Proceedings of SPE-ANTEC, p. 2012, (1998).

Goyal, S. K., *The influence of polymer structure on melt strength behavior of PE resins*, Plastics Engineering, February, pp.25-28, (1995).

Goyal, S. K., Auger, J., Karbashewski, E. and Saetre, R., *Influence of branch distribution on the rheological and processing behaviour of LLDPE resins*, Proc. SPE ANTEC, pp. 1881-1886, Atlanta, GA, (1998).

Hopper, R. W., *Coalescence of two equal cylinders: exact results for creeping viscous plain flow driven by capillarity*, Communications of the American Ceramics Society, Vol. 67, C-263, (1984)

Hornsby, P. R. and Maxwell, A. S, *Mechanism of sintering between polypropylene beads,* Journal of Materials Science, Vol. 27, pp. 2525-2533, (1992).

Hosoda, S., *Structural distribution of linear low-density polyethylene,* Polymer Journal, Vol. 20, No. 5, pp. 383-397, (1988).

Jasse, B., *Use of curve analysis to analyze overlapping bands in the IR spectra of polymers,* In "FTIR Characterization of Polymers", edited by Hatsuo Ishida, Polymer Science and Technology, Vol. 36, Plenum Press, U.S.A., (1987).

Kazatchkov, I. B., Bohnet, N., Goyal, S. K., and Hatzikiriakos, S. G., *Influence of molecular structure on the rheological and processing behaviour of polyethylene resins*, Polymer Engineering and Science, Vol. 39, No. 4, pp.804-815, (1999).

Kim, Y. S., Chung, C. I., Lai, S. Y. and Hyun, K. S., *Melt rheological and thermodynamic properties of polyethylene homopolymers and poly(ethylene/α-olefin) copolymers with respect to molecular composition and structure,* Journal of Applied Polymer Science, Vol. 59, pp. 125-137, (1996).

Koenig, J. L., *Chemical Microstructure of Polymer Chains*, John Wiley and Sons, U. S. A, (1980).

Koenig, J. L., *Spectroscopy of Polymers*, Second Edition, Elsevier Science, The Netherlands, (1999).

Koenig, J. L. and Witenhafer, D. E., *Infrared studies of polymeric chain folding I. Linear polyethylene*, Die Makromolekulare Chemie, Vol. 99, pp. 193-201, (1966).

Kontopoulou, M., Takacs, E. and Vlachopoulos, J., *An investigation of the bubble formation mechanism in rotational molding*, Rotation, Vol. IX, Issue 1, pp. 28-33, (2000).

Kuczynski, G. C., Neuville, B. and Toner, H. P., *Study of sintering of poly(methyl methacrylate)*, Journal of Applied Polymer Science, No. 14, p. 2064, (1970).

Kuczynski, G. C., *Physics and chemistry of sintering,* Adv. Colloid Interface Sci., No. 3, p. 275, (1972).

Lambert, W. S. and Phillips, P. J., *Crystallization kinetics of low molecular weight fractions of branched polyethylenes*, Macromolecules, Vol. 27, pp. 3537-3542, (1994).

Leaversuch, R. D., *Rotational molding comes of age*, Modern Plastics, June, pp. 38-41, (1989).

Liu, S. J., *A study of the sintering behaviour of polyethylene*, Rotation, pp. 20-31, Winter, (1996).

Maddams, W. F. and Southon, M. J. *The measurement of derivative IR spectra-III. The effect of band width and band shape on resolution enhancement by derivative spectroscopy*, Spectrochimica Acta, Vol. 38A, pp. 459-466, (1982).

Mazur, S., *Coalescence of polymer particles*, in "Polymer Powder Technology", Edited by M. Narkis and N. Rosenzweig, pp.157-214, John Wiley and Sons, (1995).

McDaid, J. and Crawford, R. J., *The grinding of polyethylene powders for use in rotational molding,* Proc. SPE ANTEC, Atlanta, GA, 1152-1155, (1998).

McRae, M. A. and Maddams, W. F., *Infrared spectroscopic studies of polyethylene, 2. The characterization of specific types of alkyl branches in low-branched ethylene polymers and copolymers*, Die Makromolekulare Chemie, Vol. 177, pp. 449-459, (1976).

McRae, M. A. and Maddams, W. F., *Infrared spectroscopic studies of polyethylene, 3. The bromination of unsaturated groups*, Die Makromolekulare Chemie, Vol. 177, pp. 461-471, (1976).

Muñoz-Escalona, A., Lafuente, P., Vega, J. F., and Santamaria, A., *Rheology of metallocene-catalyzed monomodal and bimodal polyethylenes*, Polymer Engineering and Science, Vol. 39, No. 11, pp. 2292-2303, (1999).

Okada, T. and Mandelkern, L., *Effect of morphology and degree of crystallinity on infrared absorption spectra of linear polyethylene*, Journal of Polymer Science Part A-2, Vol. 5, pp. 239-262, (1967).

Painter, P. C., Havens, J., Harf, W. W. and Koenig, J. L., *A fourier transform infrared spectroscopic investigation of polyethylene single crystals. I. Methylene wagging mode*, Journal of Polymer Science: Polymer Physics, Vol. 15, pp. 1223-1235, (1977a).

Painter, P. C., Havens, J., Harf, W. W. and Koenig, J. L., *A fourier transform infrared spectroscopic investigation of polyethylene single crystals. I. Fine structure of the methylene rocking mode*, Journal of Polymer Science: Polymer Physics, Vol. 15, pp. 1237-1249, (1977b).

Pandey, G. C., *Quantification of a-olefin co-polymer in linear low-density polyethylene by FTIR*, Process Control and Quality, No. 7, p. 173, (1995).

Peeters, M., Goderis, B., Vonk, C., Reynaers, H. and Mathot, V., *Morphology of homogeneous copolymers of ethene and 1-octene. I. Influence of thermal history on morphology,* Journal of Polymer Science: Part B: Polymer Physics, Vol. 35, pp. 2689-2713, (1997).

Peeters, M., Goderis, C., Reynaers, H. and Mathot, V., *Morphology of homogeneous copolymers of ethene and 1-octene. II. Structural changes on annealing,* Journal of Polymer Science: Part B: Polymer Physics, Vol. 37, pp. 83-100, (1999).

Pokluda, O., Bellehumeur, C. T. and Vlachopoulos, J., *Modification of Frenkel's model for sintering,* AIChE, Vol. 43, No. 12, pp. 3253-3258, (1997).

Poon, B., Chang, A., Chum, S. P., Tau, L., Volkenburgh, W. R., Hiltner, A. and Baer, E., *Adhesion of polyethylene to polypropylene in multi-layer films*, Proceedings of SPE-ANTEC, Dallas, TX, pp. 1668-1672, (2001).

Qureshi, N. Z, Rogunova, M., Stepanov, E. V., Capaccio, G., Hiltner, A. and Baer, E., *Self-adhesion of polyethylene in the melt. 2. Comparison of heterogeneous and homogeneous copolymers*, Macromolecules, Vol. 34, pp. 3007-3017, (2001).

Rastogi, S., Kurelec, L. and Lemstra, P. J., *Chain mobility in polymer systems: On the borderline between solid and melt. 2. Crystal size influence in phase transition and sintering of ultrahigh molecular weight polyethylene via the mobile hexagonal phase*, Macromolecules, Vol. 31, p. 5022-5031, (1998).

Riande, E., Diaz-Calleja, R., Prolongo, M. G., Masegosa, Rosa. M. and Solom, C., *Polymer Viscoelasticity, Stress and Strain in Practice*, Marcel–Dekker, New York, (2000).

Rosenzweig, N. and Narkis, M., *Coalescence phenomenology of spherical polymer particles by sintering*, Polymer, No. 21, pp. 988-989, (1980).

Rosenzweig, N. and Narkis, M., *Dimensional variations of two spherical particles during sintering*, Polymer Engineering and Science, Vol. 21, No. 10, pp. 582-585, (1981).

Rosenzweig, N. and Narkis, M., *Newtonian sintering simulator of two spherical particles*, Polymer Engineering and Science, Vol. 23, No. 1, pp. 32-35, (1983).

Rueda, D. R., Balta Calleja, F. J. and Hidalgo, A, *An IR study of the smorphous phase in melt crystallized polyethylene*, Spectrochimica Acta, Vol. 34A, pp. 475-480, (1978).

Rueda, D. R., Balta Calleja, F. J. and Hidalgo, A, *Determination of the degree of branching in polyethylene by an IR method of decomposition of bands*, Spectrochimica Acta, Vol. 35A, pp. 847-849, (1979).

Schouterden, P., Groeninckx, G., Van der Heijden, B. and Jansen, F., *Fractionation of linear low density polyethylene*, Polymer, Vol. 28, pp. 2099-2104, (1987).

Shan, C. L. P., Chu, K. J., Soares, J. B. P and Pendilis, A., *Structure-property characteristics of ethylene/1-hexene copolymers tailored short chain branching distribution*, Proc. SPE ANTEC, pp. 1616-1619, Orlando, FL (2000).

Siegmann, A., Raiter, I., Narkis, M., and Eyerer, P., *Effect of powder particle morphology on sintering behaviour of polymers*, Journal of Materials Science, Vol. 21, p. 1180-1186, (1986).

Sierra, J. D., Ospina, S., Montoya, N., Noriega, M. and Osswald, T. A., *Characterization of polyethylene blends by using novel techniques such as the successive self-nucleation and annealing and the fourier self-deconvolution IR spectroscopy (FSD-IR)*, Proceedings of SPE-ANTEC, p. 2485, (2000).

Starck, P., *Studies of the comonomer distributions in low density polyethylenes using temperature rising elution fractionation and stepwise crystallization by DSC,* Polymer International, Vol. 40, pp. 111-122, (1996).

Starck, P., Lehmus, P. and Seppala, J. V., *Thermal characterization of ethylene polymers prepared with metallocene catalysis*, Polymer Engineering and Science, Vol. 39, No. 8, pp. 1444-1455, (1999).

Stein, R. S. and Sutherland, G. B. B. M., *Interaction of methylene deformation frequencies in paraffin crystals*, Journal of Chemical Physics, Vol. 21, p. 270, (1953).

Tashiro, K., Sasaki, S. and Kobayashi, M., *Structural investigation of orhtorombic-to-hexagonal phase transition in polyethylene crystal: The experimental confirmation of the conformationally disordered structure by X-Ray diffraction and Infrared/Raman spectroscopic measurements*, Macromolecules, No. 29, pp. 7460-7469, (1996)

Tashiro, K., Sasaki, S., Gose, N. and Kobayashi, M., *Microscopically-viewed structural change of polyethylene during isothermal crystallization from the melt I. Time-resolved FT-IR spectral measurements*, Polymer Journal, Vol. 30, No. 6, pp. 485-491, (1998).

Usami, T. and Takayama, S., *Identification of branches in low-density polyethylenes by FTIR spectroscopy*, Polymer Journal, Vol. 16, No. 10, p. 731, (1984).

Vanden Eynde, S., Mathot, V. B. F., Hohne, G. W. H., Schawe, J. W. K. and Reynaers, H., *Thermal behaviour of homogeneous ethylene-1-octene copolymers and linear polyethylene at high pressures,* Polymer, Vol. 41, pp. 3411-3423, (2000a).

Vanden Eynde, S., Mathot, V. B. F., Koch, M. H. J. and Reynaers, H., *Thermal behaviour and morphology of homogeneous ethylene-propylene and ethylene-1-butene copolymers with high comonomer contents,* Polymer, Vol. 41, pp. 3437-3453, (2000b).

Vanden Eynde, S., Mathot, V. B. F., Koch, M. H. J. and Reynaers, H., *Thermal behaviour and morphology of homogeneous ethylene-1-octene copolymers with high comonomer contents,* Polymer, Vol. 41, pp. 4889-4900, (2000c).

Vega, J. F., Santamaria, A., Muñoz-Escalona, A. and Lafuente, P., *Small-amplitude oscillatory shear flow measurements as a tool to detect very low amounts of long chain branching in polyethylenes*, Macromolecules, No. 31, p. 3639-3647, (1998).

Willbourn, A. H., *Polymethylene and the structure of polyethylene: study of short-chain branching, its nature and effects*, Journal of Polymer Science, Vol. 34, pp. 569-597, (1959).

Wolf, B., Kenig, S., Klopstock, J. and Miltz, J., *Thermal fractionantion and identification of low-density polyethylenes*, Journal of Applied Polymer Science, Vol. 62, pp. 1339-1345, (1996).

Wood-Adams, P. and Dealy, J. M., *Relationship between structure and rheology of constrained geometry catalyzed and metallocene polyethylenes*, Proc. SPE ANTEC, pp. 1205-1209, New York City, NY, (1999).

Wood-Adams, P. M., Dealy, J. M., deGroot, A. W., and Redwine, O. D., *Effect of molecular structure on the linear viscoelastic behavior of polyethylene*, Macromolecules, No. 33, pp. 7489-7499, (2000).

Wu, S., *Polymer interface and adhesion*, Marcel Dekker, New York, (1982).

Zhang, M., Huang, J., Lynch, D. T. and Wanke, S. E., *Calibration of fractionated differential scanning calorimetry through temperature rising elution fraction*, Proc. SPE ANTEC, pp. 2000-2003, New York City, NY, (1999).

Zhang, M., Lynch, D. T. and Wanke, S. E., *Characterization of commercial low-density polyethylene by TREF-DSC and TREF-SEC cross-fractionation*, Journal of Polymer Science: Part B: Polymer Physics, Vol. 75, pp. 960-967, (2000).

Zhang, M., Lynch, D. T. and Wanke, S. E., *Effect of molecular structure distribution on melting and crystallization behavior of 1-butene/ethylene copolymers*, Polymer, Vol. 42, pp. 3067-3075, (2001).

Appendix A :
The Cross model

The viscosity data were fitted using the Cross model in the HAAKE RS150 software. The Cross model is given by the following equation:

$$\eta = \eta_\infty + \frac{\eta_0 - \eta_\infty}{1 + \left(\gamma / \gamma_b\right)^n}$$

where η is the shear viscosity; η_∞ the high shear rate Newtonian limit; η_0 the zero-shear viscosity; γ the shear rate; γ_b the characteristic shear rate; and n the shear thinning parameter.

Appendix B :
Processing of differential scanning calorimetry data

The data of the DSC were recorded in terms of the measurement signal U (μV) and the temperature (°C). The following equation was used to obtain thermograms with units of heat flow and temperature:

$$Q = \frac{U}{E(T)\,x\,m} \qquad (1)$$

where E(T) is the calorimetric sensitivity in μV/mW, m is the mass of the sample in mg and Q is the heat flow per unit mass in W/g. E(T) was obtained with the expression

$$E(T) = E_{In} \cdot E_{rel} \qquad (2)$$

which includes the temperature dependent and temperature independent components. In Equation 2 E_{In} is the value of E at the melting point of indium, i.e. 156.6 °C and is determined during the calibration and E_{rel} can be calculated using the equation

$$E_{rel} = A + B*T \qquad (3)$$

where A = 1.078 and B = -5.512×10^{-4} and T is in °C.

A standard procedure using Microsoft Excel was done in order to facilitate the data processing.

Appendix C :

Examples of infrared spectroscopy measurements

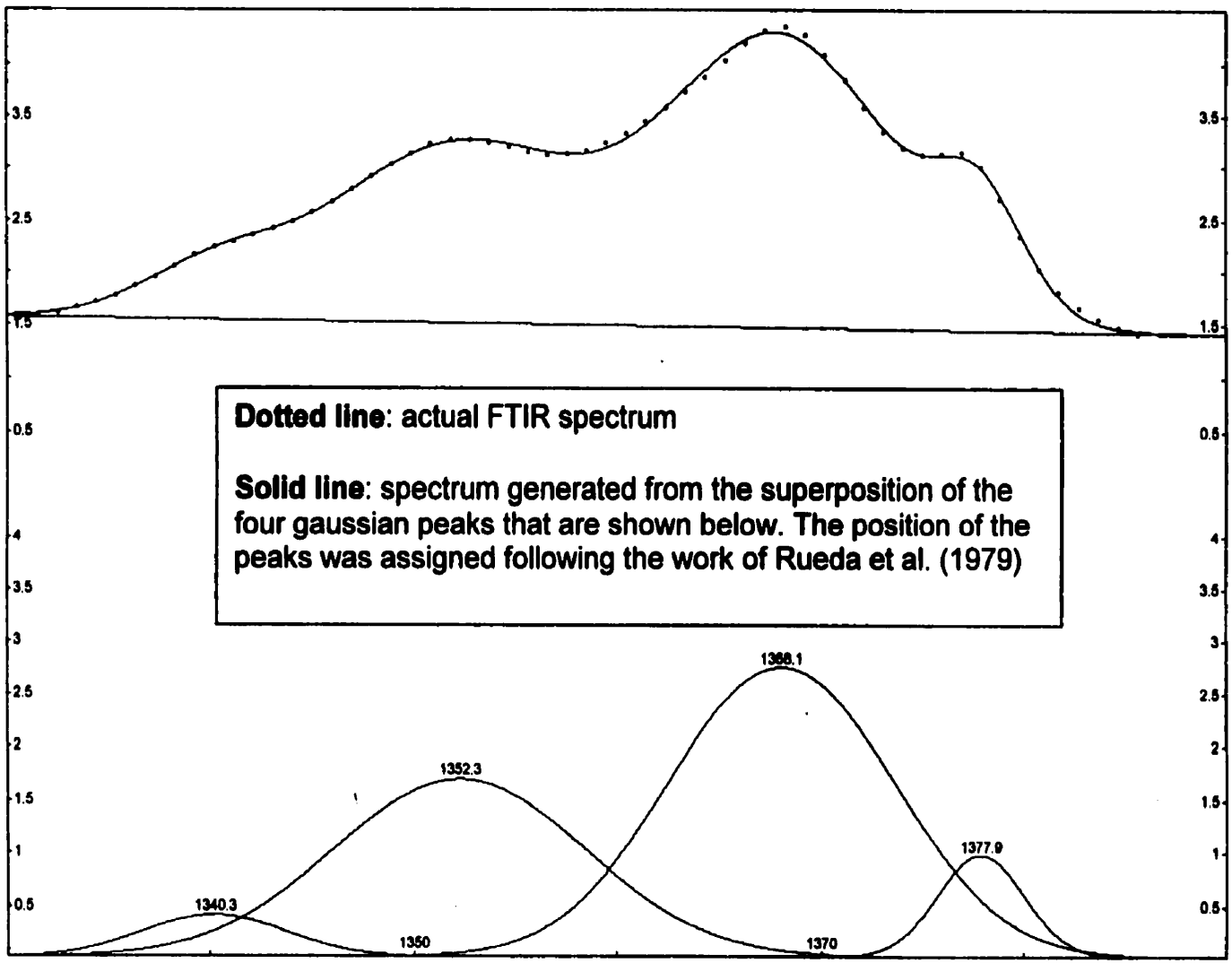

Resolution of the band located at ~1377 cm-1 associated to the methyl groups

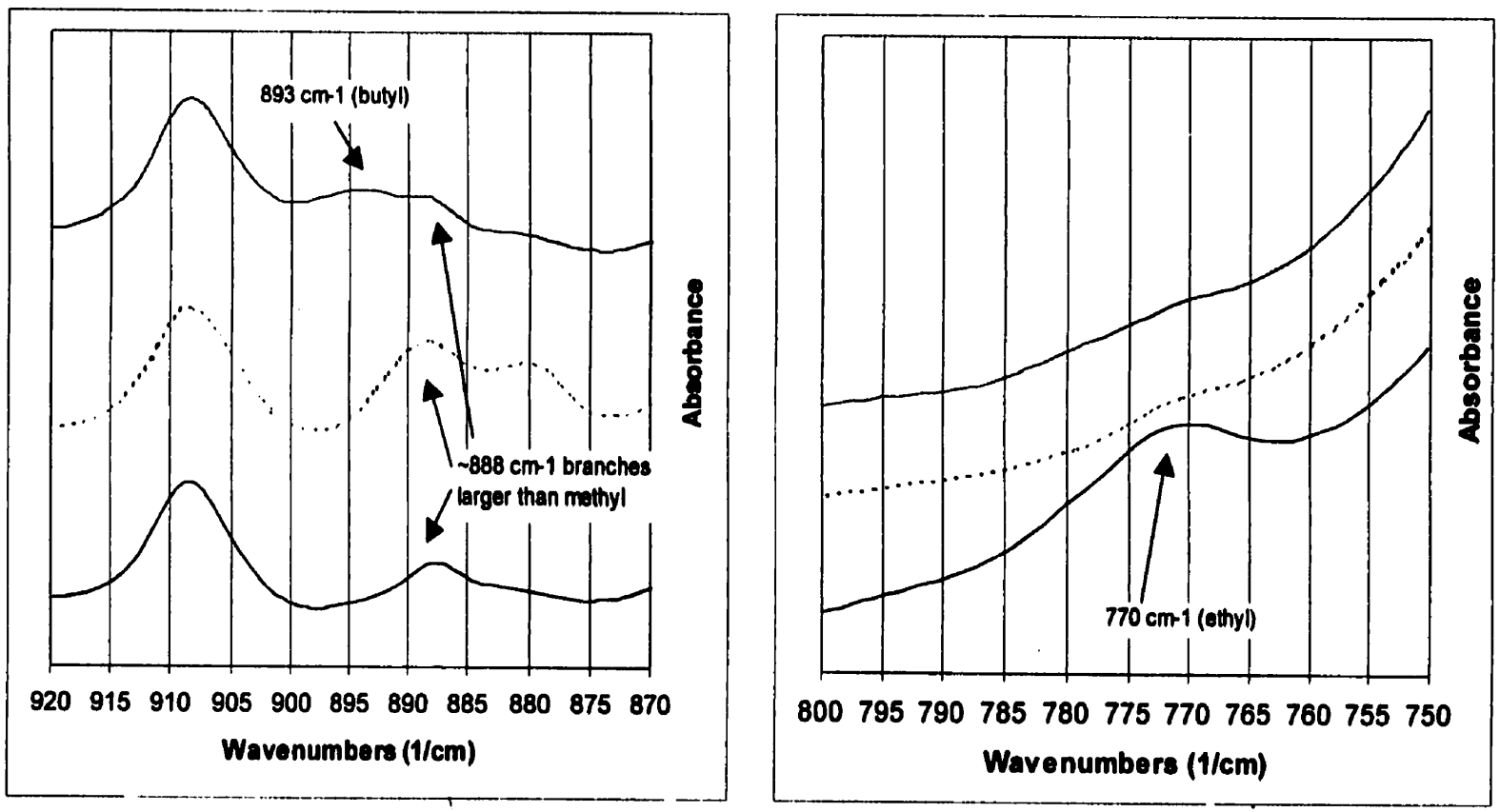

Comonomer identification using the assignments of Blitz and McFadding (1994)

Appendix D:
Calculation of the sintering neck radius (y/a)

The dimensionless sintering neck growth (y/a) is computed-based, using the partial area and the neck radius of the images (captured during the sintering process) measured by the Image-Pro Plus software. The mathematical formulation is briefly described below.

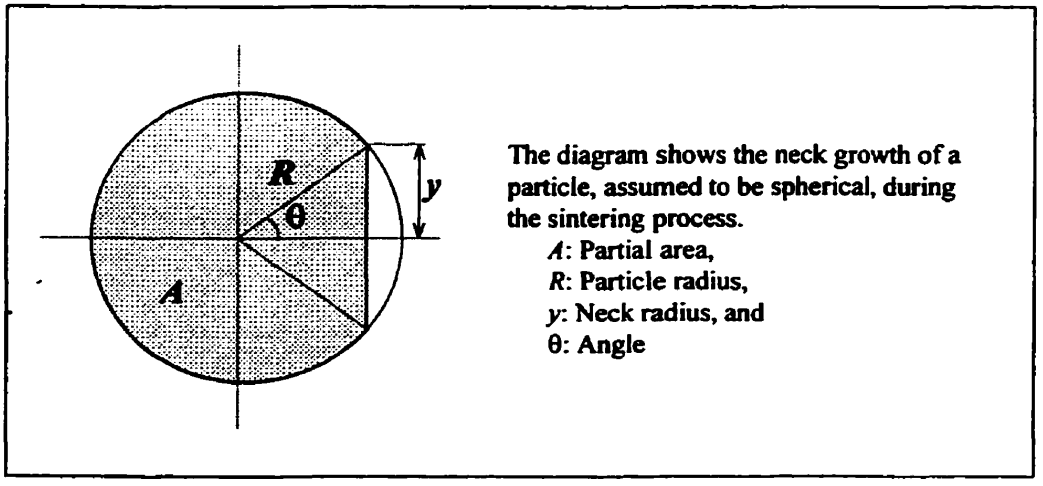

The diagram shows the neck growth of a particle, assumed to be spherical, during the sintering process.
A: Partial area,
R: Particle radius,
y: Neck radius, and
θ: Angle

The shaded area *A* shown in the diagram can be written as:

$$A = R^2\pi - R^2\theta + y\,(R\cos\theta) \qquad (1)$$

R and *y* can be related by:

$$y = R\sin\theta \quad \text{or} \quad R = y/\sin\theta \qquad (2)$$

Substituting (2) into (1):

$$A = y^2\pi/\sin^2\theta - y^2\theta/\sin^2\theta + y^2\cos\theta/\sin\theta \qquad (3)$$

Multiplying both sides of Equation (3) by $\sin^2\theta/A$, and rearranging all the terms to the right hand side:

$$0 = \sin^2\theta + (y^2/A)(\theta - \pi - \sin\theta\cos\theta) \qquad (4)$$

Since Equation (4) is a function of θ only (*y* and *A* are known data from image analysis) it can be numerically solved. The converged value of θ is then inserted into Equation (2) to calculate the particle radius *R*.

The average radius of the particle a in the sintering neck growth term (y/a) is calculated by taking the mean of the two values of *R* obtained for each particle.

Measurements of areas and length of the neck made with ImagePro®

Values generated from equations 2 and 4

Area1: A_1	Area2: A_2	Neck diam, 2y	$2a_1$	$2a_2$	
219138.3	229992.4	109.3281	528.7206	541.6210	0.2043
222282.7	234033.8	159.0156	533.5291	547.3396	0.2942
224318.5	251106.1	353.5231	552.5321	581.4631	0.6235
236805.2	267019.4	455.7408	587.5870	616.7435	0.7568
246691.9	286893.4	512.5288	614.3217	649.8104	0.8109
264147.1	297928.9	555.3741	644.7940	672.4456	0.8432
280856.6	305537.9	582.7797	668.8440	688.0532	0.8590
303471.9	304792.1	603.7591	694.4398	695.4300	0.8688
300176.3	328354.8	635.3729	705.5393	725.3136	0.8881
319153.4	327528.3	654.5074	727.2065	732.8659	0.8965
343844.8	335510.2	705.2265	767.1357	762.1289	0.9223
354033.8	353953.1	732.8453	787.2633	787.2189	0.9309
377445.2	366046.8	789.7364	831.2771	825.8089	0.9532
407941.5	390284.7	847.5774	880.4071	873.2290	0.9667

Appendix E :
Preparation of cylindrical particles

The cylinders were prepared by hot pressing the different resins on a perforated metallic plate made of aluminum. The temperature was kept below 200 °C and the heating time was less than 5 minutes to avoid degradation. Then, the plate was cooled at room temperature (20-25°C) for one hour. Cylinders with the desired thickness were cut afterwards using a razor blade. The thickness was inspected under an optical microscope and measured using the commercial software ImagePro®. Only cylinders with a thickness of 300 ± 25 μm were chosen for sintering experiments. The diameter of the cylindrical particles was approximately 500 μm.